Summer 8-13-2010

Gamma Oscillations in the Mouse Primary Visual Cortex as an Endophenotype of Schizophrenia

Cristin G. Welle
University of Pennsylvania, cgwelle@mail.med.upenn.edu

Gamma Oscillations in the Mouse Primary Visual Cortex as an Endophenotype of Schizophrenia

Abstract
Gamma oscillations (20-50 Hz) are a robust component of brain activity associated with information processing, but are also part of the background spontaneous activity during various brain states including sleep and anesthesia. Our goal was to examine the changes in gamma oscillations that result from pharmacological and genetic manipulations of glutamatergic transmission which produce endophenotypes of schizophrenia. We recorded local field potentials (LFP) and single units through the depth of the mouse primary visual cortex in vivo and examined the alterations in gamma frequency activity under both normal and pathological conditions. Our results indicate that both in awake and anesthetized animals, baseline gamma frequency power in the LFP is increased throughout the cortical lamina, and the signal-to-noise ratio of gamma oscillations produced by a visual stimulus is diminished, most notably in the superficial layers. In addition, the entrainment of single units to the local oscillations in the LFP is reduced in the supragranular (L2/3) and infragranular (L5/6) layers. This work supports the hypothesis that alterations in glutamatergic transmission result in changes to gamma oscillations in primary sensory areas and is consistent with the hypothesis that these changes are associated with disrupted sensory perception.

Degree Type
Dissertation

Degree Name
Doctor of Philosophy (PhD)

Graduate Group
Neuroscience

First Advisor
Diego Contreras

Keywords
gamma oscillations, mouse, vision, schizophrenia, spontaneous, electrophysiology

Subject Categories
Systems Neuroscience

GAMMA OSCILLATIONS IN THE MOUSE PRIMARY VISUAL CORTEX AS AN ENDOPHENOTYPE OF SCHIZOPHRENIA

Cristin Grace Welle

A DISSERTATION

in

Neuroscience

Presented to the Faculties of the University of Pennsylvania

in

Partial Fulfillment of the Requirements for the

Degree of Doctor of Philosophy

2010

Supervisor of Dissertation

*Signature*_____

Diego Contreras, Associate Professor, Neuroscience

Graduate Group Chairperson

*Signature*_____

Rita Balice-Gordon, Professor, Neuroscience

Dissertation Committee

Larry Palmer, Professor, Neuroscience

Joshua Gold, Associate Professor, Neuroscience

Brian Salzberg, Professor, Neuroscience and Physiology

Bruce Turetsky, Associate Professor, Psychiatry

ACKNOWLEDGEMENTS

I would like to acknowledge Diego Contreras for his help and advice as thesis advisor and the members of my thesis committee for their time and support. I would also like to thank the members of the Contreras lab, both past and present, for their advice and camaraderie. In particular, I would like to acknowledge Daniel Denman for his help with experiments, for writing substantial amounts of code and for contributing experimental data to this thesis. Finally, I would like to thank Steve Siegel and Yuling Liang for providing the *neuregulin* 1 knockout mice.

ABSTRACT

GAMMA OSCILLATIONS IN THE MOUSE PRIMARY VISUAL CORTEX AS AN ENDOPHENOTYPE OF SCHIZOPHRENIA

Cristin Grace Welle

Diego Contreras

Gamma oscillations (20-50 Hz) are a robust component of brain activity associated with information processing, but are also part of the background spontaneous activity during various brain states including sleep and anesthesia. Our goal was to examine the changes in gamma oscillations that result from pharmacological and genetic manipulations of glutamatergic transmission which produce endophenotypes of schizophrenia. We recorded local field potentials (LFP) and single units through the depth of the mouse primary visual cortex in vivo and examined the alterations in gamma frequency activity under both normal and pathological conditions. Our results indicate that both in awake and anesthetized animals, baseline gamma frequency power in the LFP is increased throughout the cortical lamina, and the signal-to-noise ratio of gamma oscillations produced by a visual stimulus is diminished, most notably in the superficial layers. In addition, the entrainment of single units to the local oscillations in the LFP is reduced in the supragranular (L2/3) and infragranular (L5/6) layers. This work supports the hypothesis that alterations in glutamatergic transmission result in changes to gamma oscillations in primary sensory areas and is consistent with the hypothesis that these changes are associated with disrupted sensory perception.

Table of contents *Page*

List of Illustrations *Page*

Introduction

Diversity of gamma oscillations

The oscillatory activity of neural populations has been studied for over a century. Fast frequency, referred to as gamma, oscillations were initially observed in human EEG recordings (Berger, 1929; Adrian, 1936) and have been subsequently characterized in a wide variety of species ranging from insects and invertebrates to birds and mammals. Gamma frequency oscillations are not associated with a single neurological process, but instead occur during many different brain states, both conscious and unconscious.

A large body of literature has established a clear relationship between gamma frequency activity and the processing of sensory stimuli. Across many species, gamma activity occurs in response to visual, auditory and olfactory stimuli. In the insect olfactory system, oscillatory activity between specific groups of cells depends on the characteristics of odor that is presented (Laurent, 1996; MacLeod and Laurent, 1996; Bazhenov et al., 2001; Laurent, 2002). Auditory stimuli produce an increase in gamma oscillations in the auditory cortex (Palva et al., 2002; Lakatos et al., 2005) and synchrony in the gamma range between single units with shared frequency preference (Brosch et al., 2002). In the visual system, gamma activity of single neurons and the local field potential is modulated by basic stimulus characteristics such as orientation (Frien et al., 2000) and contrast (Henrie and Shapley, 2005), in addition to top-down cognitive processes such as perceptual grouping (Keil et al., 1999). Although most work in the visual system has been performed in larger mammals such as cats, monkeys and humans, robust gamma oscillations have also been observed in the mouse primary visual cortex following the

presentation of bars or drifting gratings (Nase et al., 2003). It has yet to be determined if gamma oscillations in the mouse share similar properties to those recorded from larger mammalian species.

In addition to sensory processing, gamma frequency activity has also been implicated in relation to higher cognitive functions. In awake monkey and human subjects, shifts in selective attention are accompanied by changes in gamma band activity specific to the modality attended (Fries et al., 2001; Herrmann and Knight, 2001; Sokolov et al., 2004; Tallon-Baudry et al., 2005). In the visual system, attention modulation of gamma activity is present both in higher order processing centers (Fries et al., 2001) and in the primary visual cortex (Chalk et al., 2010). Gamma oscillations are also relevant for short and long term memory processes. During short term memory of visual cues, EEG recordings in human subjects revealed increased gamma activity in occipital areas (Jokisch and Jensen, 2007). Likewise, modulations of gamma activity occurs both during successful encoding of memories and retrieval of long term memories (Sederberg et al., 2003; Gruber et al., 2004; Axmacher et al., 2006). Finally, gamma oscillations are also relevant for the integration of sensorimotor information (Sanes and Donoghue, 1993).

Gamma frequency activity is not restricted to states of conscious information processing. In fact, gamma oscillations occur in awake animals in the absence of sensory input, during sleep, and under anesthesia (Contreras and Steriade, 1995; Steriade and Amzica, 1996; Destexhe et al., 1999). During slow wave sleep and under ketamine and xylazine anesthesia, long lasting positive waves are followed by high amplitude negative waves that are crowned with smaller amplitude gamma oscillations. During rapid eye

movement (REM) sleep and in awake animals, gamma oscillations occur consistently (Contreras and Steriade, 1995). The general frequency content and magnitude of gamma oscillations are similar in between all the states in which it occurs.

Function of gamma oscillations

Decades of research on the visual cortex has revealed an enormous organizational complexity. There are nearly 30 distinct visual areas classified in the monkey cortex and certainly as many in human or cat cortex. Hebb was the first to propose that the representation of different visual aspects of a scene might be distributed over many distinct subdivisions of the visual cortex. He referred to neurons responding to various features of an object as an 'assembly'. This concept of neural representation is appealing because it provides an economical use of neurons, yet it creates the problem of distinguishing one neural assembly from another. Realistic scenes have multiple objects that are represented, so presumably, multiple assemblies of neurons are activated. This would create an ambiguous representation unless there is a mechanism to distinguish one neural assembly from another (Hebb, 1949).

Von der Marlsburg proposed that the precise timing of action potentials at the millisecond timescale provides a cue to distinguish a given assembly. Thus, neurons representing a single object would engage in stimulus-dependant synchronous firing patterns. Studies in cat and monkey visual cortex show that spatially separate cells in the visual cortex show strong synchronization only if they are responding to the same visual stimuli. When responding to two independent stimuli, they fire in a less correlated

manner. Further studies have shown similar stimulus-dependant synchronization across the hemispheres and between sensory and motor regions (von der Malsberg and Schneider, 1986).

Gray and Singer showed that this neural synchronization occurs in the gamma frequency range. Neurons responding to the same orientation participate in gamma frequency oscillations that are precise on a millisecond timescale, even when the neurons are separated spatially by up to 7 mm. Synchronous gamma oscillations are not stimulus-locked, but generally occur about 200 to 500 ms following stimulus onset. However, the gamma oscillations between neurons responding to the same orientation are phase-locked, and thus occur synchronously between the assembly of participating neurons (Gray et al., 1989; Gray and Singer, 1989). Gamma oscillations only occur in response to coherent stimuli, and not portions of the stimuli presented independently (Engel et al., 1991; Singer and Gray, 1995). These findings suggest that gamma oscillations may serve as the mechanism by which neural assemblies are distinguished.

The most convincing evidence establishing a functional role for gamma oscillations is that performed by Gil Laurent and colleagues in the olfactory system of insects (Laurent, 1996; MacLeod and Laurent, 1996; Bazhenov et al., 2001; Laurent, 2002). This work shows that distinct groups of cells representing a given odor fire synchronously at a gamma frequency range. When the oscillations are disrupted pharmacologically, the olfactory discrimination performance of the insects is degraded. This level of causality has not yet been applied outside the insect olfactory system due to

the technical difficulties of specifically modulating gamma activity in the context of behavior.

Although there is evidence consistent with the idea that gamma oscillations may serve as a mechanism to bind different aspects of a stimulus into one unified representation, it is far from conclusive. An alternative explanation that can account for many of the experimental observations is that gamma activity is a natural by-product of increased neural activity, and thus is correlated with depolarization but does not contribute to perception directly. LFP and single unit recordings in the cat visual cortex using drifting grating stimuli shows that gamma activity increases with contrast, and thus may be more indicative of increasing recurrent cortical activity than a perceptual process (Henrie and Shapley, 2005). Additionally, the presence of gamma oscillations during states of unconsciousness, both during sleep and under many types of anesthesia, is not consistent with a direct role for gamma activity in conscious perception.

The body of work presented in this thesis does not address the functional role of gamma activity, but instead characterizes their spatiotemporal properties and their entrainment of single units throughout the depth of the cortex. However, our studies of the characteristics of gamma oscillations in different contexts do touch on this issue of a functional role. We find that gamma oscillations have different spatiotemporal properties and entrain excitatory and inhibitory networks differently when they are produced spontaneously than when they are induced by a stimulus. This suggests that the organization and the mechanisms of generation of gamma oscillations are context

dependant, and is consistent with the interpretation that gamma oscillations may serve different roles during spontaneous and stimulus-driven activity (Chapter 1).

Gamma oscillations and human disease

Another important motivation for the study of gamma frequency oscillations is the disruption of these oscillations that occurs in patients with neuropsychiatric disorders, such as schizophrenia. Schizophrenia is a disorder of altered cognition that is largely genetic in origin and is characterized by constellations of positive symptoms such as hallucinations and delusions and negative symptoms including flattened affect and disorganization of thought and language. Despite nearly a century of research on the disorder, there is no known cause of schizophrenia, and in fact, schizophrenia itself may include numerous diseases with different origins that manifest similar cognitive symptoms.

Patients with schizophrenia exhibit many electrophysiological alterations, including changes in gamma frequency activity throughout numerous areas of the brain (Kwon et al., 1999; Spencer et al., 2003; Uhlhaas and Singer, 2010). During higher-level cognitive tasks such as working memory and perceptual organization, schizophrenic patients show decreased power in the gamma band in frontal and temporal areas, and reduced synchrony of oscillations over the whole brain (Winterer et al., 2000; Cho et al., 2006; Uhlhaas et al., 2006; Haenschel et al., 2009). Even in the resting state, baseline spontaneous gamma activity is reduced in the frontal cortex compared to controls (Tekell et al., 2005; Boutros et al., 2008; Rutter et al., 2009).

Because of its symptoms, schizophrenia has long been considered a disorder of higher cognition, but work on event-related potentials (ERPs) in the primary auditory and visual cortices has demonstrated that schizophrenic patients show abnormalities even in the initial stages of sensory processing (Johnson et al., 2005; Turetsky et al., 2009). Furthermore, recent studies in primary sensory areas have shown that gamma oscillations are enhanced in patients compared to controls (Light et al., 2006; Spencer et al., 2009). Additionally, gamma oscillation power correlates with the positive symptoms of schizophrenia, most notably, hallucinations (Lee et al., 2003a; Behrendt, 2006). Patients with auditory hallucinations have increased magnitude and synchrony of gamma oscillations in the primary auditory cortex compared to patients not experiencing auditory hallucinations (Spencer et al., 2009).

One of the preeminent hypotheses for the cellular basis of schizophrenia is an alteration in glutamatergic functioning (Greene, 2001; Coyle et al., 2003; Lisman et al., 2008; Traub and Whittington, 2010). A strong line of evidence for this hypothesis stems from the observation that when humans are given the NMDA receptor antagonist ketamine, they exhibit symptoms similar to those observed in schizophrenic patients (Krystal et al., 1994). Additionally, the administration of ketamine alters gamma oscillations, increasing the power in the auditory cortex of human subjects (Plourde et al., 1997). In rodent models, ketamine produces behavioral endophenotypes of schizophrenia, such as hypolocomotion, reduced attention, visual discrimination and perceptual grouping (Nelson et al., 2002; Kurylo and Gazes, 2008). Ketamine has been shown to increase baseline gamma (Pinault, 2008; Hakami et al., 2009), and reduce the signal-to-

noise ratio of gamma oscillations in the awake rodent EEG (Lazarewicz et al., 2010). In primates, NMDA receptor antagonists alter mismatch negativity, another common endophenotype of schizophrenia (Javitt et al., 1996).

Interestingly, recent work in human neuroimmunology has identified an antibody that specifically antagonizes NMDA receptors (Dalmau et al., 2008; Hughes et al., 2010). Patients with this autoimmune disorder present with psychotic-like symptoms and are often admitted in psychiatric wards with tentative diagnosis for schizophrenia. Typically, the antibodies are produced in reaction to teratomas in the body, and following tumor resection, the patient's cognitive state is fully restored. This disorder lends support to the hypothesis that some of the psychiatric symptoms found in schizophrenia are produced by the modulation of the NMDA receptor.

A leading risk gene for schizophrenia, *neuregulin 1* (NRG1), is a synaptic structural protein that also effects NMDA-receptor mediated glutamatergic neurotransmission (Stefansson et al., 2002; Hahn et al., 2006). NRG1 has been shown to modulate NMDA receptor activation and has altered expression patterns in post mortem brain tissue from schizophrenic patients compared to controls (Hahn et al., 2006). Animal models with decreased NRG1 expression exhibit behavioral endophenotypes of schizophrenia such as mismatch negativity, contextual fear conditioning and social deficits (Ehrlichman et al., 2009b; O'Tuathaigh et al., 2010). In vitro studies of the hippocampus from NRG1 knockout animals report increased gamma oscillations (Fisahn et al., 2009).

In this body of work, we have looked at gamma oscillations specifically in the visual cortex of mice either under the influence of ketamine or with genetic reductions in NRG1 to assess the changes in gamma oscillations during baseline conditions and during the processing of sensory stimuli. We propose that changes in NMDA receptor function result in alterations of gamma oscillation in V1 (Chapter 3).

Cellular mechanisms of gamma oscillations

The cellular mechanisms of gamma oscillation production in the sensory cortex in vivo have not been fully investigated. Gamma activity in the cortex can be produced by at least three mechanisms: cell autonomous, gap junction-mediated networks between inhibitory interneurons and the network activity involving both excitatory and inhibitory neurons. Gamma oscillations in cortex can results from intrinsic oscillatory properties of excitatory cells (Llinas, 1988; Silva et al., 1991; Nunez et al., 1992), inhibitory cells (Llinas et al., 1991), and the special pyramidal cell class called fast rhythmic bursting or chattering cells (Gray and McCormick, 1996; Steriade et al., 1996b; Cardin et al., 2005). However, evidence from intracellular recordings of fast rhythmic bursting cells in cortex demonstrates that individual cells are not acting as pacemakers for gamma oscillations (Cardin et al., 2005). Instead, cortical gamma oscillations are more likely to be an emergent property of the network. Thus, synchronous gamma activity in a cortical network is likely generated either through connections between interneurons, or through reciprocal interactions between pyramidal cells and interneurons (Whittington et al., 2000; Tiesinga and Sejnowski, 2009). Interneuron generated gamma activity (ING)

occurs when a network of interneurons, potentially connected via gap junctions, receive an excitatory input and then begin to fire synchronously due to reciprocal inhibition. Alternatively, pyramidal-interneuron gamma generation (PING) occurs when pyramidal cells receive excitatory input, and depolarize inhibitory cells, which inhibit the excitatory cells and result in a network of oscillating cells. In both mechanisms, the onset of gamma generation requires a depolarizing input, and the frequency of the oscillation is determined by the decay constant of the GABAA receptor (Contreras et al., 1996; Whittington et al., 2000; Traub and Whittington, 2010).

In addition to generation by local cortical sources, gamma oscillations can be imposed onto the cortex by extracortical sources. For instance, gamma oscillations are robustly generated by thalamic cells (Steriade et al., 1993) and propagated between thalamic and cortical circuits via recurrent thalamocortical interactions (Contreras and Steriade, 1995; Jones, 2001; Llinas et al., 2005).

Experimental evidence suggests that both excitatory and inhibitory cells play some role in the production of gamma activity. A number of studies in vitro and in vivo suggest that inhibitory cell firing and IPSP timing is more closely entrained to activity in the gamma frequency range (Hasenstaub et al., 2005; Haider et al., 2007). Similarly, optogenetic stimulation of inhibitory cells at gamma frequencies produces greater gamma activity in the local field potential (LFP) than stimulation of regular spiking (RS) cells and may influence the information transmitted by sensory stimulus (Cardin et al., 2009; Sohal et al., 2009). However, a recent study showed that optogenetic excitation of RS cells in the superficial layers also produces gamma activity in L2/3 and influences firing

rates of excitatory cells in the deep layers (Adesnik and Scanziani, 2010). In our work on the entrainment of excitatory and inhibitory neurons to ongoing gamma oscillations, we find far greater entrainment of putative inhibitory cells than excitatory cells, although the precise contribution of specific cell type varies both with cortical depth and with the context of gamma production (Chapter1, Chapter 2).

The spatiotemporal characteristics of gamma oscillations in the LFP also vary through the depth of the cortex. Gamma oscillations are not thought to originate from one initial current sink, but instead, current source density profiles in anesthetized animals show multiple distributed sinks and sources over space and time (Steriade and Amzica, 1996). In addition, the magnitude of gamma oscillations in the auditory cortex of awake monkeys is larger in superficial layers than deep (Lakatos et al., 2005). In vitro studies have suggested that there may be two independent networks for generating gamma in cortex, located in the superficial and deep layers. These studies show that a cut perpendicular to the cortical surface in L4 does not prevent oscillatory activity in the beta/gamma range in either L2/3 or L5/6 (Roopun et al., 2006; van Aerde et al., 2009). In the primary sensory cortex of mice, we found that gamma oscillations showed a consistent phase shift through the layers of cortex, implying some organization of current sinks and sources. The magnitude of visually-driven gamma oscillations was largest in the superficial layers, but we did not observe a laminar profile during bouts of spontaneous activity. We manipulated gamma frequency activity in the superficial layers and found that the gamma oscillations in the deep layers were not affected, lending

support to the hypothesis of two connected, but somewhat independent, circuits for gamma generation in the cortex.

Importance of murine model in the study of gamma oscillations

Recently, studies in the field that have long relied on larger animal models such as cat and monkey have begun to move towards to the mouse model. One of the most important advantages of the murine model is the ability to genetically modify the mouse in order to model disease or to perturb a specific aspect of the neural system. In this thesis, we use the NRG1 mouse to characterize gamma oscillations as an endophenotype of schizophrenia. Modeling human disease in rodents can be an important way to make predictions about the changes that occur in disease states and allow for the testing of potential pharmacological interventions.

An additional advantage of the genetic modification of mice comes from the recent development of optogenetics. The excitation or inhibition of specific groups of neurons by light stimulation provides an opportunity to determine the contribution of specific components of a circuit. The manipulation of individual cell types in combination with recent advances in mouse behavioral paradigms, such as the recently developed visual discrimination tasks in head-fixed mice (Andermann et al., 2010; Niell and Stryker, 2010), will allow for experiments that can effectively address the mechanisms and function of gamma oscillations.

Chapter 1: Spontaneous and sensory-driven gamma oscillations engage distinct cortical circuitry

Abstract

Gamma oscillations (20-50 Hz) are a robust component of brain activity associated with information processing, but are also part of the background spontaneous activity during various brain states including sleep and anesthesia. Since the proposed functional role of gamma differs between states, we reasoned that the spatiotemporal pattern and contribution of excitatory and inhibitory networks to gamma oscillations should also be distinct. Here we compared those two states using local field potentials and single units from mouse primary visual cortex in vivo. We found that visually-driven gamma activity was preferentially increased in supragranular (L2/3) and granular (L4) layers whereas spontaneous gamma activity was homogenously distributed through the depth of the cortex. Single unit recordings of regular spiking (RS, putative excitatory) neurons showed that visual stimulation increased the number of rhythmic cells mainly in supra- and infragranular (L5/6) cortical layers, unlike during spontaneous gamma, in which rhythmic cells were homogeneously distributed throughout cortex. In contrast, fast spiking (FS, putative inhibitory) cells showed increased rhythmicity in infragranular layers during both conditions of gamma. Blockage of chloride-mediated GABAergic inhibition in supragranular layers led to a reduction in gamma oscillations in supragranular layers, a reduction in rhythmicity for both supragranular RS and FS, but a reduced rhythmicity for only RS cells in infragranular layers. Thus, our results show clear

differences in the spatiotemporal pattern of spontaneous and sensory-driven gamma and reveal an important contribution of supragranular layers to the rhythmicity of infragranular layers.

Introduction

Oscillatory activity in the gamma (20-50 Hz) frequency band is a ubiquitous rhythm throughout the brain that has been implicated in multiple aspects of information processing. Gamma oscillations have been associated with sensory representation (Gray et al., 1989; Ribary et al., 1991; Eckhorn et al., 1993), sensorimotor integration (Sanes and Donoghue, 1993) and cognitive processes including memory (Sederberg et al., 2003; Gruber et al., 2004; Herrmann et al., 2004), attention (Fries et al., 2001; Debener et al., 2003) and perception (Keil et al., 1999; Ribary, 2005). The association of gamma-band rhythmic activity and information processing is found across a wide range of species ranging from insects (Laurent, 1996) and rodents (Sukov and Barth, 1998; Nase et al., 2003) to non-human primates (Eckhorn et al., 1993) and humans (Ribary et al., 1991).

In addition to its association with information processing, gamma-frequency activity is a robust component of the ongoing background activity of the brain. Spontaneous gamma oscillations occur during REM and slow wave sleep, under various anesthesias, and in the wake state in the absence of direct sensory stimulation (Contreras et al., 1996; MacDonald et al., 1996; Steriade and Amzica, 1996; Steriade et al., 1996a; Destexhe et al., 1999; Steriade, 2006).

Experimental and theoretical studies have identified a variety of cellular mechanisms underlying the generation of gamma oscillations in cortical and thalamocortical networks. These mechanisms range from intrinsic oscillatory properties of single neurons (Llinas, 1988; Llinas et al., 1991; Silva et al., 1991; Nunez et al., 1992; Gray and McCormick, 1996; Steriade et al., 1996b; Cardin et al., 2005), to local circuit

interactions (Whittington et al., 1995; Wang and Buzsaki, 1996; Fisahn et al., 1998; Whittington et al., 2000) and recurrent thalamocortical interactions (Steriade et al., 1993; Contreras and Steriade, 1995; Jones, 2001; Llinas et al., 2005).

Despite the abundance of work delineating the mechanisms of gamma oscillations and their relevance to information representation, few studies have addressed the apparent paradox of the presence of this rhythm during ongoing, background activity. The goal of this study was to shed light on the mechanisms of gamma generation in vivo and to determine if stimulus-driven gamma activity engages columnar circuitry and excitatory and inhibitory networks in the same manner as spontaneous gamma activity. The well-documented modulation of gamma activity by visual stimuli, the robust gamma oscillations in the mouse V1 (Nase et al., 2003), and the recent characterization of its single unit response properties (Niell and Stryker, 2008) made the mouse primary visual cortex ideally suited for our study of the characteristics of gamma frequency oscillations.

We show that in the primary visual cortex of the mouse in vivo, spontaneous and visually-driven gamma oscillations have similar magnitude and peak frequency but different bandwidths and distributions over the cortical depth. In addition, the quantification of rhythmicity of regular and fast spiking neurons reveals a laminar structure that differs between the stimulus-driven and spontaneous conditions, implying differential contribution of excitatory and inhibitory networks between states. Finally, our results suggest an important contribution of L2/3 to sensory responses and to the rhythmicity of the output neurons of the cortex.

Materials and Methods

Surgery

All animal experiments were performed in accordance with the guidelines of the National Institutes of Health and the University of Pennsylvania Institutional Animal Care and Use Committee. Adult C57/B6 mice (12 – 24 weeks) were sedated with an initial dose of xyalzine (13 mg/kg) and anesthetized with brief exposure to a high concentration of isoflurane (5%). Anesthesia was maintained with light isoflurane (0.1 – 0.7 %) and the administration of booster doses of xylazine as needed, typically every 2 hours. Anesthetic level was monitored by toe pinch, respiration and pupil dilation. Body temperature was maintained at 36° – 37° F throughout the experiment with a heating pad (FHC). Mice were positioned in a stereotaxic apparatus (David Kopf Instruments) and rotated 60° so that one eye was directed towards a LCD monitor. Skin incisions were infused with lidocaine and the eye was covered with lacrilube to prevent drying. During the recording session, lacrilube was removed, and eye condition was carefully monitored. A craniotomy (~1.5 x 1.5 mm) was made above the primary visual cortex contralateral to the eye facing the monitor. The dura was removed to allow the insertion of either a silicon polytrode (NeuroNexusTechnologies) or multiple tetrodes (Thomas Recording Technologies).

Electrophysiology

Local field potential (LFP) recordings were obtained from multi-electrode probes (Neuronexus Technologies) with 16 channels arranged in a vertical configuration, with

either 50 or 100 μm spacing between probes (model a1x16-3mm50-177 or a1x16-3mm100-177), inserted normal to the surface of the cortex. In some experiments, two probes were inserted with ~1mm space between the probes. LFP signals were filtered 0.1 to 3000 Hz online (n= 18 animals, 21 probes). For single-unit recording, simultaneous extracellular and LFP recordings were obtained from multiple tetrodes inserted via a microcontroller (Thomas Recording). The extracellular signal was filtered from 600 to 9000 Hz and spiking events were detected on-line by voltage threshold crossing (N=14 animals, 47 tetrodes, 215 cells). A 1.5 ms waveform sample was acquired around the time of threshold crossing and was analyzed offline. All signals were recorded with the Cheetah 32-channel acquisition system at 30 kHz (Neuralynx).

Pharmacology

A small dose (75 μL) of picrotoxin (0.75 μM, Sigma) was applied to the surface of the cortex, and the excess was immediately wiped away. Recordings were started 5 minutes after the application of picrotoxin and lasted for ~20 minutes.

Visual stimuli

Visual stimuli were generated using a ViSaGe stimulation generation system (Cambridge Research Systems, Cambridge, UK) and the accompanying MATLAB toolbox. Stimuli were displayed on a gamma-corrected 19-inch LCD monitor configured at 75Hz refresh rate, and positioned 30cm away from the mouse's eye to occupy ~70º of visual space. Full screen drifting gratings were presented for 1s with long (2-5 s) inter-stimulus intervals to

allow for a sufficient return to baseline between trials. Stimulus parameters (95% contrast, 0.08- 0.1 cycles/degree, 3 Hz) were chosen to maximally drive the visual response in both single units (Drager, 1975; Niell and Stryker, 2008) and LFPs.

Analysis

Analysis was carried out using custom routines in Igor (Wavemetrics) except where specified. Neural signals were filtered 0.1 – 300 Hz for LFP recordings and 20 – 50 Hz to isolate gamma frequency oscillations. LFPs from the 16-channel probes were used to calculate the current source density (CSD) of the cortical stimulus-evoked responses according to the methods of Swadlow et al. (2002). Briefly, the one-dimensional CSD was derived from the second spatial derivative of the LFP data as described by Freeman and Nicholson (1975):

$$(\partial^2\Phi/\partial z^2)=[\Phi(z+2\Delta z)-2\Phi(z)+\Phi(z-2\Delta z)]/(2\Delta z)^2$$

where Φ is the LFP, z is the vertical coordinate depth of the probe, and Δz is the inter-recording site distance (50 or 100 μm in the present study). Upper and lower boundaries for CSD calculation were obtained by extrapolating recordings from the first and last recording sites.

Power spectra were generated using Fast Fourier Transform at a single trial level for 1s epochs either immediately before (baseline condition) or after (stimulus condition) the onset of the drifting grating. Baseline and stimulus spectra were averaged across trials for each electrode and then divided to give a ratio measurement of the increase above baseline. Peak frequency, amplitude and width measurements were calculated from the

ratio spectra. Latency to onset of gamma oscillations was calculated from LFP traces filtered for the gamma range (20- 50 Hz) and was measured as the time from stimulus onset to the first positive peak of the gamma filtered trace that crossed a significance threshold (2.5 SD above the mean). Coherence measurements were computed using multitapered methods and the Chronux package (http://chronux.org/)(Mitra et al., 2008) in Matlab (Mathworks). Wave triggered averages were calculated by averaging LFPs on the peaks of gamma oscillations that occurred during the presentation of the drifting grating and were above the significance threshold (2.5 SD above the mean). Representative LFPs from L2/3, L4 and L5/6 were averaged on the peaks of gamma from the L4 LFP. Phase shift was quantified by comparing the time of the center peak in the wave triggered average of LFPs from L2/3, L4 and L5/6.

Single units were first identified using an automated clustering algorithm based on the mixture-of-Gaussians model (Harris et al., 2000). Clusters were refined manually on the basis of waveform shape and interspike interval (SpikeSort3D, Neuralynx). Quality of separation was determined based on the Mahalanobis distance and L-ratio (Schmitzer-Torbert et al., 2005) using the MClust package (Matlab). Units were identified as visually responsive if they maintained an average firing rate of 0.05 Hz during at least 20 presentations of the stimulus.

All 215 units were then classified as regular or fast spiking based on properties of their average waveforms, at the electrode site with the largest amplitude. Three parameters were used for discrimination: the height of the positive peak relative to the subsequent negative trough, the time from peak to trough, and the slope of the waveform

0.5 ms after the initial peak. These parameters have been found optimal for separation of neurons in all layers of the mouse V1 (Niell and Stryker, 2008).

To determine if single units were entrained to the gamma oscillations in the LFP recorded on the same tetrode, we created peri-event histograms (PEHs) using the peaks of the gamma oscillations that crossed a significance threshold as timestamps. To ascertain if the modulation of these events was significant, we computed a rhythmicity index (RI) for each cell. The RI was calculated by averaging the spike counts of the difference between the three center peaks and troughs, and dividing this by the average of the entire histogram (Popescu et al., 2009). This calculation was repeated 1,000 times with shuffled spike times, and the RI of the cell was normalized with respect to the resulting histogram of spike-shuffled rhythmicity values. A normalized rhythmicity value of 0.95 or greater, corresponding to a RI greater than 95% of the shuffled values, was considered significant. All rhythmicity values reported in the text and figures are normalized.

Statistical analysis was performed using the Mann-Whitney U test or the Wilcoxon signed-rank test where appropriate. Variability is reported as the standard deviation (SD) unless specified to be the standard error of the mean (s.e.m.). All error bars in the figures represent the standard error of the mean.

Results

Spontaneous and visually driven gamma frequency oscillations occur robustly through the depth of V1.

Our goal was to characterize the spatiotemporal distribution of gamma oscillations (20-50 Hz) through the depth of the mouse primary visual cortex (V1) and compare visually driven oscillations with those occurring spontaneously. We recorded local field potentials (LFPs) using a multisite probe (Neuronexus, Ann Arbor, MI) with 16 evenly spaced recording sites (50 or 100 μm interelectrode distance) inserted normal to the cortical surface and spanning the cortical depth. We also recorded single cells from layers 2-6 using 5-7 independently movable tetrodes (Thomas Recordings, Giessen, Germany). Mice were anesthetized with a mix of isoflurane and xylazine in order to obtain a stable low amplitude spontaneous baseline pattern recorded in the LFPs (Fig. 1A). The visual responses described here were readily abolished or became highly variable when the anesthesia level induced slow oscillations in the background activity. We obtained recordings from 21 probes from 18 animals, from which we selected 17 probes from 13 animals for analysis based on the stability and amplitude of visual responses and the absence of slow oscillations in the baseline. Among these, we further selected 9 probes from 7 animals for the analysis of spontaneous activity in which there was enough prolonged stable baseline activity.

The presentation of high-contrast, full screen drifting gratings evoked a large response in the LFP signal, which was evident at the single trial level (Fig.1, green boxes) both in the broadband (0.1 to 300 Hz, Fig. 1A) and gamma frequency (20 – 50 Hz, Fig.

1D) filtered data. The stimulus-locked average of the visual response in the broadband LFP (Fig. 1B) consisted of a negative deflection with a latency of 90 ms after stimulus onset in layer 4 (L4). The amplitude and latency of the stimulus-locked response varied systematically with cortical depth, which we quantified using current source density (CSD) analysis (Freeman and Nicholson, 1975; Swadlow et al., 2002). In this example, the CSD revealed an initial large sink in L4 with an onset latency of 90 ms followed 92 and 111 ms later by sinks in L2/3 and L5/6, respectively (Fig. 1C). For the population, the latency to onset of the evoked response in L4 was 95.7 ± 15.5 ms, the latency to onset of the CSD response for L4 was 103±16 ms followed 69±66 and 78±73 later by sink onsets in L2/3 and L5/6. On the basis of the CSD analysis, we were able to reliably identify channels located in L2/3, L4 and L5/6. These latencies are longer than others have previously reported for rodent primary visual (Heynen and Bear, 2001; Niell and Stryker, 2008) and auditory cortex (Szymanski et al., 2009). However, this may be a function of the drifting grating stimuli, which produces a more gradual onset than a flashed or contrast reversing grating. Additionally, differences in onset latency may be anesthesia dependant.

Visual stimulation also triggered a robust increase in gamma frequency activity (Fig. 1D). Unlike the LFP evoked response, sensory driven gamma showed a variable latency from stimulus onset, and, therefore, was greatly reduced in magnitude by the stimulus-locked averaging (Fig. 1E, notice the change in vertical scale). Indeed, the CSD analysis of the averaged gamma revealed multiple sinks and sources over space and time

without any obvious layer arrangement (Fig. 1F). For this reason, our quantification of gamma frequency activity was done at the single trial level.

In addition to sensory-driven gamma, the spontaneous background activity showed bouts of gamma activity with similar amplitude and duration to those triggered by the drifting gratings. Spontaneous gamma bouts occurred robustly and regularly throughout the depth of V1 in all recording sessions (Fig. 1D, spontaneous). The presence of spontaneous gamma oscillations agrees with previous observations indicating that gamma oscillations are a robust component of the background activity of the brain (Steriade et al., 1996b).

Sensory-driven and spontaneous gamma frequency activities have distinct laminar structures.

Next, we compared the characteristics of visually-driven and spontaneous gamma through the vertical extent of the cortex. To quantify visually-driven gamma oscillations, we calculated the power spectrum from each single trial response over a 1 second window following stimulus onset. To obtain baseline spectra we used 1 second windows immediately preceding stimulus onset for each single trial. As indicated above, single trial analysis is immune to the reduction in amplitude of gamma oscillations that inevitably results from averaging the responses time locked to the stimulus. We then averaged the response and baseline single trial spectra (Fig. 2A, left panel) and calculated the ratio between the two for all 16 channels (Fig. 2A, right panel). Thus, the ratio spectra quantify the fold increase in activity along the frequency axis triggered by the visual

response with respect to the activity immediately preceding stimulus onset. The ratio spectra for this example illustrated in Figure 2A show up to a 6.36 fold increase in power in the gamma frequency band that is maximal at 26 ± 1 Hz. This increase over baseline was limited to a relatively narrow band of frequencies surrounding 26 Hz (width = 11.3±1.8 Hz). Additionally, this increase in gamma power was not uniform through cortical depth but was much stronger in granular (L4) and supragranular (L2/3) layers as illustrated by representing the ratio spectra as a 2D plot in which magnitude was color coded (Fig. 2B). The asymmetry between layers was clear in the plot of peak power frequency (26 Hz) versus cortical depth (Fig. 2B), which shows a 2.84 fold difference between L4 and L5/6.

Spontaneous gamma oscillations had distinct spectral and spatiotemporal properties compared to visually-driven gamma. We detected spontaneous gamma bouts by the crossing of a significance threshold set to 2.5 SD above the mean applied to the gamma band filtered data (see Methods). As with the visually-driven gamma, we calculated the power spectrum from each gamma bout and its corresponding 1 second preceding baseline, and averaged the single trial spectra (Fig. 2C, left panel). We then calculated the ratio spectra (spontaneous bout/baseline) for all 16 channels (Fig. 2C, right panel). Fig 2C shows an example in which spontaneous gamma bouts were similar to sensory-triggered gamma in their amplitude and peak frequency (6.17 fold increase in gamma power at 25.2 ± 1 Hz). In contrast, spontaneous gamma bouts included a much wider spectral increase (18.5 ± 1.4 Hz) and were relatively uniform in magnitude over the cortical layers. The more uniform distribution of spontaneous gamma bouts through

cortical depth is illustrated by the two-dimensional plot of the ratio spectra and by the laminar profile of the power at the peak frequency of 27 Hz (Fig. 2D). Thus, in contrast with those driven by visual stimuli, spontaneous gamma oscillations lack a distinct laminar structure.

The differences illustrated by the example in Figure 2 (A-D) were verified at the level of the population. To simplify the comparison over depth and across experiments, we averaged the responses of the channels located in the supragranular (L2/3), granular (L4) and infragranular (L5/6) laminae, as indicated by the CSD analysis. We quantified the distribution of gamma power through the depth of the cortex from the ratio spectra, to obtain a population value we arbitrarily normalized to L5/6 (Fig. 2E). The increase in visually driven gamma was significantly higher in L2/3 (1.83 fold greater, $p= 0.022$) and L4 (1.86 fold greater, $p= 0.012$) than L5/6. In contrast, the increase in gamma power during spontaneous bouts did not show significant differences between layers, despite a tendency to a larger increase in L2/3 (Fig. 2E).

The width (in Hz) of the increased power was measured from the ratio spectra as the distance between points raising 1 SD above spectral noise. The width did not change as a function of depth in either the spontaneous or stimulus-driven condition, and thus was averaged across all channels for each experiment. The width was significantly larger for spontaneous (23.2 ± 1.9 Hz) than sensory-driven (13.4 ± 2.7 Hz) (Fig. 2F), and while visually-driven increase generally fell between 20 – 50 Hz, spontaneous oscillations increased over a broader spectral range from 10 – 60 Hz. Like the example in Figure 2, the population peak frequency in the ratio spectra did not change over cortical depth and

was averaged across all channels. The frequency was not different between spontaneous (29.5 ± 3.4 Hz) and visually-driven (29.1 ± 1.8 Hz) (Fig. 2G). We quantified the latency to onset of visually-driven gamma oscillations as the time from onset of the drifting grating presentation to the first threshold-detected peak on the gamma-band filtered LFP. The population average showed no difference in onset latency between L2/3 (524 ± 246 ms) and L4 (495 ± 252 ms), but the latency in L5/6 was significantly longer than in L4 (652 ± 279 ms, $p = 0.04$). In conclusion, sensory-driven and spontaneous gamma activity showed peaks with similar frequency and magnitude but different bandwidth and distribution across cortical depth.

To further characterize the differences between spontaneous and visually-driven gamma oscillations and their distribution in the cortical depth, we investigated the phase and magnitude of gamma activity between the cortical layers. We performed coherence measurements (see Methods) between representative channels in L4, L2/3 and L5/6, in which the two non-granular channels were equidistant to L4. In the example of Figure 3A (left panel) coherence was strong between L4 and the other two layers along most of the frequency spectrum, but was consistently larger between L4 and L2/3. Coherence between supra and infragranular layers was considerably smaller throughout the spectrum, but in all three cases coherence increased in the gamma band (20-50 Hz) and it was highest for L4 and L2/3 (Fig. 3A, left panel). We quantified coherence at the gamma frequency band for the population by averaging the coherence values for frequencies from 20 - 50 Hz across the population. The coherence of L4 and L2/3 between 20- 50 Hz (0.83±0.1) was greater than the coherence of L4 and L5/6 (0.64±0.17, $p< 0.0001$).

Coherence between L2/3 and L5/6 (0.46±0.23) was lower than both of the other pairs. The coherence analysis for the spontaneous gamma oscillations produced the same results as the stimulus-driven. Thus, our results show a large degree of broadband spectral coherence within the cortical column with a strong functional coupling between L4 and L2/3. More importantly, our results show that coherence is enhanced in the gamma frequency band both for spontaneous and stimulus-driven gamma. The similar coherence values between spontaneous and visually-driven oscillations suggest that, despite the differences in laminar distribution and frequency band, the phase relations across the cortical depth are equally stable over a wide spectral band.

Coherence analysis quantifies the stability of the phase relationships between waveforms but does not provide a measure of the phase value. To quantify the phase (in ms) of gamma oscillations between layers, we averaged the gamma oscillations in all channels around the threshold-detected positive gamma cycles from one chosen electrode in L4. As illustrated by the example of Figure 3B, these wave triggered averages (WTA) centered on L4 showed a positive phase shift in supragranular layers progressively increasing towards the pia, and a negative phase shift that progressively decreased towards the white matter. To obtain a population measure of phase shift we measured the delay of the central peak with respect to L4 from the same two representative channels (L2/3 and L5/6) as for the coherence analysis (Fig. 3C). We measured the phase shift both for stimulus driven as well as spontaneous gamma. The example in Figure 3C of stimulus-driven gamma showed a L4-L5/6 negative delay of -2.58 ms and a L4-L2/3 positive delay of 2.76 ms. Population averages reveal a positive delay in L2/3 during

visually-driven gamma (2.7 ± 1.7 ms) and that is significantly larger than the positive delay during spontaneous gamma (1.9 ± 1.6 ms; p = 0.029). The average phase between L4 and L5/6, in contrast, showed a negative delay (visually-driven= -2.2 ± 1,5 ms; spontaneous = -1.95 ± 1.8 ms). In addition, the WTA analysis showed a much larger central peak for L2/3 than L5/6, emphasizing the functional coupling of the superficial layers. Thus, the large coherence values and the small phase shifts of the gamma positive peaks between layers assures effective interactions in the gamma band along the vertical axis of the cortical column. In addition, sensory-driven gamma oscillations have a better defined spatial and temporal structure than spontaneous oscillations.

Single units entrain to gamma differently through the cortical layers.

In order to determine if the laminar structure of the LFP oscillations is reflected in the spike output of V1, we recorded single units and LFPs throughout V1 using independently movable tetrodes (n=215 units). Single units in the mouse primary visual cortex respond robustly to full screen drifting gratings (mean firing rate to visual stimulation = 2.17 ± 3.2 Hz; baseline firing rate = 0.479 ± 1.07; n= 176 cells). However, since response firing rates rarely reach firing rates in the gamma range, responsive cells typically fire only once every several gamma cycles. An example of a cell responding to various orientations of a full screen drifting grating is illustrated by the rastergram in Fig. 4A. The spike response of this example cell was robust as shown by the peristimulus histogram (PSTH) at the bottom, and it faithfully followed the evoked potential recorded in the LFP from the same electrode (superimposed trace on Fig. 4A, polarity inverted for

clarity). However, despite the strong responses and the presence of gamma oscillations in the LFP no gamma frequency activity was visible in the PSTH. Therefore, to quantify the rhythmicity of cells with low firing rates, we generated perievent histograms (PEH) which are spike time histograms around the threshold-detected positive gamma peaks in the LFP (Fig. 4B). From the PEHs we calculated a rhythmicity index (RI, see methods) as the average distance between trough and peak of the first 3 peaks of the PEH (Popescu et al., 2009). We set a criteria for significance at 95% over the level of the shuffled PEH (Fig. 4C, significance level) and found that 38% of single units showed a significant entrainment to stimulus driven gamma-frequency fluctuations in the LFP (mean RI 0.99±0.6) but only 15% to the spontaneous gamma oscillations (mean RI 0.742±0.4) (Fig. 4C). For example, the PEH of the cell in Fig. 4B (green histogram, RI = 2.59) showed a strong entrainment to the visually-driven gamma oscillations, which were very robust as shown by its WTA (Fig. 4B, green line, vertical dotted line indicates the zero time of the gamma peaks). The same cell showed a much smaller entrainment to the spontaneous gamma oscillations (blue histogram, RI = 1.03) which in this example also produced a less robust WTA (Fig. 4B, blue line). Variations in the degree of entrainment of the spikes to the LFP could be a trivial result of variations in the magnitude of the gamma oscillations. However, the entrainment of a given cell could not be predicted by overall magnitude of gamma activity in the LFP rhythm or to the rhythmicity index of other cells in very close spatial proximity (Fig. 4D). In contrast, cell rhythmicity was dependent on the laminar position of the cell during visually driven gamma (Fig. 4E). The mean RIs were highest in L2/3 (1±0.6, p=0.025) and L5/6 (1.18±0.6, p=0.0039)

compared to L4 (0.78 ± 0.3). During spontaneous gamma, there were no significant differences in RI throughout the cortical depth (Fig. 4D, left panel). Similar results were obtained when examining the percent of rhythmic cells in each layer. During stimulus-driven gamma L2/3 and L5/6 had a greater percentage of rhythmic cells (38% and 58.5%, respectively) than L4 (20.9%). During spontaneous gamma, the differences were much smaller, although L4 still had the smallest percent of rhythmic cells (9.3% compared to 17.1% in L2/3 and 26.8% in L5/6; Fig 4D, right panel). Thus, both in terms of mean RI and percent rhythmic cells, neurons in L2/3 and L5/6 showed enhanced rhythmicity compared to L4 during stimulus-driven, but not spontaneous, gamma oscillations.

RS and FS cells networks entrain differently during spontaneous and stimulus-driven gamma.

In cortex, gamma oscillations rely strongly on excitatory and inhibitory network interactions. To determine the potential influence of excitatory and inhibitory cells on rhythmogenesis throughout the cortex, we classified all 215 units as putative excitatory (regular spiking, RS) or putative inhibitory (fast spiking, FS) cells on the basis of the shape of their waveform (Fig. 5A) (n= 195 RS, 20 FS) (Niell and Stryker, 2008). Unlike what has been observed in other species (Bruno and Simons, 2002), FS and RS both show high variability in firing rates and very similar mean rates during visual stimulation (FS = 2.65±2.8 Hz ; RS=2.13±3.3 Hz). However, the average rhythmicity of FS cells was much more pronounced than that of RS cells (FS = 1.42±0.7; RS = 0.95±0.5, p=0.002) and a higher percentage of FS cells were rhythmic compared to RS cells (FS = 75 %, RS

= 35%; Fig. 5B). Both FS and RS cells showed laminar structure in their rhythmicity during stimulus-driven gamma oscillations. FS cells showed no differences in average rhythmicity between L2/3 (1.12±0.6) and L4 (1.16±0.6), but rhythmicity in L5/6 was significantly greater than both of the superficial layers (2.03±0.67, p=0.02, p=0.022; Fig 5C). Similarly, the percent of rhythmic FS cells in L5/6 (100%) was higher than L2/3 (66.7%) or L4 (60%; Fig 5E). The laminar profile of the rhythmicity of RS cells during stimulus-driven gamma was distinct from that of FS cells (Fig. 5D). RS cells had significantly higher rhythmicity in L2/3 (1±0.6, p = 0.006) and L5/6 (1.06±0.46, p=0.0006) than L4 (0.73±0.25), and showed a similar pattern in the percent of rhythmic cells across layers (L2/3 = 36%; L5/6 = 52.8%; L4 = 15.8%; Fig 5F).

During spontaneous gamma, the mean RI decreased in both cell classes and across all layers However, FS cells maintained their laminar structure during spontaneous gamma, with L5/6 cells showing significantly greater rhythmicity than cells in more superficial layers (L5/6 = 1.24±0.47; L4 = 0.75±0.7, p=0.038; L2/3 = 0.82±.042, p= 0.033) (Fig. 5C). In contrast, despite the significant entrainment of cells throughout the cortex, RS cells did not show laminar specificity during spontaneous gamma (L2/3 = 0.76±0.5; L4 = 0.66±0.27; L5/6 = 0.71±0.34) (Fig 5D). The percentage of rhythmic cells followed the same trends as the mean RI for both FS and RS cells during spontaneous gamma (Fig 5E,F). Taken together, these results imply that the RS cells in L2/3 and L5/6 are specifically engaged during stimulus driven gamma activity and that both spontaneous and stimulus gamma engage more powerfully FS cells in the deep layers.

Stimulus driven, but not spontaneous, gamma frequency activity depends on GABAergic transmission between RS cells.

Anatomical and electrophysiological studies of cortical circuits have found a strong efferent drive from L2/3 to L5/6 (Thomson et al., 2002; Binzegger et al., 2009). We hypothesized that the increase in gamma frequency activity in the LFP and single units of L2/3 during stimulus gamma might be driving the increased rhythmicity seen in FS and RS cells in L5/6. To test this hypothesis, we specifically reduced gamma frequency activity in the superficial layers through the application of a weak concentration of picrotoxin (0.75 μM, 75 μL) topically to the surface of the cortex and presented drifting gratings over the course of 20-30 minutes. Within 5 – 10 minutes, the picrotoxin had noticeably increased the size of the evoked response of the LFP throughout all cortical layers (Fig.6A) and selectively reduced the magnitude of stimulus-driven gamma activity in L2/3 (Fig. 6B). The reduction of the GABAA dependant transmission also reduced the percent of rhythmic cells in L2/3 (50% reduction) and L5/6 (15%) (Fig 6C). FS and RS cells were identified on the basis of their waveform shape (n= 30 RS, 7 FS). In L2/3, the number of rhythmic cells was reduced for both FS cells (33% reduction, n = 3) and RS cells (100% reduction, n = 9). In L5/6, the percent of RS cells with significant rhythmicity was reduced (88% reduction, n=18), but the number of rhythmic FS cells in L5/6 was unchanged (n=3).

These results indicate that networks of FS and RS cells in L2/3 generate gamma oscillations driven by sensory stimulation through a mechanism that is dependent on GABAergic transmission. This network activity underlying gamma generation in L2/3

during visual stimulation contributes to the rhythmicity of RS, but not FS cells in L5/6. This result suggests a mechanism for L5/6 RS cell entrainment based either on the location of their apical dendrites in L2/3 or to excitatory vertical connectivity, and shows that networks of FS cells in L5/6 are capable of generating gamma oscillations independently of their RS neighbors and of afferent drive from L2/3. Furthermore, the magnitude of stimulus driven gamma in L5/6 is unchanged following the application of picrotoxin, suggesting that L5/6 stimulus driven gamma at a population level does not depend on activity in L2/3 or RS cell entrainment in L5/6, and is consistent with the hypothesis that FS cells are the primary drivers of gamma frequency activity in L5/6.

Figure 1

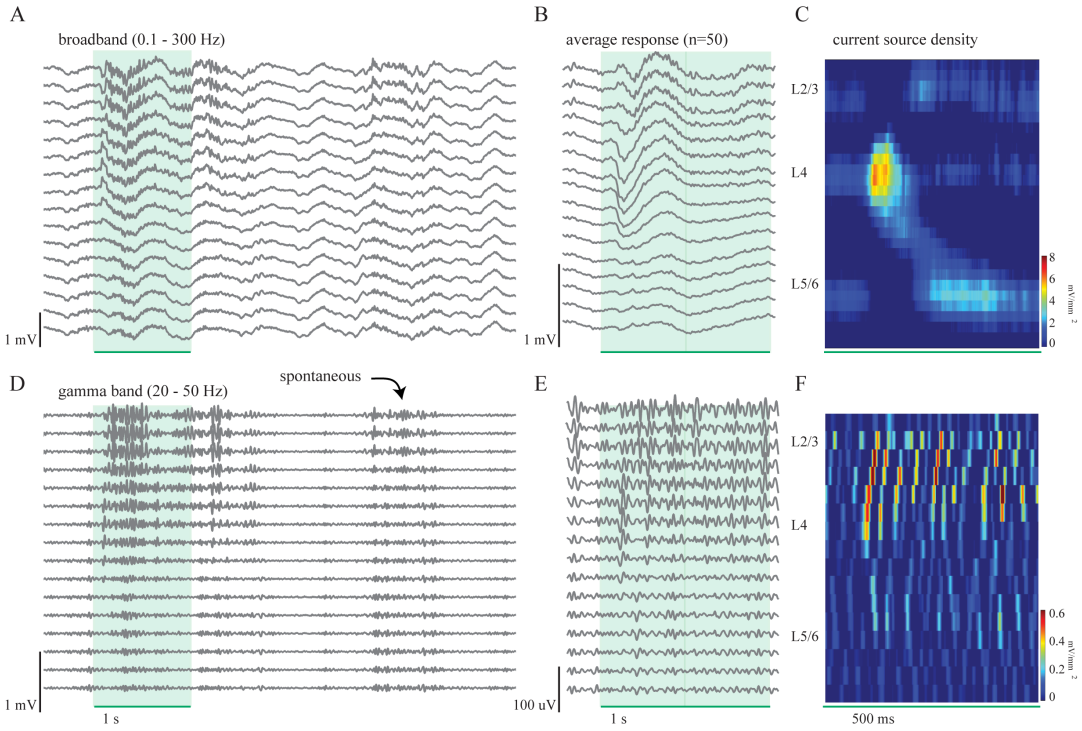
A
broadband (0.1 - 300 Hz)
1 mV
B
average response (n=50)
1 mV
C
current source density
L2/3
L4
L5/6
8
6
4
2
0
D
gamma band (20 - 50 Hz)
spontaneous
1 mV
1 s
E
100 uV
1 s
F
L2/3
L4
L5/6
0.6
0.4
0.2
0
500 ms

Figure 1. Local field potential activity during the presentation of a drifting grating. (A) Sixteen LFPs, filtered 0.1 – 300 Hz, showing the evoked response to a single presentation of a full screen vertical drifting grating (95% contrast, 3 Hz, 0.08 cycles/degree) for 1 second, as indicated by the green rectangle. An evoked response and corresponding fast frequency activity following stimulus onset are clearly visible during this single trial.

(B) Average evoked response for 50 presentations of the drifting grating. The onset of the evoked response occurs 90 ms following stimulus onset, and the largest evoked response occurs within layer 4.

(C) Current source density analysis of the average response in (B) shows a large initial sink in L4 at 90 ms, followed by sinks in L2/3 (182 ms) and L5/6 (201 ms).

(D) Same data as presented in (A) but filtered for the gamma frequency range, 20 to 50 Hz. A stimulus-driven increase in gamma activity occurs during the presentation of the drifting grating, and a spontaneous bout of gamma activity occurs several seconds later.

(E) Average evoked gamma activity for 50 presentations of the stimulus. Because gamma activity is not time-locked to stimulus onset, these averages only represent a small portion of the total gamma activity, as reflected by the smaller amplitude of the averages compared to the single trial activity in (D).

(F) Current source density analysis of the average evoked gamma. Unlike the CSD analysis of the broadband LFP (panel C), there is not one initial sink in L4 followed by distinct sinks in the other layers, but instead multiple distributed sinks and sources over space and time.

Figure 2

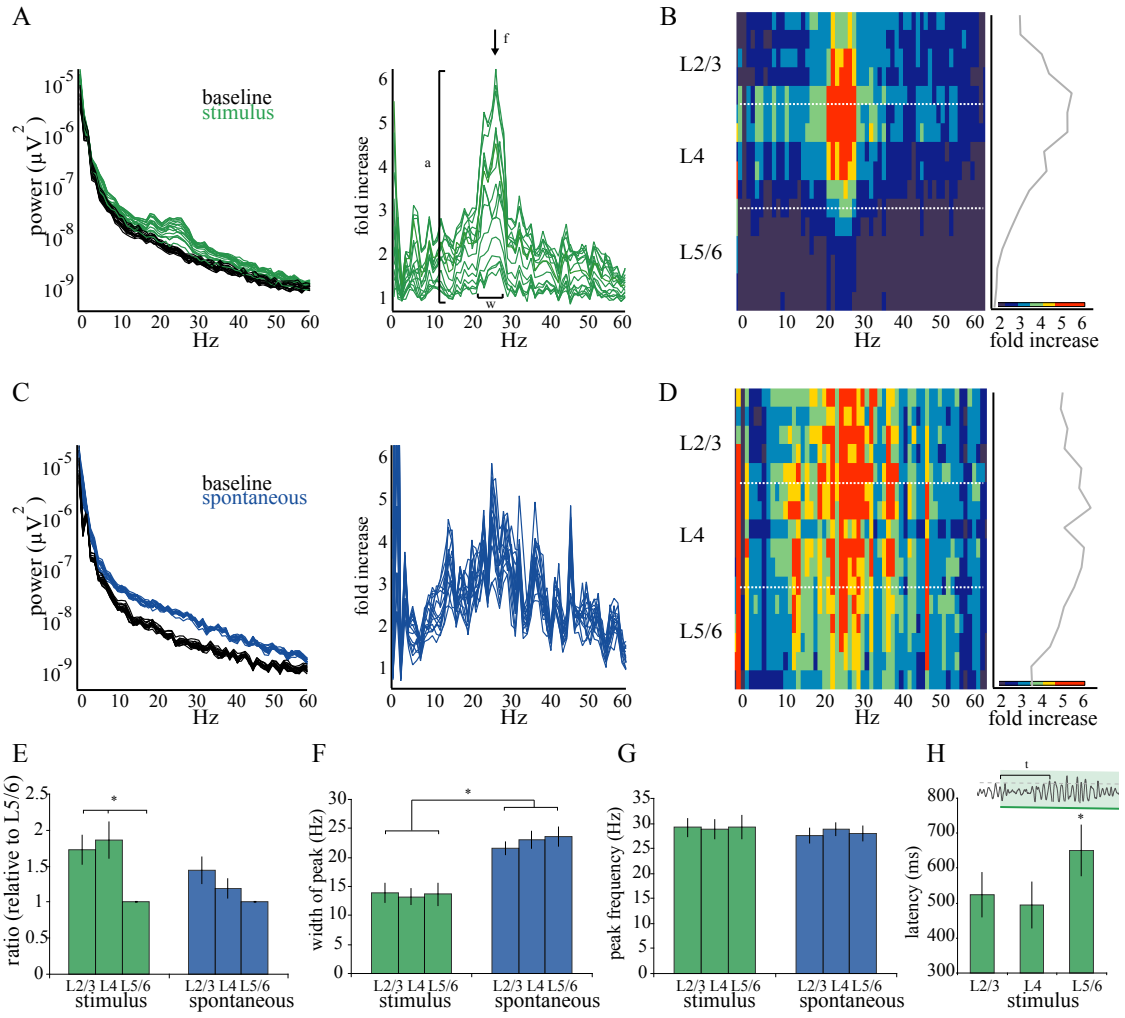
A
baseline
stimulus
power (μV²)
Hz
fold increase
f
a
w
B
L2/3
L4
L5/6
Hz
fold increase
C
baseline
spontaneous
power (μV²)
Hz
fold increase
D
L2/3
L4
L5/6
Hz
fold increase
E
ratio (relative to L5/6)
L2/3 L4 L5/6
stimulus
L2/3 L4 L5/6
spontaneous
F
width of peak (Hz)
L2/3 L4 L5/6
stimulus
L2/3 L4 L5/6
spontaneous
G
peak frequency (Hz)
L2/3 L4 L5/6
stimulus
L2/3 L4 L5/6
spontaneous
H
latency (ms)
t
L2/3
L4
L5/6
stimulus

Figure 2. Laminar characteristics of stimulus-driven and spontaneous gamma activity.

(A) Power spectra from each of the 16 channels for one experiment. Power spectra are calculated for the 1s window during the presentation of the stimulus (green) and for the baseline period 1 second immediately before the stimulus onset (black). Spectra are calculated for each single trial and then averaged across all trials. For each channel, the stimulus spectrum is divided by the baseline spectrum to reveal the frequencies with the greatest increase above baseline during the presentation of the stimulus.

(B) The values of the stimulus/baseline ratio (A, right hand graph) are plotted with respect to cortical depth. The fold increase over baseline is represented by pseudocolor, with red indicating the largest increase (~6 fold increase). Values for the frequency with the largest increase (26 ± 1 Hz, designated by arrow), are plotted with respect to depth to the right of the color plot. The width of the gamma peak is 11.3±1.8 Hz.

(C) Spontaneous bouts of gamma are identified manually and confirmed by threshold crossing (2.5 SD + mean). Power spectra are calculated in the same manner as in (A), for the 1 second window during the spontaneous bout (blue) and the 1 second baseline period immediately preceding each bout (black). The spectra during the spontaneous bout are then divided by the corresponding baseline spectra for each channel to reveal a ratio measurement.

(D) The ratio measurements calculated in (C) were plotted with respect to depth. The color scale indicated the increase over baseline and is the same as in (B). The maximum increase (~6 fold) occurs at frequency 25.2 ± 1 Hz, and the width of the gamma peak is 18.5 ± 1.4 Hz.

(E) The ratio measurements shown in (A) and (C) for stimulus and spontaneous gamma, respectively were quantified (stimulus n=18 probes, 13 animals; spontaneous n=9 probes, 7 animals). The increase over baseline was quantified as the maximum amplitude for each channel, demonstrated by "a" in panel (A). To compare between stimulus and spontaneous, these values were normalized to the value in L5/6. The increase in visually driven gamma was significantly higher in L2/3 (1.83 fold greater, p= 0.022) and L4 (1.86 fold greater, p= 0.012) than L5/6, only during stimulus driven gamma.

(F) The width of the gamma peak includes those frequencies in which the ratio measurement is greater than baseline, demonstrated by "w" in panel (A). The width of the gamma peak was similar throughout the layers of cortex, but encompassed a wider range of frequencies during spontaneous gamma (23.2 ± 1.9 Hz) than stimulus (13.4 ± 2.7 Hz, p=0.02).

(G) Peak frequency was designated as the frequency with the largest increase over baseline, demonstrated by "f" in panel (A). Peak frequency was constant through the layers of cortex and was the same during stimulus-driven (29.5 ± 3.4 Hz) and spontaneous (29.1 ± 1.8 Hz) bouts of gamma.

(H) The latency to the first bout of gamma was only calculated for stimulus-driven gamma, due to the lack of a consistent onset time for spontaneous gamma. Latency was determined by finding the first gamma peak to cross the significance threshold following the onset of the stimulus. The population average showed no difference in onset latency between L2/3 (524 ± 246 ms) and L4 (495 ± 252 ms), but the latency in L5/6 was significantly longer than in L4 (652 ± 279 ms, p = 0.04).

Figure 3

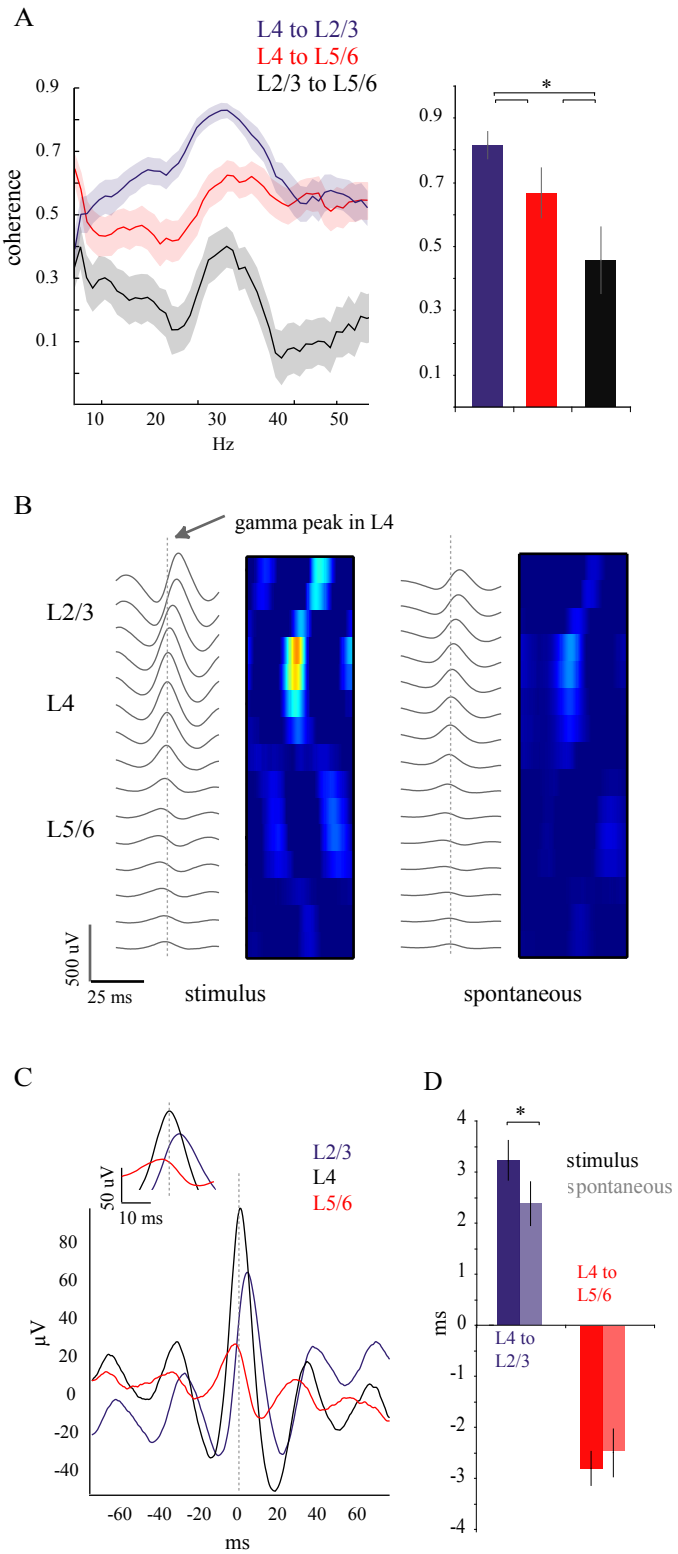
A
L4 to L2/3
L4 to L5/6
L2/3 to L5/6
coherence
0.9
0.7
0.5
0.3
0.1
10
20
30
40
50
Hz
*
B
gamma peak in L4
L2/3
L4
L5/6
500 uV
25 ms
stimulus
spontaneous
C
L2/3
L4
L5/6
50 uV
10 ms
μV
80
60
40
20
0
-20
-40
-60
-40
-20
0
20
40
60
ms
D
*
stimulus
spontaneous
L4 to
L5/6
L4 to
L2/3
ms
4
3
2
1
0
-1
-2
-3
-4

Figure 3. Coherence and phase measurements between cortical laminae.

(A) Coherence ± jackknife error measurements for 50 trials of drifting grating presentation. The coherence of L4 and L2/3 between 20- 50 Hz (0.83±0.1) was greater than the coherence of L4 and L5/6 (0.64±0.17, $p < 0.0001$). Coherence between L2/3 and L5/6 was lower than both of the other pairs (0.46±0.23). These differences were significant over the population (right panel, N=5 animals), and were similar between stimulus-driven and spontaneous gamma (not shown).

(B) Wave-triggered averages (WTAs) using the peaks of gamma oscillations in L4 as timestamps shows a distinct phase relationship through the cortical depth. The peak of each gamma cycle occurs first in L5/6, followed by L4 and then L2/3. The phase relationship is seen even more clearly in the CSD plot to the right of the WTAs. Similar phase shifts are seen in both stimulus-driven (left panel) and spontaneous (right panel) gamma activity.

(C) Detailed view of the WTA averages seen in (B) for channels from each lamina.

(D) Quantification of the phase relationships shown in (B) and (C) for the population shows a larger phase precession through the layers during stimulus-driven gamma than spontaneous (N = 5 animals). The positive delay between L2/3 and L4 is larger for visually-driven (2.7 ± 1.7 ms) than for spontaneous (1.9 ± 1.6 ms; $p = 0.029$) gamma. The average phase between L4 and L5/6, in contrast, showed a negative delay (visually-driven= -2.2 ± 1.5 ms; spontaneous = -1.95 ± 1.8 ms).

Figure 4

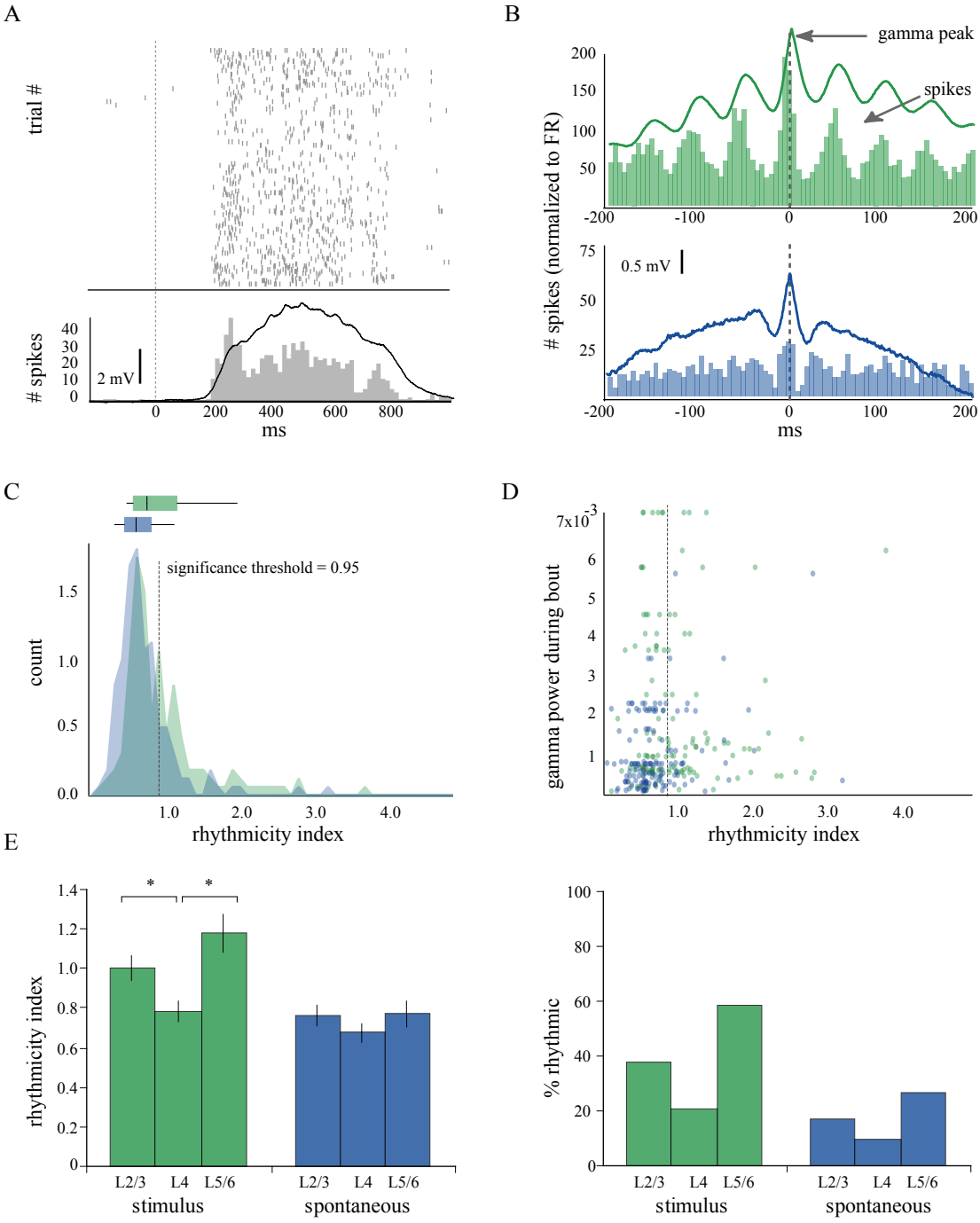
A
trial #
spikes
2 mV
ms
B
gamma peak
spikes
spikes (normalized to FR)
0.5 mV
ms
C
significance threshold = 0.95
count
rhythmicity index
D
gamma power during bout
rhythmicity index
E
rhythmicity index
stimulus
spontaneous
% rhythmic
L2/3
L4
L5/6

Figure 4. Single units are modulated by gamma oscillations differently through the cortex.

(A) Raster and PSTH from an RS cells in L2/3 during the presentation of a drifting grating. The evoked response in the LFP (inverted polarity) follows a similar time course to the PSTH of the unit.

(B) Peri-event histograms for stimulus-driven (green) and spontaneous (blue) spiking events. The positive peaks of gamma oscillations that crossed the significance threshold (2.5 SD above mean) served as timestamps.

(C) Distribution of rhythmicity indices (RIs) for 176 cells during stimulus-driven (green) and spontaneous (blue) gamma. RI for one third (38%) of the neurons were greater than the significance threshold during stimulus-driven gamma (mean RI 0.99±0.6), and RI for 15% of the neurons crossed threshold during spontaneous gamma (mean RI 0.742±0.4). Box and whisker plots demonstrate the median and quartile values for each condition (stimulus median = 0.79, lower quartile = 0.62, upper quartile = 1.16; spontaneous median = 0.66, lower quartile = 0.51, upper quartile = 0.84).

(D) The RI did not correlate with the magnitude of gamma oscillations in the LFP from the same tetrode for either spontaneous or stimulus-driven gamma.

(E) Distinct laminar differences in rhythmicity were observed during stimulus, but not spontaneous gamma. Neurons in both L2/3 (1±0.6, p=0.025) and L5/6 (1.18±0.6, p=0.0039) had significantly higher mean RI than L4 neurons (0.78 ± 0.3) (left panel). During spontaneous gamma there were no difference between the mean RIs for each layer (L2/3 = 0.76±0.45; L4 = 0.67±0.33; L5/6 = 0.77± 0.4). Similarly, a greater percent

of neurons in L2/3(38%) and L5/6 (58.5%) were rhythmic compared to L4 (20.9%) during stimulus-driven gamma (right panel). There was a similar trend during spontaneous gamma, but the differences between layers were smaller than during stimulus-driven gamma (L2/3 = 17.1%; L4 = 9.3%; L5/6 = 26.8%).

Figure 5

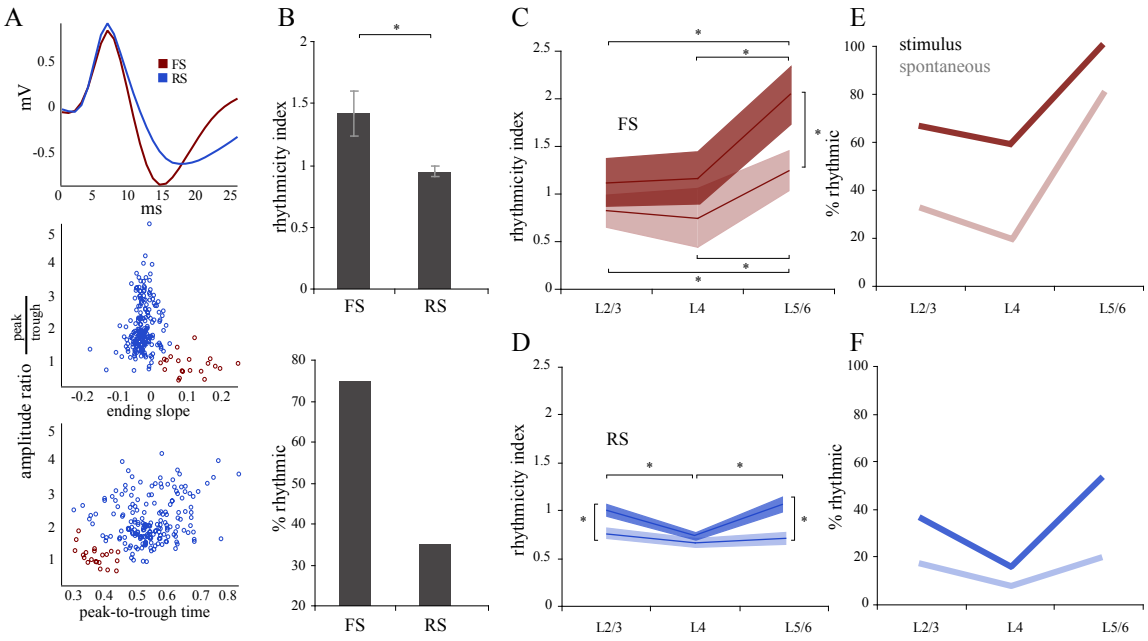
A
B
C
E
D
F
mV
ms
FS
RS
amplitude ratio
peak / trough
ending slope
peak-to-trough time
rhythmicity index
% rhythmic
FS
RS
L2/3
L4
L5/6
stimulus
spontaneous

Figure 5. FS and RS classification and modulation through the cortex.

(A) FS and RS cells were well separated on the basis of their peak/trough amplitude ratio, peak-to-trough time and ending slope of the trough.

(B) FS cells showed significantly greater rhythmicity than RS cells both in terms of the mean RI (FS 1.42±0.7; RS 0.95±0.5, p=0.002), and the percent of rhythmic cells (75% FS, 35% RS).

(C) FS cells have a laminar structure to their rhythmicity during both stimulus-driven and spontaneous gamma. During stimulus-driven gamma (dark lines) FS cells in L5/6 are more rhythmic (2.03±0.7) than those in L4 (1.16±0.6, p=0.022) or L2/3 (1.12±0.6; p= 0.02). FS cells have a similar laminar profile during spontaneous gamma (light lines) (L5/6 1.24±0.7; L4 0.75±0.7, p=0.038; L2/3 0.82±.042, p= 0.033). The rhythmicity in L5/6 is greater during stimulus-driven than spontaneous gamma activity (p=0.0217).

(D) RS cells in L2/3 (0.998±0.6) and L5/6 (1.06±0.46) showed greater rhythmicity than cells in L4 (0.734±0.25, p<0.0001). During spontaneous gamma, RS cells showed no distinct changes in rhythmicity through the depth of the cortex (L2/3 0.76±0.5, L4 0.66±0.27, L5/6 0.71±0.34). RS cell rhythmicity in both L2/3 and L5/6 is greater during stimulus-driven than spontaneous gamma activity (p<0.0001).

(E) Similar to the mean RI shown in (C), more FS cells are rhythmic in L5/6 (100%) than in L2/3 (66.7%) or L4 (60%) during stimulus-driven gamma. This same relationship holds true for spontaneous gamma (L5/6 = 80%; L2/3 = 33.3%; L4 = 20%).

(F) Like the data presented in (D), more RS cells are rhythmic in L2/3 (36%) and L5/6 (52.8%) than in L4 (15.8%), during stimulus-driven gamma. During spontaneous gamma,

there is a trend in the same direction, but the differences between layers are much smaller (L2/3 = 17%; L4 = 7.9%; L5/6 = 19.4%).

Figure 6

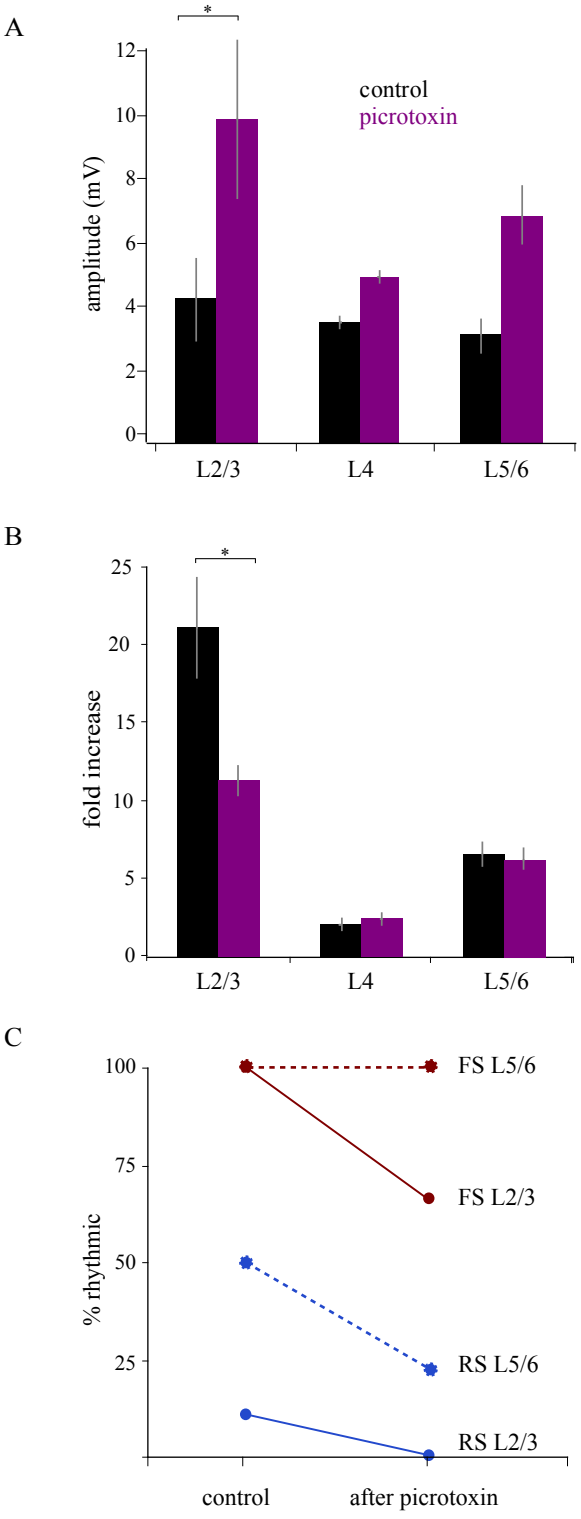
A
*
12
10
8
6
4
2
0
amplitude (mV)
control
picrotoxin
L2/3
L4
L5/6
B
*
25
20
15
10
5
0
fold increase
L2/3
L4
L5/6
C
100
75
50
25
% rhythmic
FS L5/6
FS L2/3
RS L5/6
RS L2/3
control
after picrotoxin

Figure 6. Gamma activity is reduced following the application of picrotoxin.

(A) The GABAA antagonist, picrotoxin, increases the amplitude of the evoked response in the LFP during the presentation of the drifting grating through all layers of cortex, with the largest increase in L2/3 ($n = 3$ animals, $p = 0.0215$).

(B) Picrotoxin reduces the gamma power (20-50 Hz) during the presentation of the visual stimulus in L2/3 ($p = 0.0313$).

(C) The percent of rhythmic RS cells ($n=30$) in both L2/3 and L5/6 decreases following the application of picrotoxin (100% and 88% decrease). The percent of rhythmic FS cells ($n=7$) falls in L2/3 (33% decrease) but not in L5/6 (0% decrease).

Discussion

Our goal was to compare the laminar structure and the single unit entrainment during stimulus-driven and spontaneous gamma frequency activity in the primary visual cortex of the mouse. This study was motivated by the apparent paradox between the relevance of gamma oscillations for information processing and the abundance of gamma oscillations in local field potentials and units during on-going background activity in wake, sleep and anesthesia. Our results indicate that stimulus-driven and spontaneous gamma oscillations have distinct spatiotemporal profiles and engage excitatory and inhibitory networks differently through the cortical depth. Indeed, not only does stimulus-driven gamma activity preferentially occur in the superficial layers, but it specifically entrains networks of excitatory cells in the superficial layers that contribute to the rhythmic activity of excitatory cells in L5/6. This work implies that spontaneous and stimulus-driven gamma are not functionally equivalent and is consistent with the hypothesis that stimulus-driven gamma is relevant for information processing.

Gamma oscillations are ubiquitous during sensory processing and stimulus-driven activity

Over the last several decades, many studies have provided evidence that gamma oscillations in neocortex are relevant to information representation. Initial work demonstrated increased synchrony in gamma frequency activity in single units in the primary visual cortex (Gray et al., 1989; Gray and Singer, 1989). Later studies revealed that the gamma component of local field potentials in V1 is directly modulated by

stimulus characteristics (Frien et al., 2000; Henrie and Shapley, 2005). Work in humans showed that gamma oscillations are modulated by perceptual processes, such as the interpretation of Gestalt stimuli (Keil et al., 1999; Tallon-Baudry and Bertrand, 1999), and are structured differently in patients with psychiatric disorders such as schizophrenia (Kwon et al., 1999; Spencer et al., 2004). Furthermore, results from magnetoencephalography (MEG) have shown that gamma oscillations display a specific spatiotemporal organization over the entire human cortex and which are reset by sensory stimuli (Ribary et al., 1999).

However, gamma frequency activity is present not only during information processing related activity, but also occurs as part of the background activity of the brain during the depolarization phases of anesthesia and slow wave oscillations, REM sleep, brain activation by stimulation of neuromodulatory systems of the brainstem and in the waking state not in association with motor or sensory activity (Steriade et al., 1996b); reviewed in (Steriade, 2006). Thus, from the point of view of single cells the common principle underlying the appearance of gamma oscillations is the presence of tonic depolarization.

Since gamma oscillations are generated and distributed by networks of cortical neurons and their spatiotemporal profiles correlate dynamically with the information processing task, it is of great relevance to determine if stimulus-driven and spontaneous gamma activity share the same spatiotemporal characteristics or recruit the same neural networks. Differences between stimulus-driven and spontaneous gamma activity would

suggest that the mechanisms by which gamma activity is produced and likewise, its functional role, depend on the context in which it generated.

Spatiotemporal structure of gamma oscillations during sensory processing

While there are few studies that directly compare the structure of gamma oscillations in different functional or behavioral contexts, a number of studies have described the structure of spontaneous gamma activity. It was shown that spontaneous gamma oscillations have limited spatial synchrony in the cortex of awake cats (Steriade et al., 1996a) and rats (Sirota et al., 2008), and show multiple distributed current sinks and sources through the depth of the cortex (Steriade and Amzica, 1996). The study by Steriade and Amzica (1996) reported for the first time that gamma oscillations occur in tight phase relations across the depth of the cortex and single cell firing was tightly locked to the oscillations, indicative of local generation rather than volume conduction. That LFPs are indeed local in nature has been recently quantified in cat primary visual cortex (Katzner et al., 2009). We have found a similar tight relation between cell firing and LFPs as quantified by peri-event histograms centered on the peaks of gamma oscillations in the LFP, which showed that the entrainment of single units during spontaneous gamma was uniform throughout the cortex. Furthermore, in our study we quantified the phase shift across layers and found a systematic positive shift from L4 to L2/3 of 2.76 ms and a systematic negative phase shift from L4 to L5/6 of -2.58 ms. Thus, gamma oscillations occur with very small (<6ms) shifts of their positive peaks across the

cortical depth which allows effective communication between layers of gamma frequency spikes.

The study by Amzica and Steriade also showed a homogenous distribution of amplitudes across the depth of the cortex both for spontaneous gamma and that induced by stimulation of brainstem cholinergic systems, an arrangement similar to our CSD analysis of spontaneous gamma. Brainstem cholinergic systems depolarize thalamic non-specific nuclei, which in turn globally activate the neocortex through glutamatergic transmission (Steriade, 2006). A study comparing spontaneous gamma oscillations with those evoked by stimulation of an intralaminar, non-specific thalamic nucleus showed a similar and homogenous distribution through the depth of the cortex (Sukov and Barth, 1998). The similarity between gamma oscillations due to activation of diffusely projecting thalamic nuclei and gamma occurring spontaneously is consistent with the hypothesis that non-specific thalamic inputs may be an important component of the background gamma activity that characterizes functional brain states (Llinas and Pare, 1997; Steriade, 2000; Jones, 2001) and which is altered in several pathological conditions (Llinas et al., 1999). Furthermore, it clearly distinguishes spontaneous gamma oscillations or with a non-specific thalamic contribution from those generated by specific sensory inputs as reported in this study, further supporting the idea of a physiological role of sensory-driven gamma. Finally, despite the differences in organization, our study showed the spontaneous and sensory driven gamma share a common mean frequency and spectral amplitude which is in agreement with a similar comparison made in the primary auditory cortex of the rat (Lakatos et al., 2005).

In vitro studies have suggested that there may be two independent gamma generating circuits in the cortex, one in the superficial layers and one in deep layers, because a cut in L4 does not reduce the power of pharmacologically induced gamma in either L2/3 or L5/6 (Roopun et al., 2006; van Aerde et al., 2009). Furthermore, in both in vitro studies, superficial layer gamma was dependent on chloride GABAergic transmission. The laminar functional architecture of sensory-driven gamma reported here depends on GABAergic transmission as well, since superficial application of picrotoxin abolished gamma activity in L2/3. Furthermore, picrotoxin did not reduce gamma activity in deep layers suggesting that in vivo as well there may be two related, but independent, sources of gamma generation, in the deep and superficial layers of cortex.

Our results show an increase in gamma oscillation magnitude in the superficial layers that occurs only during stimulus-driven gamma. Specific activation of L2/3 gamma oscillations during the processing of sensory stimuli is consistent with the known functional architecture of the cortex. Pyramidal cells in L2/3 have widespread horizontal connections that are known to be critical for cortico-cortical information processing. Our results are suggest that stimulus-driven, but not spontaneous gamma, may be important for coordinating widespread sensory processing.

Excitatory and inhibitory network contribution to gamma oscillations in cortex

A strong case has been made for the importance of the FS cell network, mediated by gap junctions, in the generation of cortical gamma oscillations. Inhibitory transmission is thought to carry a large portion of the gamma rhythm (Hasenstaub et al., 2005) and

rhythmic depolarization of FS cells produces gamma activity in the LFP and increases spike precision (Cardin et al., 2005). In addition, in vitro studies have shown the generation of cortical gamma to be abolished by the blockade of GABAA transmission (Traub et al., 2005; Roopun et al., 2006). However, a recent study has shown that depolarization of superficial RS cells also produces gamma activity in the LFP and drives the firing of RS cells in L5/6 (Adesnik and Scanziani, 2010), which is consistent with the known excitatory drive from L2/3 to L5/6 in sensory cortex (Thomson et al., 2002; Binzegger et al., 2009). Our work highlights the involvement of both putative excitatory and inhibitory networks in gamma rhythmogenesis, but shows a specific role for RS cells in L2/3 and L5/6 during stimulus-driven gamma. Furthermore, disruption of rhythmic activity in the superficial layers by the GABAA antagonist, picrotoxin, demonstrates that gamma activity in L2/3 contributes to the entrainment of RS cells in L5/6.

In contrast, putative inhibitory cells are more entrained to gamma activity than putative excitatory cells throughout the cortex, but show a smaller difference in their rhythmicity between stimulus and spontaneous conditions. FS cells in L5/6 show increased overall rhythmicity during stimulus-driven gamma, but this increase does not depend on gamma frequency activity in the superficial layers, as seen by the unchanged rhythmicity of L5/6 FS cells during the application of picrotoxin to the superficial layers. In addition, the magnitude of the gamma oscillations in the L5/6 LFP is also unchanged during the picrotoxin application, suggesting that L5/6 putative inhibitory cells are primarily entrained to the local LFP. The modulation of L5/6 FS cell by the L5/6 LFP is

independent of the magnitude of gamma in the superficial layers and is relatively insensitive to the context during which the gamma is generated.

Taken together, these findings show clear differences in the laminar structure of gamma frequency activity in both the LFP and single units between stimulus-driven and spontaneous gamma, suggesting that gamma activity that occurs in the presence and absence of stimuli is not functionally equivalent. Instead, the context in which gamma occurs determines the networks that are involved and the balance of excitatory and inhibitory contribution throughout the laminae. These findings are consistent with the hypothesis that gamma frequency activity is relevant to the processing of information in the cortex.

Chapter 2: The modulation of gamma frequency oscillations by stimulus characteristics in the mouse primary visual cortex.

Abstract

Our goal was to determine the modulation of gamma frequency activity by stimulus characteristics in the local field potential (LFP) and single units of the primary visual cortex (V1) of the mouse. Previous studies in animals with orientation columns have shown that gamma activity depends on stimulus intensity and is selective for stimulus orientation. Visual stimulation produces robust gamma frequency activity in the mouse visual cortex, but because the mouse lacks feature maps in V1, it was not known whether gamma was modulated by the characteristics of the stimulus. Our results indicate that the broadband and gamma component of the LFP are modulated by stimulus contrast but not by stimulus orientation. In contrast, the entrainment of single units to gamma frequency activity in the LFP depends both on the intensity and orientation of the stimulus. Both the number of cells that fire rhythmically and the amount of rhythmicity for each cell varies with stimulus characteristics. This work implies that while the entrainment of single neurons is sensitive to many aspects of the stimulus, population measures depend only on stimulus intensity.

Introduction

Information representation in cortex is based on specific spatiotemporal patterns of activation of populations of neurons. The activation patterns are a consequence of synaptic inputs generated by sensory stimuli, spontaneous background activity, the state of neuromodulation, the intrinsic electrophysiological properties of neurons and the anatomical network in which neurons are embedded. As a result of these factors, the average responses to changes in stimulus features lead to the definition of functional maps. However, maps are based on average depolarization and firing rate and, therefore, constitute a simple representation of the stimulus-locked, average response to a single stimulus parameter. Further, it is not known whether other parameters of neuronal activity may allow the distinction of new functional maps with perhaps very different functional meanings. One type of activity that appears in association with many forms of brain function and particularly in response to sensory stimulation is oscillatory activity in the gamma frequency band.

Several methods allow us to characterize and describe the activity of populations of neurons, from multiple single cells recordings to population recordings with electrophysiological and optical methods. The collective synaptic input to a local population can be measured extracellularly as local field potential (LFP), which represents electrical potential gradients in the extracellular space caused by synaptic activity driven currents.

Gamma oscillations recorded in the LFP or in the spike output of individual neurons have been proposed to play a role in information processing by providing a

common frequency to which groups of cells synchronize generating functionally meaningful neuronal ensembles (Singer and Gray, 1995). Under this assumption, changes in stimulus parameters may lead to changes in the rhythmicity of individual cells which in turn could be more meaningful for stimulus representation than changes in firing rate. Moreover, if stimulus representation is indeed associated with ensembles of rhythmic neurons, then the defining parameter of a stimulus feature would be the correlation structure of the population. More likely, firing rate and correlation in the gamma band represent different attributes of a stimulus or different levels of attributes, such as orientation and object continuity in the visual system for example.

In species such as the cat and the primate, neurons with similar stimulus selectivity are arranged in vertical columns through the depth of the cortex with a diameter of roughly 300-500 microns. Such columnar arrangement is due to convergence of specific populations of thalamic inputs and local vertical connectivity. Because of the similar selectivity of the neurons within a column the LFP associated with the sensory response shows similar stimulus selectivity. Interestingly, it has been shown in monkeys and cats that gamma oscillations are more selective to orientation than the LFP, which suggests that activity in the gamma band has a higher sensory discrimination power than the average neuronal responses (Gray and Singer, 1989; Frien et al., 2000; Berens et al., 2008).

In contrast, in the mouse visual cortex there is no evidence for such columnar arrangement (Drager, 1975; Ohki et al., 2005). Therefore, the expectation is not to find stimulus selectivity in the LFP average response but to see an increase in LFP amplitude

with increases in stimulus intensity, here represented by changes in contrast. However, it is still possible that ensembles of neurons may be synchronized through synaptic linkages specific to their response properties, or that biases in the population may lead to sharper tuning of gamma oscillations despite the lack of columns. Again, the formation of functional groups should be manifest in the correlation structure of the ensemble and become visible as selectivity in the gamma band activity recorded by the LFP.

Here we show a contrast dependent increase in power in the gamma frequency band that is that is higher in L2/3 and L4 than L5/6. The firing rate, the gamma rhythmicity (measured with respect to the LFP) and the percent of rhythmic cells at the gamma frequency also increased with contrast. However, while single cells were orientation selective, gamma oscillations or the LFP evoked-response was not selective to the orientation of the drifting gratings. Thus, our results show that in mouse gamma frequency band activity is generated by populations of cells homogeneously distributed in the cortical volume.

Methods

Surgery, electrophysiology, visual stimuli:

See Chapter 1.

Analysis:

See Chapter 1. For single unit analysis, varying sets of contrast values were used in different experiments. For the purpose of population quantification, the responses of single units to slightly different contrast values in different experiments were grouped. Responses of single units to contrasts 23-35% were grouped into the contrast group 28%; contrasts between 41 – 59% were grouped into the contrast group 50%; contrasts between 65 – 77% were grouped into the contrast group 73%. All units were presented with 5% and 95% contrast stimuli.

Orientation selectivity index (OSI) was calculated by taking the value at the preferred orientation minus the value at the orthogonal orientation, divided by the sum of the two.

Results

Our goal was to quantify the modulation of gamma oscillations (20-50 Hz) through the depth of the mouse primary visual cortex (V1) in response to changes in stimulus characteristics. Using full screen drifting sinusoidal gratings, we manipulated stimulus intensity by changing contrast and stimulus specificity by changing orientation. We recorded local field potentials (LFPs) using a multisite probe (Neuronexus, Ann Arbor, MI) with 16 evenly spaced recording sites (50 or 100 μm interelectrode distance) inserted normal to the cortical surface and spanning the cortical depth. We also recorded single cells from layers 2-6 using 5-7 independently movable tetrodes (Thomas Recordings, Giessen, Germany). Mice were anesthetized with a mix of isoflurane and xylazine in order to obtain a stable low amplitude spontaneous baseline pattern recorded in the LFPs. The visual responses described here were readily abolished or became highly variable when the anesthesia level induced slow oscillations in the background activity. We obtained recordings from 21 probes from 18 animals, from which we selected 18 probes from 13 animals for orientation analysis based on the stability and amplitude of visual responses and the absence of slow oscillations in the baseline. Among these, we further selected 5 probes from 4 animals for the analysis of contrast manipulations.

Stimulus intensity modulates gamma frequency activity in V1

To quantify visually-driven gamma oscillations as a function of stimulus contrast, we used drifting grating presentations lasting 1000 ms at 4 luminance contrasts (95%, 65%, 35% and 5%). Because gamma oscillations are not stimulus-locked but they appear

at different times during the visual response they are greatly reduced by averaging. Thus, we calculated power spectra from each single trial both during the 1 second window following the onset of the presentation of the drifting gratings and 1 second window immediately before stimulus onset (baseline). We then averaged the spectra from the visual response and baseline (Fig. 1A, left panel) and calculated the ratio between the two for all 16 channels and 4 contrasts (Fig. 1A, right panel). Thus, the ratio spectra quantify the fold increase in activity along the frequency axis in the visual response with respect to the activity immediately preceding stimulus onset. The ratio spectra for the L2/3 channel illustrated in Figure 1A show a maximal fold increase in power (8.4 fold) at 95% contrast, with smaller increases (2.8 fold) at 65% contrast and (1.4 fold) at 35%, and no change at 5%. Over the population, a stimulus with 95% contrast induced an increase of 5.03±0.39, for 65% an increase of 2.5±0.7, for 35% contrast an increase of 1.6±0.2 and for 5% an increase of 1.4±0.06.

In order to determine if contrast dependent changes in gamma power were uniform throughout the cortex, we plotted the average for all experiments of the mean fold increase of gamma at the peak frequency ± 5 Hz as a function of channel depth (Fig 1B). On average, for stimuli with high contrast the modulation was greatest in the superficial layers. To simplify the comparison over depth and across experiments, we averaged the responses of the channels located in the supragranular (L2/3), granular (L4) and infragranular (L5/6) laminae, as indicated by current source density (CSD) analysis (Fig 1C). Through the cortical depth, gamma power increased with stimulus contrast, but

at 95% contrast, L2/3 and L4 showed greater increase than L5/6 ($p= 0.04$; $p=0.005$). At 65% contrast, L4 showed greater increase than L5/6 ($p = 0.04$).

In order to determine if the modulation of the LFP oscillations by stimulus intensity was reflected in the spike output of V1, we recorded single units and LFPs throughout V1 using independently movable tetrodes. Only single units that responded robustly to full screen drifting gratings of 95% contrast were included in the analysis (n= 66 cells). To quantify the rhythmicity of single units, we generated perievent histograms (PEH) which are spike time histograms around the threshold-detected positive gamma peaks in the gamma-filtered LFP for each contrast. From the PEHs we calculated a rhythmicity index (RI, see methods) as the average distance between trough and peak of the first 3 peaks of the PEH, and used a bootstrapping technique to set a significance threshold of 95% over shuffled RIs (Popescu et al., 2009).

Both firing rate and rhythmicity increased with contrast for single units. For the L2/3 RS cell shown in Figure 2A, at the lowest contrast (5%), the cell fired at 1.4 Hz and had a RI of 0.72. At the highest contrast (95%), the firing rate increased to 7.3 Hz and the RI to 3.2. However, rhythmicity crossed the significance threshold at contrast levels 35%, 65% and 95%, so the cell was rhythmic for a majority of contrast values.

Over the population, both the firing rate and rhythmicity increased with contrast. Firing rate increased from 0.7±0.15 Hz at 5% contrast to 3.3±0.32 Hz at 95% contrast (Fig. 2B). Similarly, the rhythmicity of the single units increased from 0.59±0.04 to 1.23±0.08 (Fig. 2C, left), and the percent of rhythmic units increased from 9 to 51% (Fig. 2C, right), as the contrast increased from 5% to 95%. To more directly compare the

modulation of firing rate and rhythmicity by contrast, we normalized the average firing rate and rhythmicity values to the 95% contrast value (Fig 2D). We found that firing rate rises more rapidly with increasing contrast than rhythmicity. Thus, the rhythmicity of a cell is less modulated by contrast than is the firing rate. The average RI includes all cells, both rhythmic and non-rhythmic. Thus, there are two ways to increase the mean RI; by increasing the RI of each cell, or by increasing the number of cells with high RI scores. We tested between these two possibilities by plotting the percent rhythmic and the average rhythmicity of cells that were rhythmic for two or more contrasts. This allowed us to see if rhythmicity continues to increase with contrast even after significant rhythmicity has been reached. Only the percent of rhythmic cells was modulated by contrast, which implies that with contrast, more cells become entrained to the ongoing oscillation. Cells that are already entrained do not become more tightly entrained with contrast.

To determine the potential differences in modulation of excitatory and inhibitory cells by stimulus intensity, we classified all units as putative excitatory (regular spiking, RS) or putative inhibitory (fast spiking, FS) cells on the basis of the shape of their waveform (n= 56 RS, 10 FS) (Niell and Stryker, 2008). Unlike what has been observed in other species (Bruno and Simons, 2002), FS and RS both show high variability in firing rates and very similar mean rates over all levels of contrast (Fig. 2E). However, the average rhythmicity of FS cells was much more pronounced than that of RS cells at contrast levels greater than 28%. For instance, at 95% contrast FS cells had a greater RI (1.67±0.24) than RS (1.07±0.08; $p = 0.004$) and a larger percent of rhythmic cells (FS =

90%; RS = 45%; Fig 2F). However, at 5% contrast, FS and RS cells had comparable RIs and a similar percent of cells with rhythmic firing. Correspondingly, the difference in rhythmicity from 5% to 95% contrast seemed greater for FS cells (1.05±0.3) than RS cells (0.44±0.08), although this difference did not reach significance (Fig 2G). In addition, we measured the contrast threshold for rhythmicity, which is the contrast at which a cell that is rhythmic at 95% contrast no longer fires rhythmically (Fig 2H). FS cells have a substantially lower rhythmicity threshold than RS cells (FS = 61.4±11.6%; RS = 81.5±3.5%; $p = 0.006$; Fig. 2H), and thus begin to fire rhythmically at a lower contrast level. This is consistent with a greater rate of increase in rhythmicity with increasing contrast in FS cells compared to RS, and implies that FS cell rhythmicity is modulated more strongly by stimulus intensity than that of RS cells.

Components of the LFP are weakly selective for stimulus characteristics

Unlike many other mammals, the mouse primary visual cortex does not show a columnar organization based on orientation preference (Mangini and Pearlman, 1980; Wagor et al., 1980; Ohki et al., 2005; Niell and Stryker, 2008). Therefore, we did not expect to find strong orientation tuning of the population activity represented by the broadband LFP or gamma frequency component of the LFP. Figure 3A shows an example of the average evoked responses to 8 different orientations in three layers of cortex. The amplitude of these evoked responses is represented in Figure 3B as a tuning curve (left panel) and polar plot (right panel). The difference in amplitude between the most and least preferred orientation is typically very small. In this example, in L2/3 the

amplitude at the preferred orientation (315 º) is 0.19 mV, and the amplitude of the non-preferred orientation (180 º) is 0.12 mV. To quantify the stimulus selectivity for our population, we calculated an orientation selectivity index (OSI, see Methods) and averaged the OSI for channels corresponding to L2/3, L4 and L5/6 (Fig. 3G, white circles). The average OSI was similar through the depth of the cortex (L2/3 = 0.2±0.12; L4 = 0.18±0.14; L5/6 = 0.23±0.18), demonstrating that all layers of cortex have a similarly broad selectivity for orientation.

Although stimulus selectivity is low, orientation preference remains relatively constant through the cortical depth. In the example shown in Fig. 2A and B, the evoked response is largest in all layers when a grating of 315 º is presented. Over the population in general, the orientation preference shows only moderate variance from surface to depth. We calculated change in orientation preference as degrees difference from the preferred orientation of the most superficial channel (Fig 3C). On average, the preferred orientation changes 37±18 º over the cortical depth, with the smallest change predictably occurring at a depth of 100 µm (3±69 º) and the largest change occurring in deepest channel (68±86 º).

To quantify the orientation tuning of the gamma component in the LFP, we calculated the power spectrum from each single trial both during a 1 second window after stimulus onset and a 1 second window immediately before stimulus onset (baseline). We then averaged the response and baseline single trial spectra (Fig. 3D, top panel) and calculated the ratio between the two for each orientation (Fig. 3D, bottom panel). For the example shown in Figure 3D (bottom panel), the maximum ratio values, which occurred

at 26 Hz, ranged from 9.9 fold increase for the preferred orientation (180º) to 4.2 fold increase for the non-preferred orientation (45º). We plotted the ratio values as a two-dimensional plot of frequency vs. orientation, where color signifies the magnitude of the ratio (fold increase) of the stimulus over baseline (Fig. 3E). The frequency with the greatest increase over baseline, 26 Hz, showed a clear tuning for orientation with a preferred value of 180º (Fig. 3E, bottom panel). As described for the broadband LFP, we calculated the OSI of the gamma tuning curve. In this example, the OSI for this L2/3 channel was 0.15. For the population, the orientation selectivity is low through the cortical depths (Fig 2G, solid circles), and is somewhat, although not significantly, less than the LFP OSI (LFP:L2/3 = 0.2±0.03; L4 = 0.18±0.03; L5/6 = 0.22±0.04; gamma:L2/3 = 0.13±0.08; L4 = 0.12±0.07; L5/6 = 0.12±0.07).

The orientation preference of gamma frequency activity was relatively constant through the depth of the cortex, with an average change from the preferred orientation of the top channel of 9.8±18º. The values through the depth of the cortex ranged from 2.5±1.8º at a depth of 200 µm to a maximum of 39±2.4º at 350 µm.

In summary, although the selectivity of both the LFP and gamma frequency component were both low, the orientation preference of gamma was more consistent through the depth of the cortex. Interestingly, the preferred orientation of gamma frequency activity did not usually correspond to the preferred orientation of the LFP, as shown in Fig 2H.

Single unit rhythmicity is orientation selective

Single neurons in the mouse primary visual cortex are selective for orientation (Drager, 1975; Mangini and Pearlman, 1980; Niell and Stryker, 2008). In our population (n = 176 cells), the average selectivity (measured as the OSI) was much greater in L2/3 (0.49±0.03, n= 92) and L4 (0.43±0.04, n=43) than in L5/6 (0.26±0.03, n= 41, $p < 0.0001$; $p = 0.002$)(Fig. 4A). We set a threshold for selectivity of 0.5 and found that 46% of cells in L2/3, 35% of cells in L4 and 7% of cells in L5/6 were selective (Fig. 4B). For a subset of the population (n = 73), we then performed a rhythmicity calculation for the spiking response to each individual orientation and plotted the RI as a function of the degrees from the preferred orientation of the cell, as determined by the cell's firing rate (Fig. 4C). Cells showed higher rhythmicity at 0º and 180º from the cell's own preferred orientation, implying that the rhythmicity of the cell is somewhat for orientation, but not for direction.

We classified the units on the basis of their waveform as either fast-spiking (FS, n = 11) or regular-spiking (RS, n = 62). Both the average selectivity and firing rate of FS and RS cells were similar (FS:FR = 2.66±0.7, OSI = 0.35±0.06; RS:FR = 2.13±0.26, OSI = 0.43±0.02) (Fig. 4D). When we examined the rhythmicity for each orientation, FS cells fired rhythmically for 2±0.7 out of 8 orientations, while RS cells were rhythmic for <1 out of 8 orientations (0.77±0.18; $p = 0.006$; Fig. 4E). Similarly, FS cells have a higher RI at every orientation than RS cells (Fig. 4F). In addition, the rhythmicity of FS cells was significantly higher for the preferred orientation (0.95±0.4) than for the orthogonal (0.66±0.3; $p = 0.02$), while RS cell rhythmicity was greater for the opposite orientation (0.73±0.4) than for the orthogonal (0.6±0.3; $p = 0.009$). Thus, although the selectivity of

RS and FS cells was similar, the rhythmic behavior of FS cells showed higher stimulus selectivity than RS cells.

Figure 1

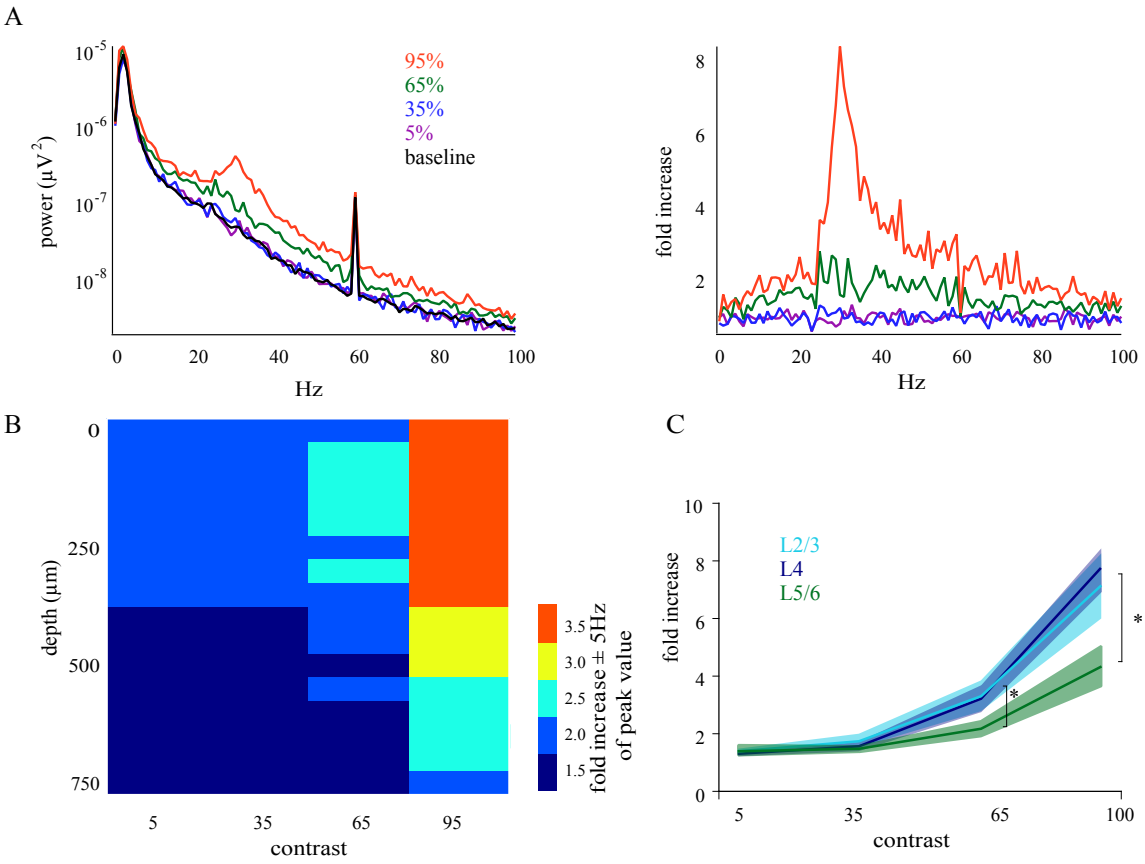
A
95%
65%
35%
5%
baseline
power (μV²)
Hz
fold increase
B
depth (μm)
contrast
fold increase ± 5Hz of peak value
C
L2/3
L4
L5/6
fold increase
contrast
*
*

Figure 1. Contrast modulates gamma oscillation power.

(A) Example of the change in induced gamma power at different level of contrasts in a L2/3 channel. Power spectra for four levels of contrast and baseline are shown in the left panel. Ratio of each power spectrum during the stimulus over the baseline power spectrum show in right panel.

(B) Average ratio value for peak value ±5 Hz for every channel through the depth of the cortex at 4 contrast levels (n= 5 probes, 4 animals).

(C) Population statistics of the maximum ratio value produced at four levels of contrast in L2/3, L4 and L5/6 (n= 5 probes, 4 animals). At 95% contrast, the ratio values for L2/3 (7.1±1.1; $p = 0.04$) and L4 (7.7±0.8; $p = 0.005$) were significantly larger than L5/6 values (4.3±0.7). At 65% contrast, ratio values for L4 (3.2±1; $p = 0.04$) were significantly larger than L5/6 values (2.2±0.6).

Figure 2

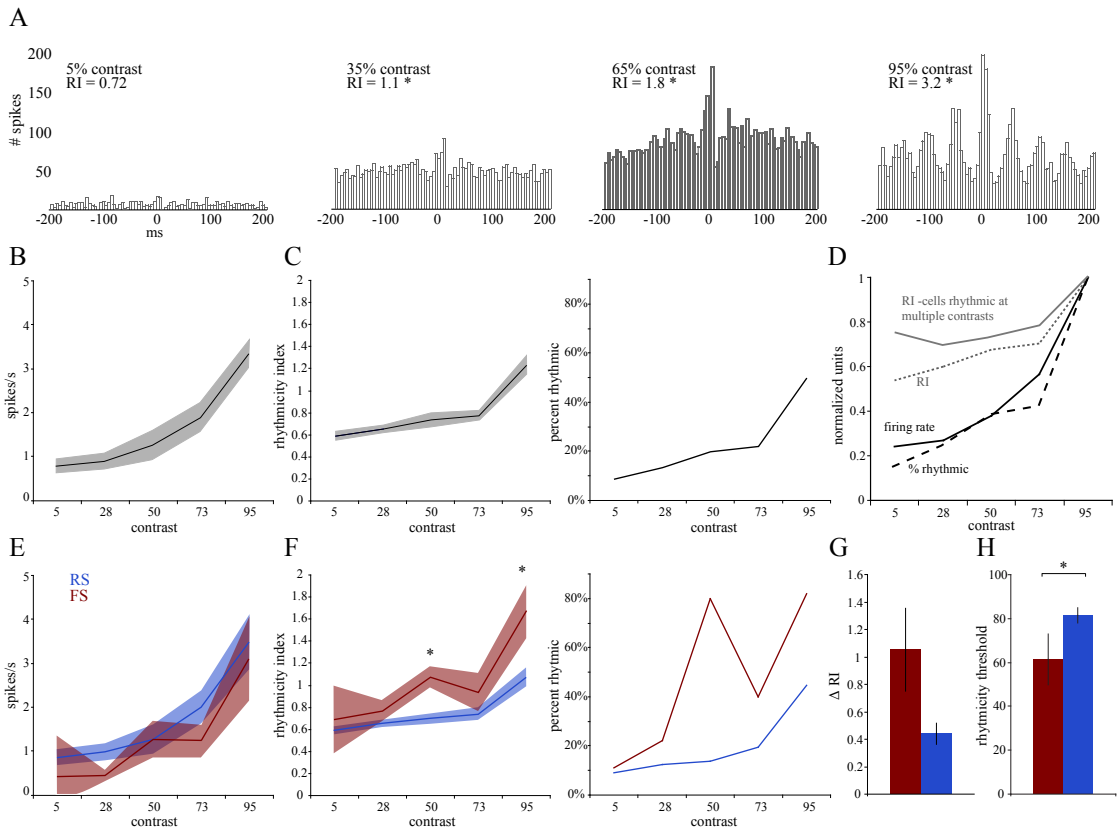
A
5% contrast
RI = 0.72
35% contrast
RI = 1.1 *
65% contrast
RI = 1.8 *
95% contrast
RI = 3.2 *
# spikes
ms
B
spikes/s
contrast
C
rhythmicity index
percent rhythmic
D
normalized units
RI -cells rhythmic at multiple contrasts
RI
firing rate
% rhythmic
E
RS
FS
F
G
Δ RI
H
rhythmicity threshold

Figure 2. Contrast modulates the entrainement of single neurons.

(A) Peri-event histogram (PEH) demonstrating the rhythmicity of an RS neuron in L2/3. Firing rate (FR) and rhythmicity index (RI) both decrease with contrast (FR 95% = 7.3 Hz ; 5% = 1.4 Hz), but the rhythmicity of the cell remains significant until 5% contrast. * = significant RI.

(B) The firing rate of single units depends on contrast. Firing rate increases from 0.7±0.15 Hz at 5% contrast to 3.3±0.32 Hz at 95% contrast.

(C) The rhythmicity of the single units increased from 0.59±0.04 at 5% to 1.23±0.08 at 95% contrast (left panel). Similarly, the percent of rhythmic neurons increased from 9% to 51% as contrast increased from 5% to 95%.

(D) Population values for FR, RI, percent rhythmic, and mean significant RI for neurons that are rhythmic at 2 or more contrasts. Values are normalized to 95% contrast value to aid comparison. Rhythmicity is less modulated by contrast than the firing rate (n = 66 units).

(E) Firing rate at different contrast levels for RS (blue) and FS cells (red). There are no significant differences in firing rate between RS and FS cells.

(F) Rhythmicity over different contrast levels for RS and FS cells. Both for average RI (left panel) and percent of cells that are significantly rhythmic (right panel), FS cells show increased rhythmicity at all levels of contrast until 5%. (95% FS = 1.67±0.24, RS = 1.07±0.08; 73% FS = 0.94±0.17, RS = 0.74±0.05; 50% = FS 1.07±0.09, RS = 0.7±0.05; 28% FS = 0.76±0.09, RS = 0.65±0.03; 5% FS = 0.69±0.09, RS = 0.59±0.04). *$p<0.004$.

(G) FS cells are more modulated by contrast than RS cells. The difference in rhythmicity score between 95% and 5% contrast was greater in FS cells (1.05±0.3) than for RS cells (0.44±0.08).

(H) FS cells have a lower threshold for rhythmicity than RS cells. Rhythmicity threshold was defined as the highest contrast stimuli that did not induce rhythmic firing in the cell. Average FS rhythmicity threshold (61.4±11.6%) was substantially lower than the average rhythmicity threshold of RS cells (81.5±3.5%; $p = 0.006$).

Figure 3

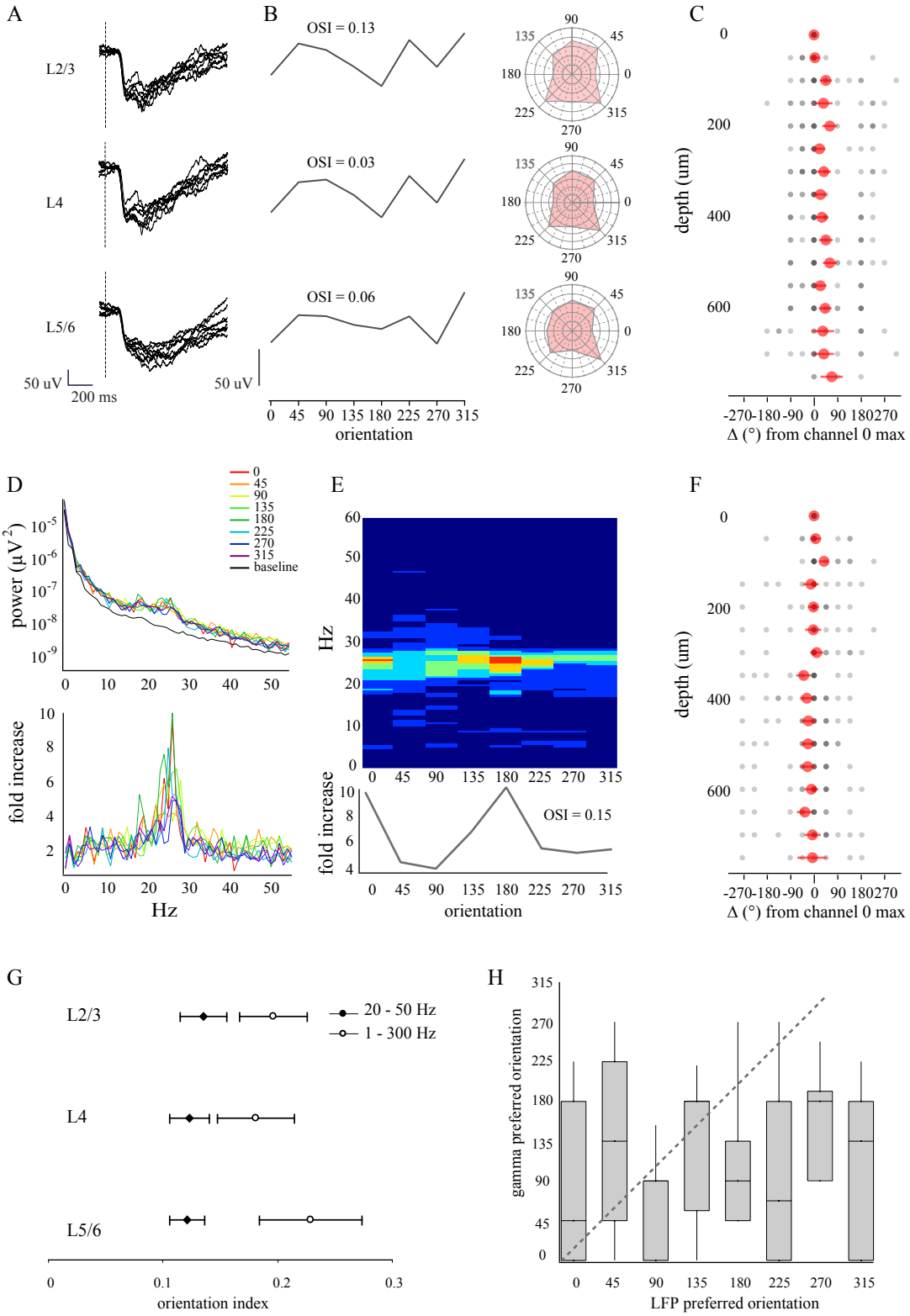
A
L2/3
L4
L5/6
50 uV
200 ms
B
OSI = 0.13
OSI = 0.03
OSI = 0.06
50 uV
0 45 90 135 180 225 270 315
orientation
C
depth (um)
0
200
400
600
-270 -180 -90 0 90 180 270
Δ (°) from channel 0 max
D
power (μV²)
0
45
90
135
180
225
270
315
baseline
fold increase
Hz
E
Hz
fold increase
OSI = 0.15
orientation
F
depth (um)
Δ (°) from channel 0 max
G
L2/3
L4
L5/6
20 - 50 Hz
1 - 300 Hz
orientation index
H
gamma preferred orientation
LFP preferred orientation

Figure 3. Population measures are not well tuned for orientation.

(A) Average evoked responses in the LFP of a representative channel from each cortical layers in response to gratings of 8 different orientations.

(B) Orientation tuning curves (left panel) and polar plots (right panel) for the amplitude of the evoked response (seen in A). The preferred orientation for each of these channels is 315º, but the tuning is very broad.

(C) Population statistics for orientation preference with respect to depth. The preferred orientation of the most superficial channel is plotted as 0, and the preferred orientation for the other 15 channels is plotted as the degrees from the preferred orientation of channel 1. Data from 18 experiments is represented by the grey dots, and the color intensity signifies the number of data points at that dot. Average values are shown in red. The average degrees away from the preferred orientation is less than 90º.

(D) Power spectra for one channel during the presentation of 8 gratings with different orientations (upper panel). Baseline spectra shown in black. Ratio of the spectrum for each orientation divide by the baseline spectrum (lower panel). Peak ratio values range from 9.9 for 180 º to 4.2 for 45 º.

(E) Power spectra from (D, lower panel) plotted with respect to depth. Color signifies the magnitude of the ratio over baseline. Orientation tuning curve for peak frequency (26 Hz).

(F) Population data for the orientation preference of gamma oscillations with respect to depth, plotted as in (C).

(G) Orientation selectivity indices for the LFP (1 – 300 Hz) and gamma oscillations (20 – 50 Hz) for the cortical layers. Both show broad orientation tuning, and although the gamma oscillations have slightly lower index values than the LFP index values, the difference is not significant (LFP:L2/3 = 0.2±0.03; L4 = 0.18±0.03; L5/6 = 0.22±0.04; gamma:L2/3 = 0.13±0.08; L4 = 0.12±0.07; L5/6 = 0.12±0.07).

(H) Gamma oscillations and LFPs from the same electrode do not share orientation preference. Descriptive statistics of the preferred orientation for gamma are plotted as a function of LFP preferred orientation.

Figure 4

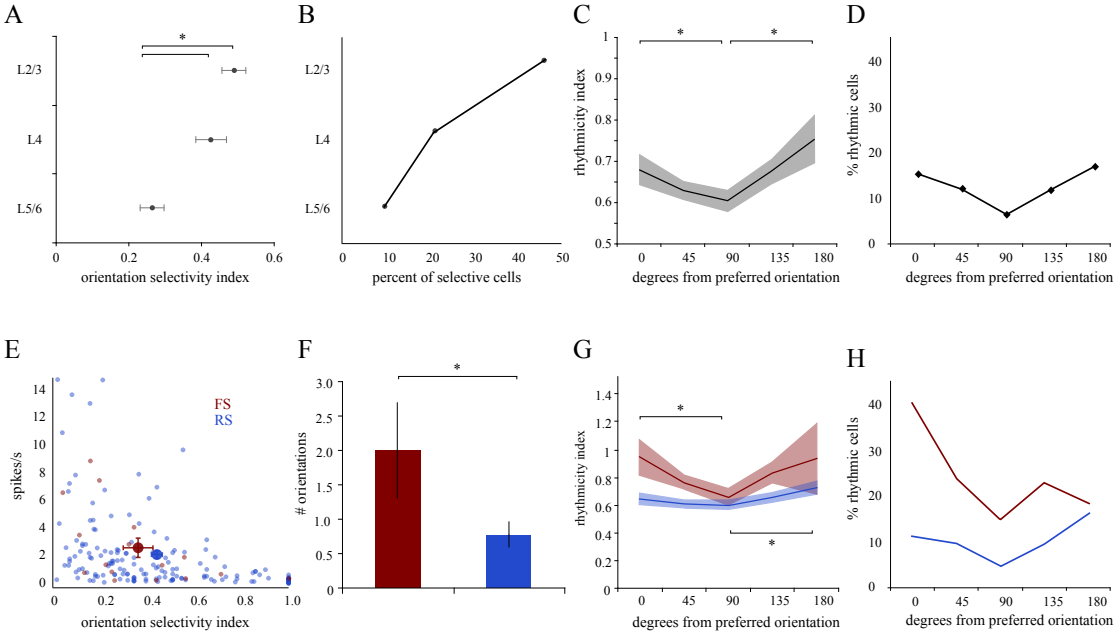
A
B
C
D
L2/3
L4
L5/6
orientation selectivity index
percent of selective cells
rhythmicity index
% rhythmic cells
degrees from preferred orientation
E
F
G
H
FS
RS
spikes/s
orientations

Figure 4. The entrainment of single units is orientation selective.

(A) Orientation selectivity index for single units. The OSI of L2/3 (0.49±0.03, n= 92) and L4 (0.43±0.04, n=43) are both greater than L5/6 (0.26±0.03, n= 41, $p < 0.0001$; $p < 0.0024$).

(B) Percent of single units with OSI > 0.5, by layer. 46% of cells in L2/3, 35% of cells in L4 and 7% of cells in L5/6 were selective.

(C) Rhythmicity of single unit firing was determined for 8 orientations. On average, cells showed the higher rhythmicity at the preferred (0.68±0.3) and opposite (0.76±0.5) orientations, compared to orthogonal (0.61±0.3; $p = 0.04$; $p = 0.008$).

(D) FS and RS cells show similar firing rates and selectivity (FS fr = 2.66±0.7, osi = 0.35±0.06; RS fr = 2.13±0.26, osi = 0.43±0.02).

(E) When rhythmicity was calculated for 8 orientations, on average, FS cells fired rhythmically for 2±0.7 orientations, compared to 0.77±0.18 orientations for RS cells($p = 0.006$).

(F) FS cells showed higher rhythmicity across all orientations than RS cells, but both cell types showed some selectivity in their rhythmicity. The rhythmicity of FS cells was significantly higher for the preferred orientation (0.95±0.4) than for the orthogonal (0.66±0.3; $p = 0.02$), while RS cell rhythmicity was greater for the opposite orientation (0.73±0.4) than for the orthogonal (0.6±0.3; $p = 0.009$).

Discussion

Our results show a selective increase in gamma frequency band in the local field potentials (LFP) recorded from mouse V1 in response to increases in stimulus contrast. The increase in gamma activity was more pronounced in supragranular (L2/3) and granular (L4) layers than in infragranular (L5/6). Single cells responded to increasing stimulus contrast with an increase in firing rate and an increase in their rhythmicity index. Increasing contrast also increased the percent of rhythmic cells.

Our results also show that neither gamma band activity, nor the LFP stimulus-locked response was modulated by stimulus orientation. This was in contrast with the population of single cells which were orientation selective particularly in L2/3 and L4, but also in L5/6. Both in response to increasing contrast and in response to changes in orientation, fast spiking (FS) neurons showed a stronger rhythmicity in the gamma band than regular spiking (RS) cells.

Our selectivity values were slightly lower than those reported previously (Drager, 1975; Mangini and Pearlman, 1980; Niell and Stryker, 2008) presumably because we did not match our stimuli for the receptive field of each cell, but instead we used full screen drifting gratings of constant spatial and temporal frequencies. Preliminary studies with the presentation of optimal stimuli resulted in higher selectivity (not shown). In addition, we did not find a significant difference between the firing rate or selectivity index of FS and RS cells, which was also likely due to the full screen grating stimuli. Similar to what has been previously reported, we found that the greatest average selectivity and highest

percent of selective neurons occurred in the superficial layers (L2/3 and L4) (Drager, 1975; Mangini and Pearlman, 1980; Niell and Stryker, 2008).

The increase in power driven by the visual stimulus was limited to a band between 20-60 Hz and more often between 20-50 Hz. We did not see peaks at higher frequencies as reported in behaving cat V1 (Siegel and Konig, 2003) or a broadband increase in power above 20Hz as in monkey V1 (Henrie and Shapley, 2005). Because the frequency band of increased power was so specific we did not compare its behavior to other frequency bands in response to visual stimuli, but instead used that power in the gamma frequency band across stimulus conditions.

Contrast increased the percentage of rhythmic cells albeit with a much smaller effect on the average rhythmicity index. Once cells became rhythmic, their overall rhythmicity changed very little with firing rate. This effect resulted from the fact that the RI of many cells is hovering below significance and an increase in contrast brings all those cells above significance level without large changes in the value of RI. Thus, the main effect of stimulus contrast was to entrain more cells to the ongoing gamma oscillations in the LFP.

It is conceivable that the increase in gamma oscillations by contrast could be due to volume conduction as the electrode would see progressively larger populations of neurons entrained by the increasing contrast. Also, the lack of modulation in gamma band by orientation could be explained by volume conduction as the electrode would not distinguish among distant populations with different orientation preferences. However, volume conduction is an unlikely explanation. Several lines of evidence show that LFP

originates within a small area around the recording electrode of a few hundred microns (Kruse and Eckhorn, 1996). Simultaneous intracellular recordings in the vicinity of the field recording electrode have demonstrated the similarity of the intracellular voltage with the LFP(Contreras and Steriade, 1995; Steriade et al., 1996b; Penttonen et al., 1998; McCormick et al., 2003), indicating the validity of the LFP as a measure of local population activity driven by synaptic currents and neuronal intrinsic properties. Finally, the rapid decay of spatial correlation in the gamma frequency band, but not in slower frequencies, both in the anesthetized (Steriade et al., 1996b) and non-anesthetized (Destexhe et al., 1999; Siegel and Konig, 2003) cat, further supports the notion that gamma oscillations in the LFP are generated locally. Therefore, an increase in power in the gamma band reflects an increase in the synchronization of local populations of neurons. In species with orientation maps such as the cat (Gray et al., 1989; Bonhoeffer and Grinvald, 1991; Katzner et al., 2009) and monkey (Friedman-Hill et al., 2000; Frien et al., 2000; Berens et al., 2008) such increase in synchrony reflects coordinated activity of neurons with similar selectivity. However, rodents do not have orientation maps (Ohki et al., 2005) and therefore cells with similar selectivity are spatially scattered, so the relationship between connectivity and functional properties is not known.

Our cells were well tuned for orientation, but gamma band oscillations in the LFP were not. This result indicates that the populations of cells engaged by the stimulus changes with orientation but the overall activity of the network remains relatively stable. Furthermore, it suggests that the distribution of cells with different orientations is

sufficiently homogeneous around the recording electrode as to not demonstrate any bias neither in the LFP response nor in the gamma frequency band activity.

Surprisingly, both the LFP and gamma oscillations showed little variance along the depth of the cortex in the orientation that evoked the maximum response. The gamma component showed less variability than LFP. In the initial studies of the mouse visual cortex, Drager (1975) reported that on penetrations normal to the cortical surface there was on average 30° difference in orientation preference of single units, implying that despite the lack of an orientation map, there may be cortical 'microcolumns' that share orientation preference (Drager, 1975; Hubener, 2003). Our results are consistent with this interpretation.

The selective increase in the gamma frequency band of the spectrum upon visual stimulation suggests a critical role for inhibitory interneurons in shaping network activity. Even though interneurons account for only 20% of the total cells in cortex, their divergent connections and the strong conductance change associated with $GABA_A$ IPSPs (Connors, 1984; van Brederode and Spain, 1995; Borg-Graham et al., 1996; Contreras et al., 1996) make interneurons ideal for pacing network activity and generating synchronization under conditions of depolarization. Indeed, the duration of $GABA_A$ mediated IPSPs in neocortex is between 20 and 50 ms (Connors, 1984; Berman et al., 1991; Contreras et al., 1996) which results in oscillatory frequencies between 20 and 50 Hz. In addition, some populations of interneurons demonstrate intrinsic oscillatory properties in the gamma frequency range (Llinas et al., 1991). Our data support of the critical role of inhibitory interneurons by showing that FS cells have a lower contrast

threshold for significant rhythmicity, there is a higher percentage of rhythmic FS cells and individual FS cells have higher degree of rhythmicity with respect to the LFP.

It has been shown in monkey V1 that gamma oscillations saturate at higher contrasts than single neuron activity suggesting that higher contrasts are encoded by changes in neuronal coherence rather than firing rate (Henrie and Shapley, 2005). A similar proposition has been made for the effects on attention on monkey V4 (Fries et al., 2001). Our single cell recordings show that in mouse V1 contrast sensitivity is low and only a few cells saturate their firing rates at the highest contrast of 95% measured here, so it is possible that such a mechanism for encoding high contrast stimuli evolved later in species with a very large dynamic range and in which the visual system is capable of operating with high acuity under very low stimulus contrast such as in primates.

The robust increase in gamma oscillations with the increase in contrast of a drifting grating and the lack of modulation with orientation suggest that gamma oscillations mainly represent the degree of activation of the local network rather than a specific code for stimulus features. Such a conclusion is supported by results showing that increasing input noise with random dot motion stimuli increases the oscillations strength at gamma frequency as measured with autocorrelation (Nase et al., 2003). Thus, under conditions of sufficient activation, gamma oscillations are the preferential output frequency and are selectively enhanced simply because of the powerful nature and the duration of GABAA IPSPs. This notion is supported by the higher frequency rates of inhibitory interneurons in response to increases in contrast (Contreras and Palmer, 2003).

Chapter 3: Alterations in gamma frequency activity in the mouse primary visual cortex as an endophenotype of schizophrenia

Abstract

Schizophrenia has long been regarded as a disorder of higher cognition, but recent electrophysiological studies in patients have revealed evidence of disruptions in basic sensory processing as well (Johnson et al., 2005; Spencer et al., 2009; Turetsky et al., 2009). In particular, gamma oscillations in the primary auditory cortex show increased magnitude at baseline and a decreased signal-to-noise ratio during a stimulus, and these changes correlate with the presence of auditory hallucinations (Spencer et al., 2009). Our goal was to examine the changes in gamma oscillations that result from pharmacological and genetic manipulations of glutamatergic transmission which produce endophenotypes of schizophrenia. We recorded local field potentials (LFP) and single units through the depth of the mouse primary visual cortex in vivo and examined the alterations in gamma frequency activity under both normal and pathological conditions. Our results indicate that both in awake and anesthetized animals, baseline gamma frequency power in the LFP is increased throughout the cortical lamina, and the signal-to-noise ratio of gamma oscillations produced by a visual stimulus is diminished, most notably in the superficial layers. In addition, the entrainment of single units to the local oscillations in the LFP is reduced in the supragranular (L2/3) and infragranular (L5/6) layers. This work supports

the hypothesis that alterations in glutamatergic transmission result in changes to gamma oscillations in primary sensory areas and is consistent with the hypothesis that these changes are associated with disrupted sensory perception.

Introduction

Gamma frequency activity is a robust characteristic of neural activity and has been associated with basic sensory processing and cognitive functions in a wide range of species. In humans, visual and auditory stimuli have been shown to increase gamma frequency oscillations throughout the brain (Ribary et al., 1991; Marshall et al., 1996; Revonsuo et al., 1997; Keil et al., 1999; Lachaux et al., 2000; Ribary, 2005). Gamma is also modulated by attentional processes (Fries et al., 2001; Herrmann and Knight, 2001; Tallon-Baudry et al., 2005) and may serve in the formation of memories (Sederberg et al., 2003; Gruber et al., 2004; Axmacher et al., 2006).

In addition, gamma oscillations are altered in patients with neuropsychiatric disorders such as schizophrenia (Kwon et al., 1999; Spencer et al., 2003; Behrendt, 2006). These patients have increased baseline gamma frequency activity (Tekell et al., 2005) but a relatively smaller increase in gamma in response to sensory stimuli compared to controls (Spencer et al., 2003; Gallinat et al., 2004; Uhlhaas et al., 2006). These abnormalities in gamma have been correlated to both the positive and negative symptoms of schizophrenia (Baldeweg et al., 1998; Lee et al., 2003a; Spencer et al., 2004), and may be responsible for the impaired sensory processing that is characteristic of patients with schizophrenia.

Although schizophrenia has long been regarded as a higher level cognitive disorder, there is mounting evidence of electrophysiological abnormalities even in basic sensory areas. ERP studies have revealed differences between schizophrenic patients and non-affected relatives in both primary auditory (Turetsky et al., 2009) and primary visual

cortex (Johnson et al., 2005). Increased synchrony of gamma oscillations in the auditory cortex were identified in patients during auditory stimulation, and the synchrony correlated with the patient's propensity for auditory hallucinations(Spencer et al., 2009).

Schizophrenia has long been associated with changes in glutamatergic function in the cortex (Greene, 2001; Coyle et al., 2003; Lee et al., 2003b; Lisman et al., 2008). The administration of a sub-anesthetic dose of an NMDA receptor antagonist produces schizophrenia-like symptoms in humans and behavioral endophenotypes of schizophrenia in animals. In addition, numerous genetic mutations associated with schizophrenia are associated with changes in excitatory neurotransmission. For instance, the *neuregulin 1* gene has been implicated in multiple linkage studies to schizophrenia and has been shown to modulate NMDA receptor activation (Stefansson et al., 2002; Hahn et al., 2006).

Gamma oscillations are produced by complex interactions between glutamatergic and gabaergic systems. Pharmacological disruption of either neurotransmitter system can alter neural activity in the gamma range. NMDA receptor antagonists have been shown to increase gamma frequency activity in EEG of rodents (Ehrlichman et al., 2008; Pinault, 2008; Hakami et al., 2009) and to reduce the signal-to-noise ratio of the EEG in response to an auditory click (Lazarewicz et al., 2010).

The goal of this study was to determine if altered glutamatergic transmission produced changes in gamma oscillations in primary sensory cortex. We show that pharmacological and genetic manipulations of the glutamatergic system alter the power of gamma oscillations in the mouse primary visual cortex in vivo. Both the administration

of the NMDA receptor antagonist ketamine and the knockout of *neuregulin-1* produce an increase in the ongoing baseline gamma power. As a result, the signal-to-noise ratio of gamma activity induced by a sensory stimulus is decreased. Our results suggest that alterations in gamma oscillations found in patients with neuropsychatric disorders may results from perturbed glutamaterigic function, and may contribute to aberrant sensory perception.

Methods

Acute animals

Nrg1$^{+/-}$ mice were obtained from S. Siegel (Ehrlichman et al., 2008). The Siegel lab previously obtained the mice from C. Birchmeier (Meyer and Birchmeier, 1995) and bred the mice on a C57BL/6/129 hybrid background at the University of Pennsylvania. Briefly, exon 6 of the neuregulin gene is fused to beta-galactosidase, which results in partial deletion of the EGF like domains of all three major types of Nrg1.

Surgery, electrophysiology, visual stimuli:

See Chapter 1.

Chronic animals

Surgery

All animal experiments were performed in accordance with the guidelines of the National Institutes of Health and the University of Pennsylvania Institutional Animal Care and Use Committee. Adult C57/B6 mice (12 – 24 weeks) were sedated with an initial dose of xylazine (13 mg/kg) and anesthetized with brief exposure to a high concentration of isoflurane (5%). Anesthesia was maintained with isoflurane (0.5 – 1 %). Anesthetic level was monitored by toe pinch, respiration and pupil dilation. Body temperature was maintained at 36° – 37° F throughout the experiment with a heating pad (FHC). Skin incisions were infused with lidocaine and the eye was covered with lacrilube to prevent drying . Mice were positioned in a stereotaxic apparatus (David Kopf Instruments) and one incision was made at midline to allow skin to be pulled to the sides and the skull be

exposed. Skull was cleaned with hydrogen peroxide and allowed to dry thoroughly, before a layer of superglue was applied to the surface of the skull. A very small craniotomy (~ 1mm x 1 mm) was drilled over V1 and another of the same size over the contralateral parietal cortex. The dura over the V1 craniotomy was removed to allow the insertion of a silicon polytrode (NeuroNexusTechnologies) with the same specifications as used in acute recordings. The ground wire was placed into the other craniotomy. The probe and ground wire were affixed to the head with dental cement (Dentsply). The mouse was given a dose of Metacam (4 mg/kg) and allowed to wake up gradually. The animal was checked every 8 hours for the next 24 hours and given additional Metacam as needed. All animals were allowed to recover for at least one week following surgery before the first recording session.

Electrophysiology

Local field potential (LFP) recordings were obtained from the implanted multi-electrode probes (Neuronexus Technologies) with 16 channels arranged in a vertical configuration, with 50 μm spacing between probes (model c1x16-3mm50-177). LFP signals were filtered 1 to 300 Hz online (n= 2 animals, 4 recording sessions). All signals were recorded with the Cheetah 32-channel acquisition system at 30 kHz (Neuralynx). Animals were allowed to freely circumnavigate their home cage during the recording session. During visual stimulation an LED was illuminated in an otherwise dark room for 1 second epochs.

Pharmacology

A sub-anesthetic dose of ketamine (30 mg/kg, i.p.) was administered. The animal was allowed to recover for ~5 minutes before visual stimulation was resumed.

Analysis:

See Chapter 1 and 2.

Results

Human patients with neuropsychiatric disorders such as schizophrenia have altered patterns of gamma frequency activity. Changes in gamma oscillations occur not just in the higher cognitive areas that have long been associated with the disease state, but also in basic sensory processing areas such as primary visual and auditory cortex. To understand in greater detail the changes in gamma activity in basic sensory areas associated with schizophrenia, we characterized the alterations in gamma activity in the primary visual cortex of mice with endophenotypes of schizophrenia. We used two well established manipulations, namely, subanesthetic injections of ketamine and the NRG1 knockout mouse, that have been shown to produce behavioral and physiological endophenotypes of schizophrenia in the mouse., We recorded local field potentials (LFPs) with a multisite probe inserted perpendicular to the cortical surface, or single units using individually moveable tetrodes. For acute recordings of LFPs and single units, mice were anesthetized with a mix of isoflurane and xylazine in order to obtain a stable low amplitude spontaneous baseline pattern recorded in the LFPs. For chronic recordings of LFP, a multisite probe was implanted normal to the cortical surface and allowed to stabilize for one week before recording.

Increased baseline gamma frequency activity and reduced signal-to-noise ratio in LFP of mice with pharmacological endophenotypes of schizophrenia.

To quantify baseline levels of gamma oscillations we recorded LFPs using a multisite probe (Neuronexus, Ann Arbor, MI) with 16 evenly spaced recording sites (50 or 100 μm

interelectrode distance) inserted normal to the cortical surface and spanning the cortical depth. We calculated power spectra from multiple 1 second epochs throughout the recording session, and averaged the spectra for each channel. To determine the total power in the gamma range, we quantified the area under the curve for the frequencies between 20 – 50 Hz.

Following our initial recordings to determine gamma activity under control conditions, we gave the mice a sub-anesthetic dose of ketamine (30 mg/kg, i.p.). The level of isoflurane was reduced to keep the anesthetic state of the animal stable. After waiting five minutes for the ketamine to take effect, we repeated our recordings.

Ketamine strongly increased the magnitude of gamma oscillations in mouse primary visual cortex. This increase was visible by eye in LFP traces filtered for the gamma range (Fig. 1A) and was evident in the average power spectra for each channel (Fig. 1B, ketamine = red). To examine the laminar profile of the increase in gamma activity, we plotted the power spectra with respect to depth, with warmer colors representing higher power (Fig. 1D). In the left and center panels of Figure 1D are the spectra for the control and ketamine conditions, respectively. To emphasize the changes in power that occur during ketamine, the right panel shows the ratio between the ketamine spectra over the control spectra, and the line profile shows the average ratio value for each channel between 20 – 50 Hz. In this example, the increase in power is greatest between 20 and 40 Hz, and is relatively uniform through the depth of the cortex, with a slightly larger increase in the deep layers. This pattern holds true over the population (n= 6 animals, 9 probes), with ketamine significantly increasing baseline

gamma activity in all cortical layers (L2/3 p = 0.04; L4 p = 0.04; L5/6 p = 0.008; Fig. 1C).

To compare visually-driven gamma oscillations before and after ketamine, we used full screen drifting grating presentations of either 500 or 1000 ms at 100% contrast. We calculated power spectra from each single trial both during the 1 second window during the presentation of the drifting gratings and 1 second window immediately before stimulus onset (baseline). We then averaged the response (green) and baseline (gray) single trial spectra for each channel (Fig. 2B, top panel) and calculated the ratio between the two for each channel (Fig. 2B, middle panel). Thus, the ratio spectra quantify the fold increase in activity along the frequency axis in the visual response with respect to the activity immediately preceding stimulus onset. The ratio spectra for the control condition illustrated in Figure 2B show a maximal fold increase in power (6.5 fold) at 20 Hz. To determine the laminar distribution of the increase in gamma activity, we plotted the ratio spectra as a function of depth (Fig 2B, bottom panel) with warmer colors representing larger fold increase above baseline power. In this example, the increase is greater in the superficial layers than deep layers.

Following the administration of ketamine, visual stimulation still produces a robust increase in gamma oscillations, as seen in the single trial illustrated in Figure 2A (green rectangle = stimulus). However, it is apparent even at the level of a single trial that the magnitude of gamma activity induced by the stimulus is not larger than the ongoing, background gamma activity. Comparison between the baseline and visually-driven gamma activity was quantified in the same manner as during the control condition. For

each single trial, the power spectrum for the epoch during the visual stimulus and for the epoch immediately before the stimulus onset were calculated and averaged across trials. There is no difference between the baseline (gray) and response (green) spectra (Fig. 2C, top panel), and the ratio between the two lacks a discernable peak in the gamma range at any depth in the cortex (middle and bottom panels).

Over the population, the total power induced during a visual stimulus was similar for control (gray) and ketamine (red) conditions (Fig. 2D), but the fold increase of stimulus-driven over baseline gamma was diminished by ketamine in L2/3 (5.4±0.9 vs. 2.4±0.4; $p = 0.01$) and L4 (5.5±0.8 vs. 2.5±0.5; $p = 0.001$), but not in L5/6 (Fig. 2E). Because of the increase in baseline gamma power, the same visually-driven induction of gamma frequency activity produces a smaller ratio between the signal and the ongoing background noise, potentially compromising the ability of the primary visual cortex to faithfully process incoming visual stimuli.

Ketamine alters gamma oscillations in awake, behaving mice.

At doses larger than given in this study, ketamine can act as anesthetic agent. To ensure that the results reported in Figures 1 and 2 were not a result of a change in the anesthetic state of the animal or of previously unknown response to a mixture of anesthetics, we chronically implanted the same 16-channel, multisite probe (Neuronexus, Ann Arbor, MI) into the primary visual cortex of c57 male mice (n=4). After 1 week of post-operative recovery, LFPs from the mice were recorded on multiple days. The mouse being recorded was kept in its home cage in a dark room, and a very bright LED was

illuminated for trials of 1 second duration. After 20 minutes of recording time, the mouse was injected with a single subanesthetic dose of ketamine (30 mg/kg, i.p.) and allowed to recover for 5 – 10 minutes before the next recording session.

Illumination of the LED produced a robust evoked response throughout the cortex during both the control (gray) and ketamine (red) conditions (Fig. 3A). When the LFPs from the example in part (A) are filtered for gamma frequency (20 – 50 Hz), it is apparent that the LED induces increased gamma activity under control conditions, and that after ketamine there is more spontaneous, baseline gamma activity (Fig. 3B). Power spectra of baseline activity during control and ketamine conditions show that ketamine increases gamma (Fig. 3C), and when the baseline power spectra are plotted with respect to depth (Fig. 3E), the increase produced by gamma is relatively uniform throughout the cortex. The increase in gamma produced by ketamine holds true over the population ($n = 2$ animals, 4 recording sessions; $p < 0.0001$; Fig. 3D). For the example shown in Figure 3B, the ratio of gamma activity produced by LED illumination over baseline activity is much greater in the control than during ketamine, particularly in the deep layers (Fig. 3F). However, because the LED is not a complex stimulus, it does not reliably increase gamma frequency activity under control conditions, so we were unable to quantify the ratio measures over our population.

Increased baseline gamma frequency activity and reduced signal-to-noise ratio in LFP of mice with genetic endophenotypes of schizophrenia.

We next wanted to determine if these findings extend to another model of glutamatergic hypofunction. We performed acute LFP and single unit recordings as described previously in mice heterozygous for the *neuregulin-1* gene (NRG1). These mice have been shown to have behavioral and biochemical endophenotypes of schizophrenia. We recorded from 8 probes in 7 NRG1 animals and 7 probes in 5 wildtype littermates.

In the absence of visual stimulation, the NRG1 animals have greater baseline gamma frequency activity, seen in the example in Figure 4A and quantified for the population in Figure 4C ($p = 0.05$). The presentation of the drifting grating reliably induces gamma frequency oscillations in NRG1 mice (Fig. 4B). When the ratio of the stimulus-driven over the baseline power spectra is plotted with respect to depth for wild type (Fig. 4E, left panel) and a NRG1 littermate (Fig. 4E, right panel), it is clear that visual stimulation increases gamma activity in the superficial layers of both mice. However, the ratio for the wild type mouse at 20 Hz in L2/3 (6.5 fold increase) and L4 (4.8 fold increase) was greater than the ratio for the NRG1 mouse (L2/3 = 2.4 fold; L4 = 2.8 fold increase). The ratio values at 20 Hz for each mouse are plotted in the line profile to the right, showing smaller increases for the NRG1 mouse throughout the superficial layers. Over the population, NRG1 mice showed smaller increase in gamma activity over baseline ($p = 0.0002$; Fig. 4D). Taken together, these results suggest that the NRG1 mice have a greater baseline gamma component and a smaller signal-to-noise ratio in the gamma range, consistent with the findings in the ketamine-injected animals.

Decreased selectivity and rhythmicity in single units of mice with endophenotypes of schizophrenia.

In order to determine if the alterations of gamma oscillations in mice with glutamatergic transmission deficits were reflected in the spike output of V1, we recorded single units and LFPs throughout V1 using independently movable tetrodes in both the mice injected with ketamine and in NRG1 mice. Only single units that responded robustly to full screen drifting gratings of 95% contrast were included in the analysis (wt = 40 cells; ketamine = 39 cells; NRG1 = 32 cells). To quantify the rhythmicity of single units, we generated perievent histograms (PEH) which are spike time histograms around the threshold-detected positive gamma peaks in the LFP for each level of contrast presented. From the PEHs we calculated a rhythmicity index (RI, see methods) as the average distance between trough and peak of the first 3 peaks of the PEH, and used a bootstrapping technique to set a significance threshold of 95% over shuffled RIs (Popescu et al., 2009). We also quantified the orientation selectivity of the cells (see Methods) and set a threshold for selectivity of 0.5.

Mice with endophenotypes of schizophrenia showed decreased rhythmicity throughout the superficial layers of cortex. In Figure 5A, the PEHs of a L2/3 cell before and after the administration of ketamine shows a decrease in rhythmicity during ketamine (control RI = 1.2, significant; ketamine RI = 0.8), causing the cell's rhythmicity to fall below the significance threshold. For the population, single units in the non-granular layers (L2/3 and L5/6) also showed a decrease in rhythmicity during ketamine. In L2/3, the average RI fell from 1.3±0.3 to 0.63±0.07 ($p = 0.01$) and in L5/6 the average RI

decreased from 1.3±0.17 to 0.59±0.04 ($p = 0.0002$; Fig. 5B). In addition, the percent of rhythmic neurons decreased in L2/3 from 58% to 7.7% and in L5/6 from 58% to 0%. Both the RI and the percent of rhythmic neurons in L4 remained relatively constant. Neurons from the NRG1 mice showed similar rhythmicity as neurons from the mice under ketamine. The RI of NRG1 mice was lower than wildtype mice in L5/6 (0.55±0.06, $p = 0.005$), in L2/3 (0.82±0.08), although the difference in L2/3 did not reach significance. When grouped across all layers, the rhythmicity of cells from the NRG1 animals (0.89±0.1) and was lower than that of wildtype animals (1.2±0.1, $p = 0.013$). In addition, the percent of rhythmic cells was lower in the NRG1 animals in L2/3 (31%) and L5/6 (0%) than for wildtypes, but was not different in L4 (Fig. 5C).The orientation selectivity of neurons in mice with endophenotypes of schizophrenia also decreased. Figure 5D shows the orientation tuning curve of a single unit in L2/3 before (gray) and after (red) the injection of ketamine. The orientation selectivity of the neuron is decreased following the ketamine injection. At the level of the population, the percent of neurons that are selective (OSI>= 0.5) is smaller during ketamine in L2/3 (8.3%) and in L4(25%) than in wt mice (L2/3 = 50%; L4 = 37%). Likewise, fewer neurons from NRG1 animals are selective in the superficial layers (L2/3 = 15%; L4 = 15%) than from wild type animals.

Defects in glutamatergic transmission decrease the ability of the cell in V1 to entrain to the oscillations of the LFP. In addition, single units do not detect characteristics of the stimulus as well.

Figure 1

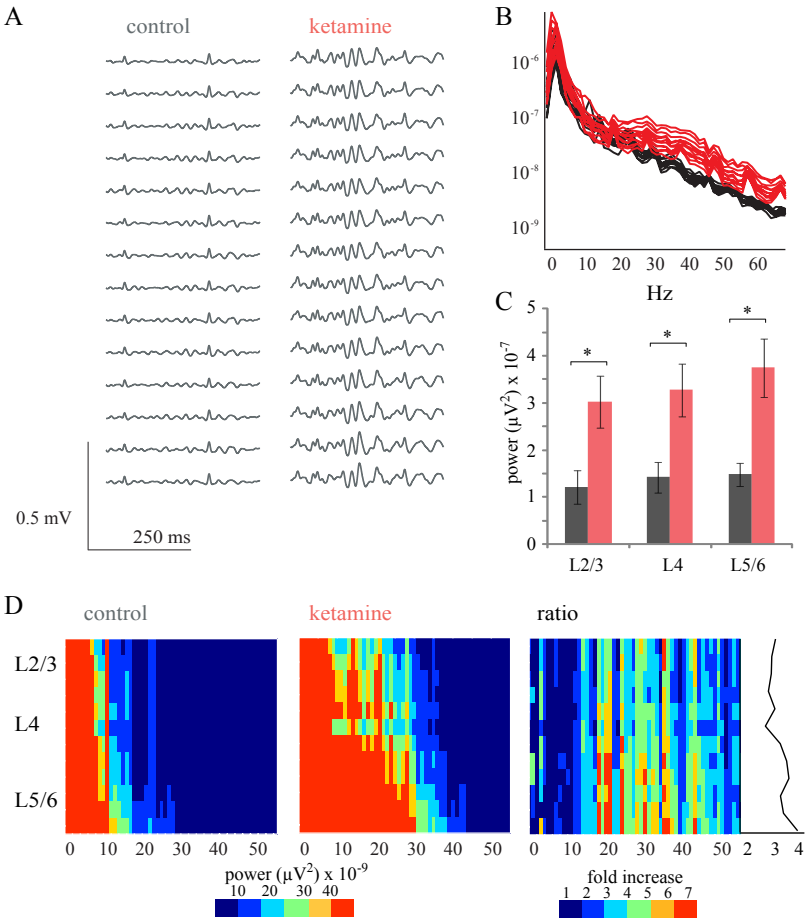
A
control
ketamine
0.5 mV
250 ms
B
Hz
C
power (μV²) x 10⁻⁷
L2/3
L4
L5/6
D
control
ketamine
ratio
L2/3
L4
L5/6
power (μV²) x 10⁻⁹
fold increase

Figure 1. Ketamine increases baseline gamma oscillation power.

(A) Sixteen local field potentials (LFPs) filtered for the gamma range (20 – 50 Hz) recorded in the absence of visual stimulation. Adminstration of ketamine (30 mg/kg, i.p.) causes a marked increase in gamma frequency activity (right panel) as compared to baseline conditions (right panel).

(B) Power spectra of multiple 1 second epochs of baseline activity before (black) and after (red) the injection of ketamine.

(C) For the population (n= 6 animals, 9 probes), ketamine substantially increased the power of gamma frequency activity at baseline conditions through the depth of the cortex (L2/3 $p = 0.04$; L4 $p = 0.04$; L5/6 $p = 0.008$). Although the increase in L5/6 was larger than that of L2/3 or L4, the difference was not significant.

(D) Power spectra shown in (B) are plotted with respect to depth under control (left panel) and ketamine (center panel) conditions, and then the ratio between the ketamine and control plots to show the change in power at each frequency. Ketamine induces a generalized increase in frequencies between 20 – 50 Hz that is relatively similar throughout the depth of the cortex, as demonstrated by the line profile to the right of the ratio plot. The line profile is a mean of ratio amplitudes from 20 – 50 Hz for each channel.

Figure 2

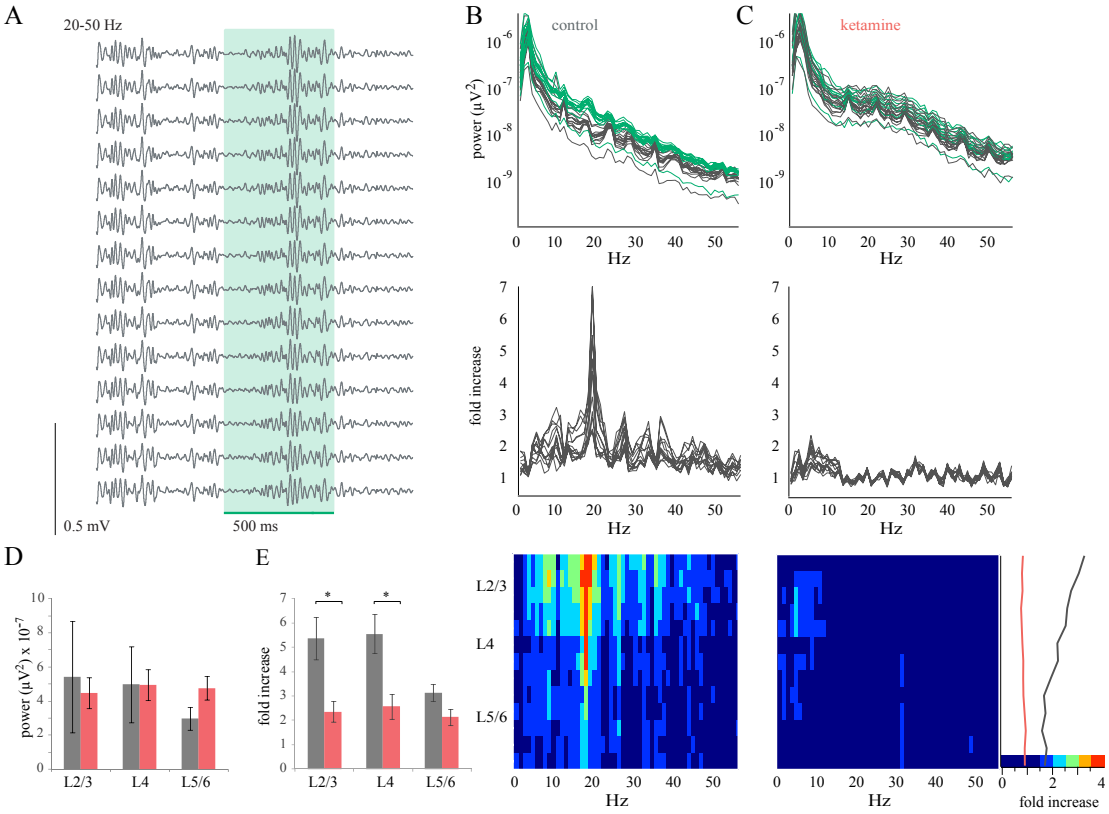
A
20-50 Hz
0.5 mV
500 ms
B
control
power (μV²)
Hz
fold increase
C
ketamine
Hz
fold increase
D
power (μV²) x 10⁻⁷
L2/3
L4
L5/6
E
fold increase
L2/3
L4
L5/6
Hz
Hz
fold increase

Figure 2. Ketamine reduces the signal-to-noise ratio.

(A) Sixteen LFPs filtered for the gamma range (20 – 50 Hz) recorded following the administration of ketamine. Green rectangle indicates the time during the presentation of 500 ms full screen drifting grating at full contrast. The visual stimulus induces robust gamma frequency activity, but note that the activity is no larger than the ongoing gamma activity that occurs before stimulus onset.

(B) Average power spectra from each channel from epochs either during the presentation of the stimulus (green) or during the baseline epoch immediately preceding stimulus onset (gray) for a single experiment (top panel). The ratio of each power spectrum during the stimulus over the corresponding power spectrum at baseline is show in the middle panel. In the bottom panel, each ratio is plotted as a function of depth. These ratio measurements show that the largest increase in power (6.5 fold increase) occurs at 20 Hz and is predominantly located in the superficial layers.

(C) Data from the same experiment as (B), following the injection of ketamine. Top panel shows average power spectra from baseline epoch (gray) and stimulus epoch (green) for each channel. The ratio of stimulus spectrum over baseline spectrum for each channel shown in the center panel. Note the lack of a distinct peak in the gamma range. The ratio measurements are plotted with respect to depth in the bottom panel. To the right of the bottom panel are line profiles from the pre-ketamine condition (gray) and ketamine condition (red) showing the ratio value at 20 Hz for each channel.

(D) Population measurements (n = 6 animals, 9 probes) of gamma power (20 – 50 Hz) during the presentation of the stimulus during control (gray bars) conditions and

following the injection of ketamine (red bars). There are no significant differences in power between the two conditions.

(E) Maximum ratio values for the population. The average ratio value was greater under control conditions (gray) than under ketamine (red) in L2/3 (5.4±0.9 vs. 2.4±0.4; $p = 0.01$) and L4 (5.5±0.8 vs. 2.5±0.5; $p = 0.001$) but not in L5/6 (3.1±0.4 vs. 2.1±0.3).

Figure 3

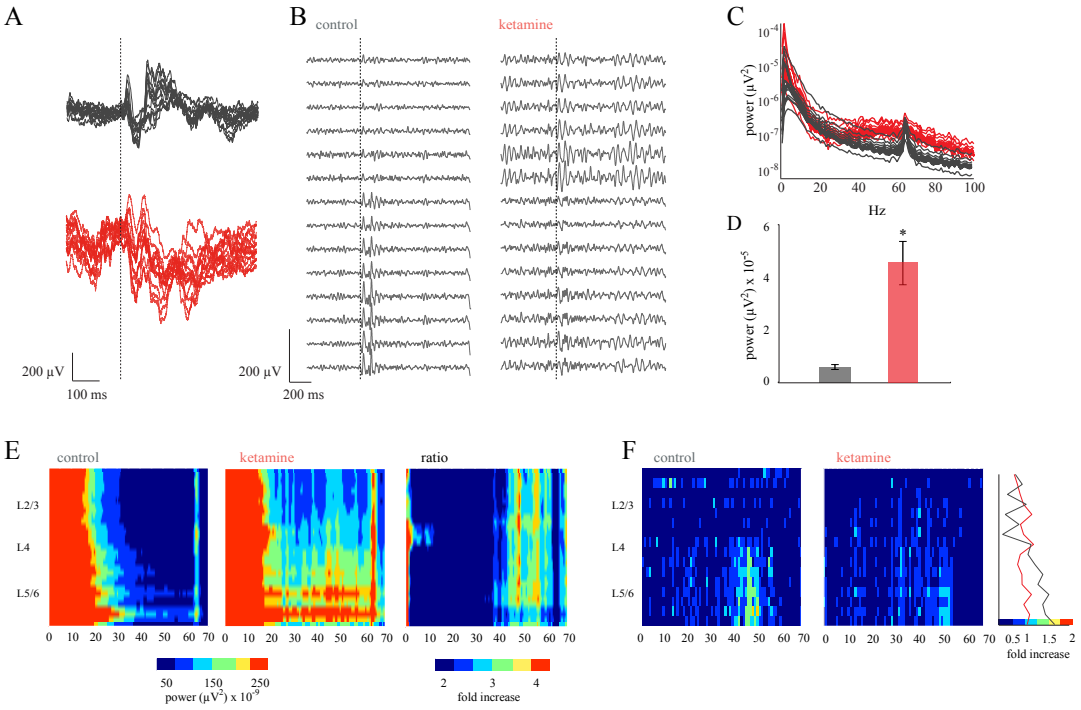
A
B
control
ketamine
C
power (μV²)
Hz
D
power (μV²) x 10⁻⁵
200 μV
100 ms
200 μV
200 ms
E
control
ketamine
ratio
L2/3
L4
L5/6
power (μV²) x 10⁻⁹
fold increase
F
control
ketamine
L2/3
L4
L5/6
fold increase

Figure 3. Ketamine increases baseline gamma oscillations in awake mice.

(A) LFPs from an awake, behaving mouse with an implanted 16 channel multi-site probe. The average evoked response for each channel during visual stimulation with an LED (onset indicated by dotted line, 1 second duration) under control conditions (gray) and following the injection of ketamine (30 mg/kg; i.p.).

(B) LED stimulation in an awake mouse induces gamma frequency ac tivity. Sixteen LFPs recorded through the depth of the cortex filtered for the gamma range (20 – 50 Hz) before (left panel) and after the injection of ketamine (right panel). An increase in overall gamma frequency activity can be seen in the traces recorded under ketamine.

(C) Power spectra for each of sixteen channels for activity in the absence of visual stimulation during control (gray) conditions and following the administration of ketamine (red). The spike at 60Hz is line noise.

(D) Quantification of baseline power (no visual stimulation) for the population (n = 2 animals, 4 trials). The power of gamma frequency activity during ketamine ($4.6\pm0.8 \times 10^{-5}$ μV^2) is much greater than during control conditions ($0.6\pm0.08 \times 10^{-5}$ μV^2; $p < 0.0001$).

(E) Power spectra shown in (C) plotted with respect to depth during control (left panel) and ketamine (center panel) conditions. The ratio of the ketamine plot divided by the control plot reveals the frequencies of greatest increase, in this example between 40 – 60 Hz. The increase is relatively constant through the depth of the cortex.

(F) Ratio of the power spectrum during the LED stimulation over the power spectrum from the epoch that immediately precedes LED onset for each channel plotted with respect to cortical depth. Under control conditions (left panel), LED stimulus increases

gamma activity in L4 (1.4 fold increase) and L5/6 (1.8 fold increase) at ~ 45 Hz. Following the injection of ketamine (right panel) the increases in L4 (1.1 fold) and L5/6 (1.1 fold) are much smaller than under control conditions. Line profiles at right show the values for control (gray) and ketamine (red) at 50 Hz.

Figure 4

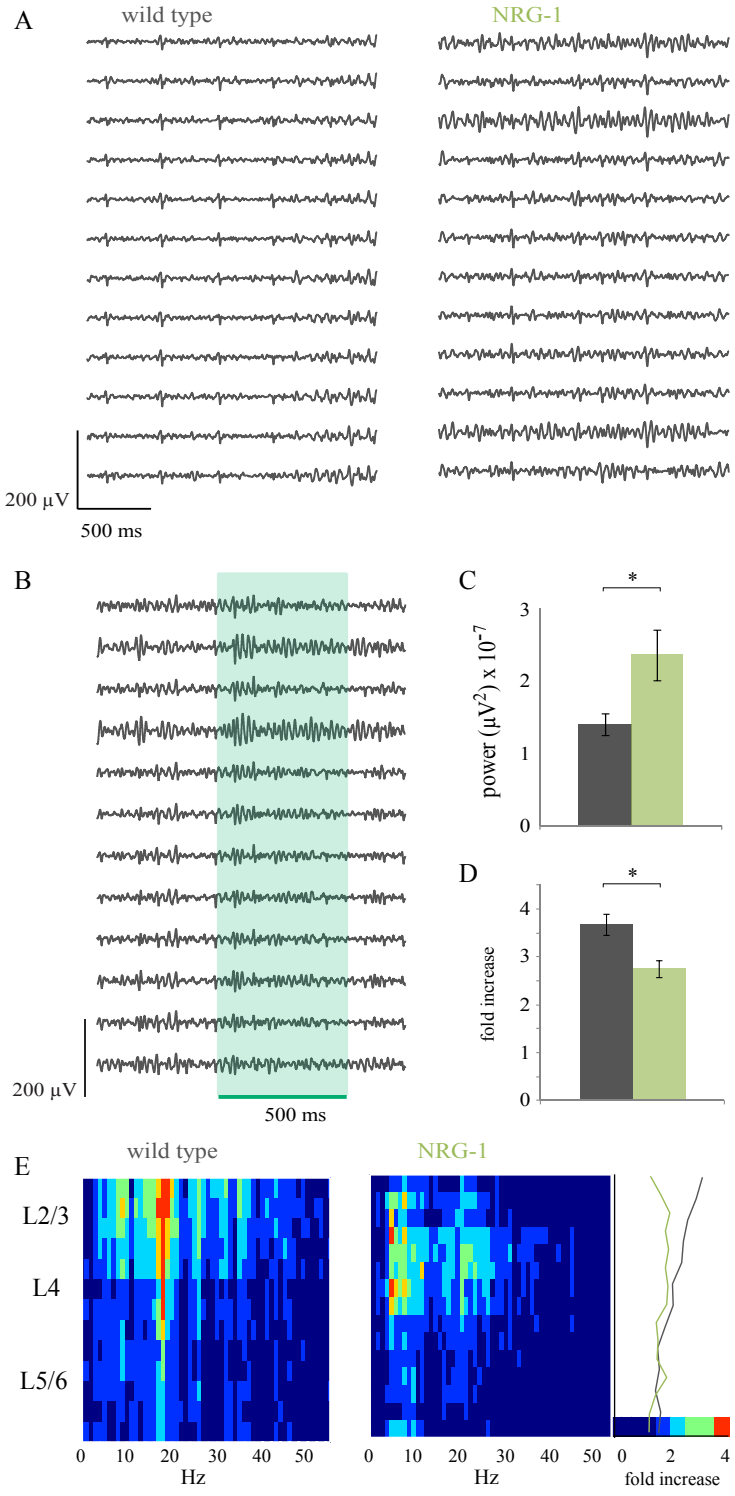
A
wild type
NRG-1
200 µV
500 ms
B
200 µV
500 ms
C
*
power (µV²) x 10⁻⁷
3
2
1
0
D
*
fold increase
4
3
2
1
0
E
wild type
NRG-1
L2/3
L4
L5/6
0 10 20 30 40 50
Hz
0 10 20 30 40 50
Hz
0 2 4
fold increase

Figure 4. NRG1 mice show increased baseline gamma and reduced signal-to-noise ratio.

(A) Gamma frequency activity in LFPs filtered 20 – 50 Hz recorded on multiple electrodes through the depth of the cortex in a NRG1 (right panel) and a wildtype littermate (right panel) mouse under baseline conditions. Larger amplitude gamma oscillations are visible in the recordings from the NRG1 mouse.

(B) Gamma frequency activity in an NRG1 mouse during the presentation of a full screen drifting grating (green rectangle).

(C) Baseline gamma power over the population (wt = 5 animals, 7 probes; NRG1 = 7 animals, 8 probes) and all recording channels. NRG1 (green) gamma power at baseline ($2.4\pm0.4 \times 10^{-7}$ μV^2) is greater than their wt (gray) littermates ($1.4\pm0.1 \times 10^{-7}$ μV^2; $p = 0.05$).

(D) Ratio of gamma power during the presentation of visual stimulus over the baseline epoch immediately preceding stimulus onset for all channels from the population. The ratio values for NRG1 (green) animals (2.7 ± 0.2) is less than the ratio for wt littermates (3.7 ± 0.2; $p = 0.0002$).

(E) Ratio values representing the increase in power induced by visual stimulation for a NRG1 mouse and a wt littermate. The wt mouse shows an increase in L2/3 (6.5 fold increase) and L4 (4.8 fold increase) that are greater than for the NRG1 (L2/3 = 2.4 fold; L4 = 2.8 fold increase). The ratio value at 20 Hz for each channel is plotted in the line profile (right).

Figure 5

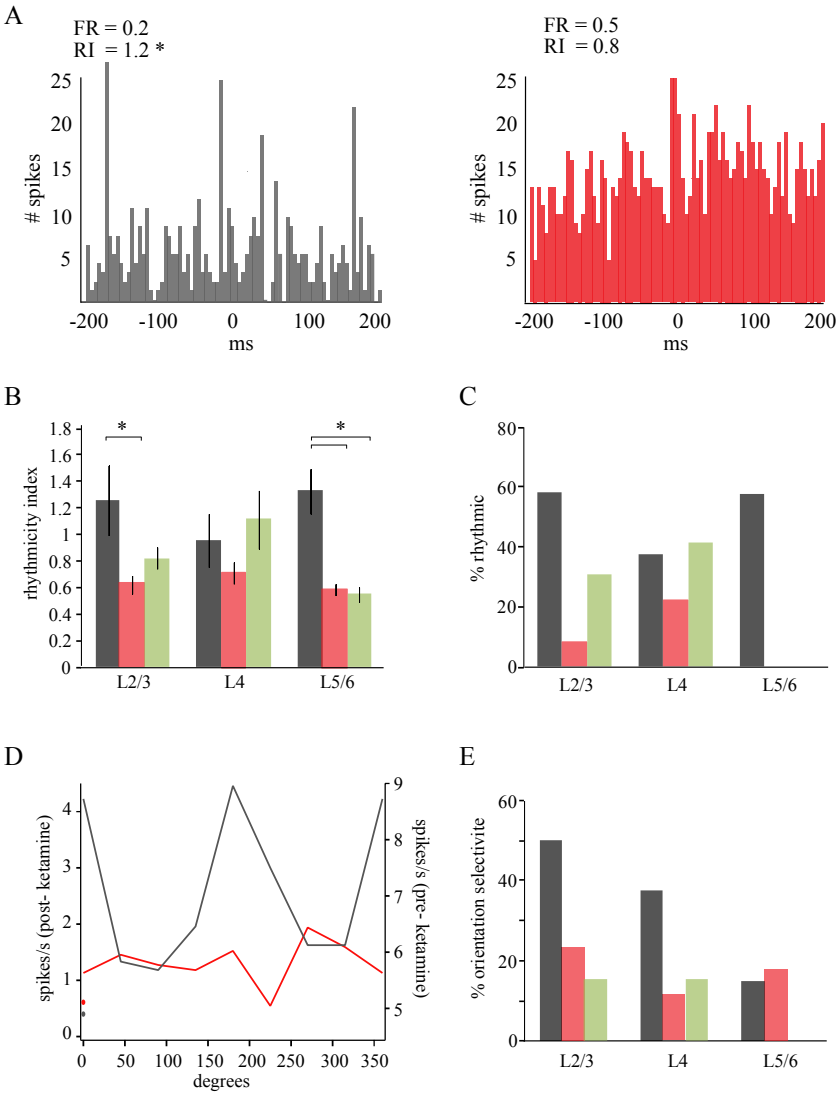
A
FR = 0.2
RI = 1.2 *
# spikes
ms
FR = 0.5
RI = 0.8
B
rhythmicity index
L2/3
L4
L5/6
C
% rhythmic
D
spikes/s (post- ketamine)
spikes/s (pre- ketamine)
degrees
E
% orientation selectivite

Figure 5. Single units from ketamine and NRG1 mice show decreased rhythmicity and orientation selectivity.

(A) Perievent histogram (PEH) for a L2/3 RS cell before and after the injection of ketamine. Although the firing rate is slightly increased during ketamine (baseline 0.2 Hz, ketamine 0.5 Hz), the rhythmicity index of the cell drops below the significance threshold to 0.8, from 1.2 (significant) during baseline conditions.

(B) The rhythmicity of neurons from wt animals (gray; n = 40) compared to neurons during ketamine administration (red; n = 39) and in NRG1 mice (green; n= 32). The average rhythmicity index (RI) is decreased both during ketamine and in NRG1 mice in L5/6 (k = 0.59±0.04, p = 0.0002; NRG1 = 0.55±0.06, p = 0.005), and in L2/3 (k = 0.63±0.07, p = 0.011; NRG1 = 0.82±0.08, p= 0.08, n.s.) as compared to wt (1.3±0.3; 1.3±0.17).

(C) Likewise, the percent of neurons that are rhythmic (RI>= 0.95) is smaller during ketamine and in NRG1 mice in L2/3 (k = 7.7%; NRG1 = 31%) and in L5/6 (k = 0%; NRG1 = 0%) than in wt mice (58%; 58%).

(D) Orientation tuning curve of of an RS cell in L2/3 before (gray) and after an injection of ketamine (red).

(E) The orientation selectivity of neurons from wt animals (gray; n = 40) compared to neurons during ketamine administration (red; n = 39) and in NRG1 mice (green; n= 32). The percent of neurons that are selective (OSI>= 0.5) is smaller during ketamine and in NRG1 mice in L2/3 (k = 8.3%; NRG1 = 15%) and in L4 (k = 25%; NRG1 = 15%) than in wt mice (50%; 37%).

Discussion

Our goal was the evaluate changes in gamma frequency oscillations following genetic and pharmacological perturbations of glutamatergic transmission in the mouse primary visual cortex in vivo. These manipulations are known to create behavioral endophenotypes of schizophrenia in rodents, so we hypothesized that they may produce electrophysiological endophenotypes as well. Our work shows that both the administration of ketamine and the reduction of NRG1 increase baseline gamma frequency activity in the primary sensory cortex and reduce the signal-to-noise ratio of gamma oscillations in response to visual stimuli. In addition, entrainment of neurons in the superficial and deep layers to gamma oscillations in the LFP was reduced and orientation selectivity was diminished. These results show that changes in glutamatergic functioning associated with pathology in schizophrenia alters gamma activity in primary sensory areas in vivo, and suggests that electrophysiological abnormalities in primary sensory areas may contribute to the deficits observed in patients with neuropsychiatric disorders.

Gamma oscillations at rest are increased in V1

Many studies in humans regarding aberrations in gamma oscillations find decreased magnitude and synchrony of gamma oscillations in the frontal and temporal cortex during the presentation of sensory stimuli (Spencer et al., 2003; Uhlhaas et al., 2006) and during rest (Boutros et al., 2008; Rutter et al., 2009). These results were somewhat in conflict with electrophysiological studies performed in mice with behavioral endophenotypes of

schizophrenia of gamma. In these animals, whole brain EEG recordings showed increased gamma oscillations following the administration of ketamine (Pinault, 2008). However, more recent electrophysiological recordings in the primary auditory cortex of schizophrenic patients and controls show an increase in gamma activity in patients compared to controls (Spencer et al., 2009), implying that the direction of change in baseline gamma oscillation magnitude varies with brain region. Our acute recordings in mice under the effects of ketamine and with decreased NRG1 signaling, along with our chronic recordings in mice with sub-anesthetic doses of ketamine support the hypothesis that gamma oscillations in primary sensory areas are increased when glutamatergic function is compromised. These results are consistent with the observed increases in human patients with schizophrenia, but do not exclude the hypothesis that gamma oscillations in other areas such as the frontal and temporal cortex are reduced in schizophrenics.

Signal-to-noise ratio of gamma oscillations during sensory stimulus is reduced

Human EEG recordings demonstrate a reduced signal-to-noise ratio between background gamma oscillations and those induced by a sensory stimulus (Spencer et al., 2003; Gallinat et al., 2004). Whole brain EEG recordings in mice given ketamine show overall reductions in the signal-to-noise ratio following an auditory click (Ehrlichman et al., 2009a; Lazarewicz et al., 2010). However, animal studies have not yet evaluated changes in LFP oscillations in primary sensory areas. Our work evaluates the ratio of the power of visually-driven gamma over baseline gamma and finds that reductions that are consistent

with previous studies and acute experiments and additionally suggest that these changes primarily occur in the superficial layers of cortex.

In anesthetized animals, we find that the ratio of the power of visually-driven gamma activity over baseline to be largest in L2/3 and L4, compared to L5/6. Correspondingly, we find that the reduction in the ratio produced by changes to glutamatergic transmission is largest in these superficial layers. This is consistent with the known architecture of the cortex, in which L2/3 and also L4 have many recurrent, horizontal connections that generate large amounts of recurrent excitatory activity, causing network depolarization that produces gamma oscillations. The full screen, high contrast drifting grating stimulus that we present for a long duration is optimal for generating recurrent activity and gamma oscillations.

During chronic recordings, we provided non-specific illumination via an LED stimulus instead of a drifting grating due to our lack of control of the mouse's eye position. The LED is less complex stimulus than a drifting grating with a variable level of contrast depending on the direction of the mouse's gaze during LED illumination. Although the LED consistently produced an evoked response in the broadband LFP throughout all layers of cortex, gamma oscillations varied between testing periods, even within the same animal,. In the example in Fig 3F, gamma is induced in the deep layers, but not in L2/3, in contrast to our results in the acute experiments, where the stimulus produces the largest gamma increase in L2/3. While this difference between chronic and acute recordings may be due to anesthesia, it is even more likely to be a consequence of

the different visual stimuli. The LED stimulus may not be sufficiently complex to induce recurrent activity in L2/3 and L4 of cortex that generate large amounts of gamma.

Single neuron rhythmicity is decreased

Alterations in glutamatergic signaling increase baseline gamma activity in LFP oscillations, but reduce the entrainment of single neurons to gamma oscillations in L2/3 and L5/6 during the visual stimulus. One potential explanation for this observed decrease in rhythmicity is that neurons are entrained to the increased spontaneous gamma, and thus are decoupled from gamma oscillations by incoming excitation from a stimulus. In wild-type animals under control conditions, cells are not strongly entrained to ongoing gamma frequency activity in the LFP. When a sensory stimulus is presented, putative excitatory cells in superficial and deep layers and putative inhibitory cells in deep layers become more entrained to the induced gamma oscillations. Under conditions of altered glutamatergic function, cells maybe already entrained to the strong ongoing oscillations and the incoming sensory stimuli decouples the cells. This hypothesis predicts that the entrainment of neurons under altered glutamatergic signaling is higher during spontaneous gamma activity than stimulus-driven. Future analysis will address this prediction.

NMDA receptor modulation and cell type

A number of very recent studies have suggested that both NMDA receptor antagonists and NRG1 may not act direct on excitatory transmission, but instead have the largest

effect on inhibitory neurons. In slice recordings, bath application of the NMDA receptor antagonist MK801 actually increases pyramidal cell activity, but decreases GABAergic neural activation (Homayoun and Moghaddam, 2007). Similarly, NRG1 has recently been shown to act as trophic factor that acts specifically on inhibitory interneurons (Wen et al., 2010), and the ligand for NRG1, ErbB4, is only expressed in inhibitory cells in the rat hippocampus (Vullhorst et al., 2009). In previous work, we showed that putative excitatory and inhibitory neurons were modulated differently during stimulus driven gamma than during spontaneous gamma. In future experiments, we would like to isolate putative inhibitory and excitatory neurons and determine if ketamine and reductions in NRG1 modulate inhibitory neurons more than excitatory.

Conclusions

The work presented in this thesis was developed from a desire to investigate in vivo the changes in gamma frequency activity of the LFP and single units that occur in the primary visual cortex in models of glutamatergic hypofunction in schizophrenia. Previous electrophysiological characterizations of changes associated with schizophrenia have either been measured with a single whole-brain EEG in vivo, or performed in vitro. In vivo animal studies with a single EEG measurement lack the resolution necessary to understand the circuit dynamics that underlie the observed changes in gamma oscillation magnitude. It is possible to probe circuit and cellular dynamics in vitro, however, gamma oscillations are not normally observed in vitro and must be created pharmacologically. The degree of similarity between pharmacologically induced oscillations in slice and those occurring in vivo has not yet been documented. In the slice preparation, the circuits involved in gamma oscillation production have been altered fundamentally. Physical connections have been severed, and the neuromodulators that are essential for normal cortical function have been eliminated (Steriade, 2001). Thus, a detailed characterization of changes in gamma oscillations associated with altered glutamatergic function is not reducible to the slice, and has not been investigated in vivo. Here, we have a provided a detailed circuit-level investigation of gamma oscillations during both normal and pathological conditions associated with schizophrenia.

Spontaneous and stimulus-driven gamma oscillations

Spontaneous activity in cortex has been long ignored as ‘noise’ that detracts from the processing of the incoming ‘signal’. However, recent work on population activity in cortex has suggested that ongoing spontaneous activity may modulate cortical responsiveness and contribute to information processing. Studies that directly compare the spatiotemporal profile of spontaneous and stimulus-driven broadband LFP activity have found that they show remarkable similarity (Arieli et al., 1995; Tsodyks et al., 1999; Kenet et al., 2003; Fiser et al., 2004; Hasenstaub et al., 2005; Haider et al., 2007), although the observed differences may be evidence of cortico-cortical processing during stimulus-driven activity (Nauhaus et al., 2009). Gamma frequency activity has also been reported to have similar spatiotemporal structure through the cortical depth and across the cortical surface (MacDonald et al., 1996; Lakatos et al., 2005). However, we have performed more detailed measurements that highlight changes over baseline, and we find that spontaneous and stimulus-driven gamma have distinct spatiotemporal profiles and entrain excitatory and inhibitory single units differently. These results imply that gamma frequency activity engages cortical circuitry differently during spontaneous and visually-driven contexts, and are consistent with the hypothesis that gamma activity is relevant for sensory processing.

Modulation of gamma oscillations by stimulus characteristics

Neurons in the visual cortex of rodents share many similar properties with those of larger mammals, including orientation tuning, but they lack the anatomical organization of an orientation map (Drager, 1975; Ohki et al., 2005; Niell and Stryker, 2008). In mammals

that have orientation maps, the broadband and gamma frequency component of the LFP are tuned to orientation (Frien et al., 2000). We hypothesized that orientation tuning of these population components may be due to the close proximity of single units with a shared orientation preference, and that the population components of mice may show less tuning. Indeed, in the mouse V1, we find very little evidence for orientation tuning of the broadband or gamma frequency LFP, suggesting that orientation tuning of LFP components depends on the map structure.

In contrast to the LFP, single neurons in the mouse V1 are tuned to orientation, and the entrainment of the unit depends on the orientation preference of the neuron. Thus although the population gamma oscillations are not tuned to orientation, the cells fire more rhythmically with respect to the gamma oscillations during preferred orientation than non-preferred. This implies that the phase relationship between the single unit firing and the local gamma oscillation may have some relevance in stimulus discrimination.

However, as found in other mammals, gamma frequency component of the LFP in mice is modulated by contrast. This indicates that ongoing oscillations are reflective of the general depolarization state of the cortex. The average rhythmicity of the single units increased with contrast, and this increase was primarily due to a larger number of neurons engaging in rhythmic firing, rather than a general increase in rhythmicity across all neurons. This implies that with increasing depolarization of the network, a larger percentage of neurons are recruited by oscillations of increasing magnitude. Presumably, the rhythmic firing of these neurons contributes to the ongoing oscillation of the population, entraining more neurons to rhythmic firing.

The contribution of inhibitory and excitatory networks in gamma oscillation production

Very little work has been done to delineate the cellular mechanisms of visually evoked gamma oscillations in vivo in the cortex. Intracellular recordings in pyramidal neurons of anesthetized cats have revealed that membrane depolarization is a critical component for fast frequency oscillations (Contreras and Steriade, 1995; Cardin et al., 2005). In vitro work in the hippocampus has observed that pyramidal neurons and inhibitory interneurons oscillate in phase and the frequency of the oscillation is determined by the time constant of the GABAa receptor, although these findings have not been validated in vivo (Traub and Whittington, 2010).

Inhibitory neurons have been proposed to have greater influence in the production of gamma oscillations than excitatory neurons. In vitro recordings in L5 neurons show that FS cells discharge more strongly in relation to LFP gamma and IPSPs shape spike firing in RS cells (Hasenstaub et al., 2005). In addition, optogenetic excitation of inhibitory interneurons at gamma frequency produces greater power gamma oscillations in the LFP than excitation of excitatory pyramidal cells (Sohal et al., 2009; Cardin et al., 2010). However, optogenetic depolarization of excitatory pyramidal neurons is sufficient to induce gamma oscillations in the population (Adesnik and Scanziani, 2010), implying that excitatory neurons in L2/3 are also capable of initiating gamma oscillations. Taken together, these results lend support to the idea that gamma oscillations, at least in the

superficial layers, are a result of pyramidal-interneuron generated gamma (PING), and are not solely dependent on interneuron activation.

We find that both excitatory and inhibitory neurons are entrained to the ongoing gamma oscillations, but a greater percentage of inhibitory neurons are rhythmic, implying a greater correspondence between inhibitory neuron firing and gamma oscillations than excitatory neuronal activity. However, closer examination of cell type-specific rhythmicity as a function of cortical depth reveals a more subtle role for the contribution of each cell type. Inhibitory interneurons in L5/6 show particularly high entrainment during spontaneous gamma and an increase in rhythmicity during a stimulus, compared to the other layers. During spontaneous gamma, excitatory neurons have low entrainment to the LFP through all layers, but stimulus presentation increases rhythmicity in L2/3 and L5/6 excitatory neurons. Presumably, this increase in rhythmicity of excitatory neurons is due to the observed increase in gamma oscillations in the L2/3 LFP during stimulus presentation. Thus, although inhibitory neurons have generally greater entrainment to the ongoing LFP and likely contribute strongly to gamma activity throughout the cortex, excitatory neurons may also be critically involved in the stimulus-driven gamma in the superficial layers.

Previous work in vitro has suggested that there may be two somewhat independent networks for gamma generation in the cortex. L2/3 and L5/6 are both capable of generating gamma oscillations even when connections between the layers are severed (Roopun et al., 2006; van Aerde et al., 2009). When we reduce L2/3 gamma oscillations pharmacologically in vivo, we find no change in the magnitude or frequency

of gamma oscillations in L5/6, implying that L5/6 oscillations do not depend on those in superficial layers, and supporting the idea of two, somewhat independent gamma generating networks.

However, we did see a reduction in rhythmicity of excitatory neuron in L5/6, and based on previous work showing that excitatory cells in L2/3 drive L5/6 excitatory neurons (Adesnik and Scanziani, 2010), we conclude that the rhythmic RS cells in L2/3 drive rhythmicity in L5/6. There was no reduction in the rhythmicity of L5/6 inhibitory neurons, suggesting that the rhythmicity of these inhibitory neurons is not dependant on oscillations in L2/3, or on the rhythmicity of L5/6 excitatory neurons. Thus, gamma oscillations in L5/6 may be largely dependent on connections between inhibitory interneurons, perhaps dependant on gap junctions.

Changes in glutamatergic transmission in schizophrenia

We find evidence that alteration in glutmatergic function increases baseline gamma oscillations throughout the depth of the primary visual cortex in both awake and anesthetized animals. These changes in glutamate transmission produce behavioral endophenotypes of schizophrenia. Both the systemic injection of ketamine and genetic reduction in NRG1 are thought to influence signaling at the NMDA receptor. Interestingly, in the cortex, reductions in NMDA receptor signaling most likely reduce the activity of inhibitory interneurons.

In vivo iontophoresis studies have shown that ketamine only produces behavioral endophenotypes of schizophrenia and accompanying increases in firing rates of cells in

the prefrontal cortex when it is administered systemically, and not when it is locally injected into the cortex (Suzuki et al., 2002; Lopez-Gil et al., 2007). In addition, systemic administration of ketamine produces a large increase in the amount of glutamate and acetylcholine in the cortex as measured by microdialysis, but local injection of ketamine does not increase these neurotransmitter levels (Lopez-Gil et al., 2007). On the basis of these findings, it has been proposed that ketamine blocks NMDA receptors on inhibitory interneurons in subcortical structures such as the thalamus and basal forebrain, which reduces the inhibitory drive of these structures on the cortex, leading to increased glutamateric and cholinergic input into the cortex.

Neuregulin 1 is a synaptic structural protein that can modulate NMDA receptor activation. However, recent evidence suggests that this modulatory role may primarily affect inhibitory neurons. NRG1 has recently been identified as a trophic factor that stimulates GABA release from parvalbumin-positive inhibitory interneurons onto pyramidal neurons (Wen et al., 2010). Structurally, in the rat hippocampus, the NRG1 receptor (ErbB4) is only found on inhibitory interneurons, although it is not yet known if this is also true for other brain areas (Vullhorst et al., 2009). Thus, under normal circumstances, NRG1 seems to stimulate inhibitory neurons via NMDA receptor modulation to reduce the excitation in pyramidal neurons. In NRG1 knockout animals, the NMDA receptor activation of inhibitory interneurons may be reduced, leading to increased depolarization of excitatory neurons in cortex and other brain areas.

A similar effect may be responsible for schizophrenia-like symptoms observed in patients with NMDA-receptor mediated encephalitis. In these patients, the body produces

an antibody to the NMDA receptor that is shown to reduce the NMDA current in hippocampal neurons, and is likely most efficacious on inhibitory neurons (Dalmau et al., 2008; Hughes et al., 2010). Removal of the antibody through immunotherapy and surgical intervention reverses the symptoms of the patient. However, the gamma component of the EEG in these patients has not yet been evaluated.

Although not identical, both ketamine and NRG1 seem to affect similar pathways involving the NMDA receptor modulation of inhibitory interneurons, resulting in decreased inhibitory activity and consequently increased depolarization of pyramidal neurons in the cortex. This modulated increase in depolarization in the cortex seems to produce an increase in spontaneous gamma frequency oscillations in the LFP. However, it is important to note that the modulation of inhibitory neurons via the NMDA receptor seems to increase gamma oscillations; the complete antagonism of inhibitory by picrotoxin eliminates gamma oscillations, suggesting a non-linear effect that is dose dependant.

Future directions

In order to determine a functional role for gamma oscillations, it is necessary to specifically manipulate gamma oscillations in the context of behavior. Recent advances in optogenetic tools will allow the control of distinct circuit components, such as inhibitory and excitatory cells to allow for the dissection of the circuits that control gamma oscillations. For instance, precise modulation of the activity of inhibitory cells will test their precise role in the generation of gamma oscillations. In addition, recent

advances in mouse behavioral tasks, and particularly head fixed recordings during tasks of visual discrimination (Andermann et al., 2010; Niell and Stryker, 2010), will allow for the testing of the role of gamma oscillations in visual discrimination.

Bibliography

Adesnik H, Scanziani M (2010) Lateral competition for cortical space by layer-specific horizontal circuits. Nature 464:1155-1160.

Adrian ED (1936) The spread of activity in the cerebral cortex. J Physiol 88:127-161.

Andermann ML, Kerlin AM, Reid RC (2010) Chronic cellular imaging of mouse visual cortex during operant behavior and passive viewing. Front Cell Neurosci 4:3.

Arieli A, Shoham D, Hildesheim R, Grinvald A (1995) Coherent spatiotemporal patterns of ongoing activity revealed by real-time optical imaging coupled with single-unit recording in the cat visual cortex. J Neurophysiol 73:2072-2093.

Axmacher N, Mormann F, Fernandez G, Elger CE, Fell J (2006) Memory formation by neuronal synchronization. Brain Res Brain Res Rev.

Baldeweg T, Spence S, Hirsch SR, Gruzelier J (1998) Gamma-band electroencephalographic oscillations in a patient with somatic hallucinations. Lancet 352:620-621.

Bazhenov M, Stopfer M, Rabinovich M, Abarbanel HD, Sejnowski TJ, Laurent G (2001) Model of cellular and network mechanisms for odor-evoked temporal patterning in the locust antennal lobe. Neuron 30:569-581.

Behrendt RP (2006) Dysregulation of thalamic sensory 'transmission' in schizophrenia: neurochemical vulnerability to hallucinations. J Psychopharmacol 20:356-372.

Berens P, Keliris GA, Ecker AS, Logothetis NK, Tolias AS (2008) Feature selectivity of the gamma-band of the local field potential in primate primary visual cortex. Front Neurosci 2:199-207.

Berger H (1929) Uber das Elektroenkephalogramm des Menschen. Arch Psychiatr Nervenkrankh 87:527 - 570.

Berman NJ, Douglas RJ, Martin KA, Whitteridge D (1991) Mechanisms of inhibition in cat visual cortex. J Physiol 440:697-722.

Binzegger T, Douglas RJ, Martin KA (2009) Topology and dynamics of the canonical circuit of cat V1. Neural Netw 22:1071-1078.

Bonhoeffer T, Grinvald A (1991) Iso-orientation domains in cat visual cortex are arranged in pinwheel-like patterns. Nature 353:429-431.

Borg-Graham L, Monier C, Fregnac Y (1996) Voltage-clamp measurement of visually-evoked conductances with whole-cell patch recordings in primary visual cortex. J Physiol Paris 90:185-188.

Boutros NN, Arfken C, Galderisi S, Warrick J, Pratt G, Iacono W (2008) The status of spectral EEG abnormality as a diagnostic test for schizophrenia. Schizophr Res 99:225-237.

Brosch M, Budinger E, Scheich H (2002) Stimulus-related gamma oscillations in primate auditory cortex. J Neurophysiol 87:2715-2725.

Bruno RM, Simons DJ (2002) Feedforward mechanisms of excitatory and inhibitory cortical receptive fields. J Neurosci 22:10966-10975.

Cardin JA, Palmer LA, Contreras D (2005) Stimulus-dependent gamma (30-50 Hz) oscillations in simple and complex fast rhythmic bursting cells in primary visual cortex. J Neurosci 25:5339-5350.

Cardin JA, Carlen M, Meletis K, Knoblich U, Zhang F, Deisseroth K, Tsai LH, Moore CI (2009) Driving fast-spiking cells induces gamma rhythm and controls sensory responses. Nature 459:663-667.

Cardin JA, Carlen M, Meletis K, Knoblich U, Zhang F, Deisseroth K, Tsai LH, Moore CI (2010) Targeted optogenetic stimulation and recording of neurons in vivo using cell-type-specific expression of Channelrhodopsin-2. Nat Protoc 5:247-254.

Chalk M, Herrero JL, Gieselmann MA, Delicato LS, Gotthardt S, Thiele A (2010) Attention reduces stimulus-driven gamma frequency oscillations and spike field coherence in V1. Neuron 66:114-125.

Cho RY, Konecky RO, Carter CS (2006) Impairments in frontal cortical gamma synchrony and cognitive control in schizophrenia. Proc Natl Acad Sci U S A 103:19878-19883.

Connors BW (1984) Initiation of synchronized neuronal bursting in neocortex. Nature 310:685-687.

Contreras D, Steriade M (1995) Cellular basis of EEG slow rhythms: a study of dynamic corticothalamic relationships. J Neurosci 15:604-622.

Contreras D, Palmer L (2003) Response to contrast of electrophysiologically defined cell classes in primary visual cortex. J Neurosci 23:6936-6945.

Contreras D, Timofeev I, Steriade M (1996) Mechanisms of long-lasting hyperpolarizations underlying slow sleep oscillations in cat corticothalamic networks. J Physiol 494 (Pt 1):251-264.

Coyle JT, Tsai G, Goff D (2003) Converging evidence of NMDA receptor hypofunction in the pathophysiology of schizophrenia. Ann N Y Acad Sci 1003:318-327.

Dalmau J, Gleichman AJ, Hughes EG, Rossi JE, Peng X, Lai M, Dessain SK, Rosenfeld MR, Balice-Gordon R, Lynch DR (2008) Anti-NMDA-receptor encephalitis: case series and analysis of the effects of antibodies. Lancet Neurol 7:1091-1098.

Debener S, Herrmann CS, Kranczioch C, Gembris D, Engel AK (2003) Top-down attentional processing enhances auditory evoked gamma band activity. Neuroreport 14:683-686.

Destexhe A, Contreras D, Steriade M (1999) Spatiotemporal analysis of local field potentials and unit discharges in cat cerebral cortex during natural wake and sleep states. J Neurosci 19:4595-4608.

Drager UC (1975) Receptive fields of single cells and topography in mouse visual cortex. J Comp Neurol 160:269-290.

Eckhorn R, Frien A, Bauer R, Woelbern T, Kehr H (1993) High frequency (60-90 Hz) oscillations in primary visual cortex of awake monkey. Neuroreport 4:243-246.

Ehrlichman RS, Maxwell CR, Majumdar S, Siegel SJ (2008) Deviance-elicited changes in event-related potentials are attenuated by ketamine in mice. J Cogn Neurosci 20:1403-1414.

Ehrlichman RS, Gandal MJ, Maxwell CR, Lazarewicz MT, Finkel LH, Contreras D, Turetsky BI, Siegel SJ (2009a) N-methyl-d-aspartic acid receptor antagonist-induced frequency oscillations in mice recreate pattern of electrophysiological deficits in schizophrenia. Neuroscience 158:705-712.

Ehrlichman RS, Luminais SN, White SL, Rudnick ND, Ma N, Dow HC, Kreibich AS, Abel T, Brodkin ES, Hahn CG, Siegel SJ (2009b) Neuregulin 1 transgenic mice display reduced mismatch negativity, contextual fear conditioning and social interactions. Brain Res 1294:116-127.

Engel AK, Kreiter AK, Konig P, Singer W (1991) Synchronization of oscillatory neuronal responses between striate and extrastriate visual cortical areas of the cat. Proc Natl Acad Sci U S A 88:6048-6052.

Fisahn A, Pike FG, Buhl EH, Paulsen O (1998) Cholinergic induction of network oscillations at 40 Hz in the hippocampus in vitro. Nature 394:186-189.

Fisahn A, Neddens J, Yan L, Buonanno A (2009) Neuregulin-1 modulates hippocampal gamma oscillations: implications for schizophrenia. Cereb Cortex 19:612-618.

Fiser J, Chiu C, Weliky M (2004) Small modulation of ongoing cortical dynamics by sensory input during natural vision. Nature 431:573-578.

Freeman JA, Nicholson C (1975) Experimental optimization of current source-density technique for anuran cerebellum. J Neurophysiol 38:369-382.

Friedman-Hill S, Maldonado PE, Gray CM (2000) Dynamics of striate cortical activity in the alert macaque: I. Incidence and stimulus-dependence of gamma-band neuronal oscillations. Cereb Cortex 10:1105-1116.

Frien A, Eckhorn R, Bauer R, Woelbern T, Gabriel A (2000) Fast oscillations display sharper orientation tuning than slower components of the same recordings in striate cortex of the awake monkey. Eur J Neurosci 12:1453-1465.

Fries P, Reynolds JH, Rorie AE, Desimone R (2001) Modulation of oscillatory neuronal synchronization by selective visual attention. Science 291:1560-1563.

Gallinat J, Winterer G, Herrmann CS, Senkowski D (2004) Reduced oscillatory gamma-band responses in unmedicated schizophrenic patients indicate impaired frontal network processing. Clin Neurophysiol 115:1863-1874.

Gray CM, Singer W (1989) Stimulus-specific neuronal oscillations in orientation columns of cat visual cortex. Proc Natl Acad Sci U S A 86:1698-1702.

Gray CM, McCormick DA (1996) Chattering cells: superficial pyramidal neurons contributing to the generation of synchronous oscillations in the visual cortex. Science 274:109-113.

Gray CM, Konig P, Engel AK, Singer W (1989) Oscillatory responses in cat visual cortex exhibit inter-columnar synchronization which reflects global stimulus properties. Nature 338:334-337.

Greene R (2001) Circuit analysis of NMDAR hypofunction in the hippocampus, in vitro, and psychosis of schizophrenia. Hippocampus 11:569-577.

Gruber T, Tsivilis D, Montaldi D, Muller MM (2004) Induced gamma band responses: an early marker of memory encoding and retrieval. Neuroreport 15:1837-1841.

Haenschel C, Bittner RA, Waltz J, Haertling F, Wibral M, Singer W, Linden DE, Rodriguez E (2009) Cortical oscillatory activity is critical for working memory as revealed by deficits in early-onset schizophrenia. J Neurosci 29:9481-9489.

Hahn CG, Wang HY, Cho DS, Talbot K, Gur RE, Berrettini WH, Bakshi K, Kamins J, Borgmann-Winter KE, Siegel SJ, Gallop RJ, Arnold SE (2006) Altered

neuregulin 1-erbB4 signaling contributes to NMDA receptor hypofunction in schizophrenia. Nat Med 12:824-828.

Haider B, Duque A, Hasenstaub AR, Yu Y, McCormick DA (2007) Enhancement of visual responsiveness by spontaneous local network activity in vivo. J Neurophysiol 97:4186-4202.

Hakami T, Jones NC, Tolmacheva EA, Gaudias J, Chaumont J, Salzberg M, O'Brien TJ, Pinault D (2009) NMDA receptor hypofunction leads to generalized and persistent aberrant gamma oscillations independent of hyperlocomotion and the state of consciousness. PLoS One 4:e6755.

Harris KD, Henze DA, Csicsvari J, Hirase H, Buzsaki G (2000) Accuracy of tetrode spike separation as determined by simultaneous intracellular and extracellular measurements. J Neurophysiol 84:401-414.

Hasenstaub A, Shu Y, Haider B, Kraushaar U, Duque A, McCormick DA (2005) Inhibitory postsynaptic potentials carry synchronized frequency information in active cortical networks. Neuron 47:423-435.

Hebb DO (1949) The organization of behavior. New York: Wiley.

Henrie JA, Shapley R (2005) LFP power spectra in V1 cortex: the graded effect of stimulus contrast. J Neurophysiol 94:479-490.

Herrmann CS, Knight RT (2001) Mechanisms of human attention: event-related potentials and oscillations. Neurosci Biobehav Rev 25:465-476.

Herrmann CS, Munk MH, Engel AK (2004) Cognitive functions of gamma-band activity: memory match and utilization. Trends Cogn Sci 8:347-355.

Heynen AJ, Bear MF (2001) Long-term potentiation of thalamocortical transmission in the adult visual cortex in vivo. J Neurosci 21:9801-9813.

Homayoun H, Moghaddam B (2007) NMDA receptor hypofunction produces opposite effects on prefrontal cortex interneurons and pyramidal neurons. J Neurosci 27:11496-11500.

Hubener M (2003) Mouse visual cortex. Curr Opin Neurobiol 13:413-420.

Hughes EG, Peng X, Gleichman AJ, Lai M, Zhou L, Tsou R, Parsons TD, Lynch DR, Dalmau J, Balice-Gordon RJ (2010) Cellular and synaptic mechanisms of anti-NMDA receptor encephalitis. J Neurosci 30:5866-5875.

Javitt DC, Steinschneider M, Schroeder CE, Arezzo JC (1996) Role of cortical N-methyl-D-aspartate receptors in auditory sensory memory and mismatch negativity generation: implications for schizophrenia. Proc Natl Acad Sci U S A 93:11962-11967.

Johnson SC, Lowery N, Kohler C, Turetsky BI (2005) Global-local visual processing in schizophrenia: evidence for an early visual processing deficit. Biol Psychiatry 58:937-946.

Jokisch D, Jensen O (2007) Modulation of gamma and alpha activity during a working memory task engaging the dorsal or ventral stream. J Neurosci 27:3244-3251.

Jones EG (2001) The thalamic matrix and thalamocortical synchrony. Trends Neurosci 24:595-601.

Katzner S, Nauhaus I, Benucci A, Bonin V, Ringach DL, Carandini M (2009) Local origin of field potentials in visual cortex. Neuron 61:35-41.

Keil A, Muller MM, Ray WJ, Gruber T, Elbert T (1999) Human gamma band activity and perception of a gestalt. J Neurosci 19:7152-7161.

Kenet T, Bibitchkov D, Tsodyks M, Grinvald A, Arieli A (2003) Spontaneously emerging cortical representations of visual attributes. Nature 425:954-956.

Kruse W, Eckhorn R (1996) Inhibition of sustained gamma oscillations (35-80 Hz) by fast transient responses in cat visual cortex. Proc Natl Acad Sci U S A 93:6112-6117.

Krystal JH, Karper LP, Seibyl JP, Freeman GK, Delaney R, Bremner JD, Heninger GR, Bowers MB, Jr., Charney DS (1994) Subanesthetic effects of the noncompetitive NMDA antagonist, ketamine, in humans. Psychotomimetic, perceptual, cognitive, and neuroendocrine responses. Arch Gen Psychiatry 51:199-214.

Kurylo DD, Gazes Y (2008) Effects of Ketamine on perceptual grouping in rats. Physiol Behav 95:152-156.

Kwon JS, O'Donnell BF, Wallenstein GV, Greene RW, Hirayasu Y, Nestor PG, Hasselmo ME, Potts GF, Shenton ME, McCarley RW (1999) Gamma frequency-range abnormalities to auditory stimulation in schizophrenia. Arch Gen Psychiatry 56:1001-1005.

Lachaux JP, Rodriguez E, Martinerie J, Adam C, Hasboun D, Varela FJ (2000) A quantitative study of gamma-band activity in human intracranial recordings triggered by visual stimuli. Eur J Neurosci 12:2608-2622.

Lakatos P, Shah AS, Knuth KH, Ulbert I, Karmos G, Schroeder CE (2005) An oscillatory hierarchy controlling neuronal excitability and stimulus processing in the auditory cortex. J Neurophysiol 94:1904-1911.

Laurent G (1996) Dynamical representation of odors by oscillating and evolving neural assemblies. Trends Neurosci 19:489-496.

Laurent G (2002) Olfactory network dynamics and the coding of multidimensional signals. Nat Rev Neurosci 3:884-895.

Lazarewicz MT, Ehrlichman RS, Maxwell CR, Gandal MJ, Finkel LH, Siegel SJ (2010) Ketamine modulates theta and gamma oscillations. J Cogn Neurosci 22:1452-1464.

Lee KH, Williams LM, Haig A, Gordon E (2003a) "Gamma (40 Hz) phase synchronicity" and symptom dimensions in schizophrenia. Cognit Neuropsychiatry 8:57-71.

Lee KH, Williams LM, Breakspear M, Gordon E (2003b) Synchronous gamma activity: a review and contribution to an integrative neuroscience model of schizophrenia. Brain Res Brain Res Rev 41:57-78.

Light GA, Hsu JL, Hsieh MH, Meyer-Gomes K, Sprock J, Swerdlow NR, Braff DL (2006) Gamma band oscillations reveal neural network cortical coherence dysfunction in schizophrenia patients. Biol Psychiatry 60:1231-1240.

Lisman JE, Coyle JT, Green RW, Javitt DC, Benes FM, Heckers S, Grace AA (2008) Circuit-based framework for understanding neurotransmitter and risk gene interactions in schizophrenia. Trends Neurosci 31:234-242.

Llinas R, Pare D (1997) Coherent oscillations in specific and non-specific thalamocortical networks and their role in cognition. Amsterdam: Elsevier.

Llinas R, Urbano FJ, Leznik E, Ramirez RR, van Marle HJ (2005) Rhythmic and dysrhythmic thalamocortical dynamics: GABA systems and the edge effect. Trends Neurosci 28:325-333.

Llinas RR (1988) The intrinsic electrophysiological properties of mammalian neurons: insights into central nervous system function. Science 242:1654-1664.

Llinas RR, Grace AA, Yarom Y (1991) In vitro neurons in mammalian cortical layer 4 exhibit intrinsic oscillatory activity in the 10- to 50-Hz frequency range. Proc Natl Acad Sci U S A 88:897-901.

Llinas RR, Ribary U, Jeanmonod D, Kronberg E, Mitra PP (1999) Thalamocortical dysrhythmia: A neurological and neuropsychiatric syndrome characterized by magnetoencephalography. Proc Natl Acad Sci U S A 96:15222-15227.

Lopez-Gil X, Babot Z, Amargos-Bosch M, Sunol C, Artigas F, Adell A (2007) Clozapine and haloperidol differently suppress the MK-801-increased glutamatergic and serotonergic transmission in the medial prefrontal cortex of the rat. Neuropsychopharmacology 32:2087-2097.

MacDonald KD, Brett B, Barth DS (1996) Inter- and intra-hemispheric spatiotemporal organization of spontaneous electrocortical oscillations. J Neurophysiol 76:423-437.

MacLeod K, Laurent G (1996) Distinct mechanisms for synchronization and temporal patterning of odor-encoding neural assemblies. Science 274:976-979.

Mangini NJ, Pearlman AL (1980) Laminar distribution of receptive field properties in the primary visual cortex of the mouse. J Comp Neurol 193:203-222.

Marshall L, Molle M, Bartsch P (1996) Event-related gamma band activity during passive and active oddball tasks. Neuroreport 7:1517-1520.

McCormick DA, Shu Y, Hasenstaub A, Sanchez-Vives M, Badoual M, Bal T (2003) Persistent cortical activity: mechanisms of generation and effects on neuronal excitability. Cereb Cortex 13:1219-1231.

Meyer D, Birchmeier C (1995) Multiple essential functions of neuregulin in development. Nature 378:386-390.

Mitra P, Bokil H, NetLibrary Inc. (2008) Observed brain dynamics. In, pp xxii, 381 p. Oxford ; New York: Oxford University Press.

Nase G, Singer W, Monyer H, Engel AK (2003) Features of neuronal synchrony in mouse visual cortex. J Neurophysiol 90:1115-1123.

Nauhaus I, Busse L, Carandini M, Ringach DL (2009) Stimulus contrast modulates functional connectivity in visual cortex. Nat Neurosci 12:70-76.

Nelson CL, Burk JA, Bruno JP, Sarter M (2002) Effects of acute and repeated systemic administration of ketamine on prefrontal acetylcholine release and sustained attention performance in rats. Psychopharmacology (Berl) 161:168-179.

Niell CM, Stryker MP (2008) Highly selective receptive fields in mouse visual cortex. J Neurosci 28:7520-7536.

Niell CM, Stryker MP (2010) Modulation of visual responses by behavioral state in mouse visual cortex. Neuron 65:472-479.

Nunez A, Amzica F, Steriade M (1992) Voltage-dependent fast (20-40 Hz) oscillations in long-axoned neocortical neurons. Neuroscience 51:7-10.

O'Tuathaigh CM, Harte M, O'Leary C, O'Sullivan GJ, Blau C, Lai D, Harvey RP, Tighe O, Fagan AJ, Kerskens C, Reynolds GP, Waddington JL (2010) Schizophrenia-related endophenotypes in heterozygous neuregulin-1 'knockout' mice. Eur J Neurosci 31:349-358.

Ohki K, Chung S, Ch'ng YH, Kara P, Reid RC (2005) Functional imaging with cellular resolution reveals precise micro-architecture in visual cortex. Nature 433:597-603.

Palva S, Palva JM, Shtyrov Y, Kujala T, Ilmoniemi RJ, Kaila K, Naatanen R (2002) Distinct gamma-band evoked responses to speech and non-speech sounds in humans. J Neurosci 22:RC211.

Penttonen M, Kamondi A, Acsady L, Buzsaki G (1998) Gamma frequency oscillation in the hippocampus of the rat: intracellular analysis in vivo. Eur J Neurosci 10:718-728.

Pinault D (2008) N-methyl d-aspartate receptor antagonists ketamine and MK-801 induce wake-related aberrant gamma oscillations in the rat neocortex. Biol Psychiatry 63:730-735.

Plourde G, Baribeau J, Bonhomme V (1997) Ketamine increases the amplitude of the 40-Hz auditory steady-state response in humans. Br J Anaesth 78:524-529.

Popescu AT, Popa D, Pare D (2009) Coherent gamma oscillations couple the amygdala and striatum during learning. Nat Neurosci 12:801-807.

Revonsuo A, Wilenius-Emet M, Kuusela J, Lehto M (1997) The neural generation of a unified illusion in human vision. Neuroreport 8:3867-3870.

Ribary U (2005) Dynamics of thalamo-cortical network oscillations and human perception. Prog Brain Res 150:127-142.

Ribary U, Cappell J, Mogilner A, Hund-Georgiadis M, Kronberg E, Llinas R (1999) Functional imaging of plastic changes in the human brain. Adv Neurol 81:49-56.

Ribary U, Ioannides AA, Singh KD, Hasson R, Bolton JP, Lado F, Mogilner A, Llinas R (1991) Magnetic field tomography of coherent thalamocortical 40-Hz oscillations in humans. Proc Natl Acad Sci U S A 88:11037-11041.

Roopun AK, Middleton SJ, Cunningham MO, LeBeau FE, Bibbig A, Whittington MA, Traub RD (2006) A beta2-frequency (20-30 Hz) oscillation in nonsynaptic networks of somatosensory cortex. Proc Natl Acad Sci U S A 103:15646-15650.

Rutter L, Carver FW, Holroyd T, Nadar SR, Mitchell-Francis J, Apud J, Weinberger DR, Coppola R (2009) Magnetoencephalographic gamma power reduction in patients with schizophrenia during resting condition. Hum Brain Mapp 30:3254-3264.

Sanes JN, Donoghue JP (1993) Oscillations in local field potentials of the primate motor cortex during voluntary movement. Proc Natl Acad Sci U S A 90:4470-4474.

Schmitzer-Torbert N, Jackson J, Henze D, Harris K, Redish AD (2005) Quantitative measures of cluster quality for use in extracellular recordings. Neuroscience 131:1-11.

Sederberg PB, Kahana MJ, Howard MW, Donner EJ, Madsen JR (2003) Theta and gamma oscillations during encoding predict subsequent recall. J Neurosci 23:10809-10814.

Siegel M, Konig P (2003) A functional gamma-band defined by stimulus-dependent synchronization in area 18 of awake behaving cats. J Neurosci 23:4251-4260.

Silva LR, Amitai Y, Connors BW (1991) Intrinsic oscillations of neocortex generated by layer 5 pyramidal neurons. Science 251:432-435.

Singer W, Gray CM (1995) Visual feature integration and the temporal correlation hypothesis. Annu Rev Neurosci 18:555-586.

Sirota A, Montgomery S, Fujisawa S, Isomura Y, Zugaro M, Buzsaki G (2008) Entrainment of neocortical neurons and gamma oscillations by the hippocampal theta rhythm. Neuron 60:683-697.

Sohal VS, Zhang F, Yizhar O, Deisseroth K (2009) Parvalbumin neurons and gamma rhythms enhance cortical circuit performance. Nature 459:698-702.

Sokolov A, Pavlova M, Lutzenberger W, Birbaumer N (2004) Reciprocal modulation of neuromagnetic induced gamma activity by attention in the human visual and auditory cortex. Neuroimage 22:521-529.

Spencer KM, Niznikiewicz MA, Nestor PG, Shenton ME, McCarley RW (2009) Left auditory cortex gamma synchronization and auditory hallucination symptoms in schizophrenia. BMC Neurosci 10:85.

Spencer KM, Nestor PG, Niznikiewicz MA, Salisbury DF, Shenton ME, McCarley RW (2003) Abnormal neural synchrony in schizophrenia. J Neurosci 23:7407-7411.

Spencer KM, Nestor PG, Perlmutter R, Niznikiewicz MA, Klump MC, Frumin M, Shenton ME, McCarley RW (2004) Neural synchrony indexes disordered perception and cognition in schizophrenia. Proc Natl Acad Sci U S A 101:17288-17293.

Stefansson H et al. (2002) Neuregulin 1 and susceptibility to schizophrenia. Am J Hum Genet 71:877-892.

Steriade M (2000) Corticothalamic resonance, states of vigilance and mentation. Neuroscience 101:243-276.

Steriade M (2001) The Intact and Sliced Brain. In, p 322 p. Cambridge, Mass.: MIT Press.

Steriade M (2006) Grouping of brain rhythms in corticothalamic systems. Neuroscience 137:1087-1106.

Steriade M, Amzica F (1996) Intracortical and corticothalamic coherency of fast spontaneous oscillations. Proc Natl Acad Sci U S A 93:2533-2538.

Steriade M, Curro Dossi R, Contreras D (1993) Electrophysiological properties of intralaminar thalamocortical cells discharging rhythmic (approximately 40 HZ) spike-bursts at approximately 1000 HZ during waking and rapid eye movement sleep. Neuroscience 56:1-9.

Steriade M, Amzica F, Contreras D (1996a) Synchronization of fast (30-40 Hz) spontaneous cortical rhythms during brain activation. J Neurosci 16:392-417.

Steriade M, Contreras D, Amzica F, Timofeev I (1996b) Synchronization of fast (30-40 Hz) spontaneous oscillations in intrathalamic and thalamocortical networks. J Neurosci 16:2788-2808.

Sukov W, Barth DS (1998) Three-dimensional analysis of spontaneous and thalamically evoked gamma oscillations in auditory cortex. J Neurophysiol 79:2875-2884.

Suzuki Y, Jodo E, Takeuchi S, Niwa S, Kayama Y (2002) Acute administration of phencyclidine induces tonic activation of medial prefrontal cortex neurons in freely moving rats. Neuroscience 114:769-779.

Swadlow HA, Gusev AG, Bezdudnaya T (2002) Activation of a cortical column by a thalamocortical impulse. J Neurosci 22:7766-7773.

Szymanski FD, Garcia-Lazaro JA, Schnupp JW (2009) Current source density profiles of stimulus-specific adaptation in rat auditory cortex. J Neurophysiol 102:1483-1490.

Tallon-Baudry C, Bertrand O (1999) Oscillatory gamma activity in humans and its role in object representation. Trends Cogn Sci 3:151-162.

Tallon-Baudry C, Bertrand O, Henaff MA, Isnard J, Fischer C (2005) Attention modulates gamma-band oscillations differently in the human lateral occipital cortex and fusiform gyrus. Cereb Cortex 15:654-662.

Tekell JL, Hoffmann R, Hendrickse W, Greene RW, Rush AJ, Armitage R (2005) High frequency EEG activity during sleep: characteristics in schizophrenia and depression. Clin EEG Neurosci 36:25-35.

Thomson AM, West DC, Wang Y, Bannister AP (2002) Synaptic connections and small circuits involving excitatory and inhibitory neurons in layers 2-5 of adult rat and cat neocortex: triple intracellular recordings and biocytin labelling in vitro. Cereb Cortex 12:936-953.

Tiesinga P, Sejnowski TJ (2009) Cortical enlightenment: are attentional gamma oscillations driven by ING or PING? Neuron 63:727-732.

Traub RD, Whittington MA (2010) Cortical oscillations in health and disease. Oxford: Oxford University Press.

Traub RD, Bibbig A, LeBeau FE, Cunningham MO, Whittington MA (2005) Persistent gamma oscillations in superficial layers of rat auditory neocortex: experiment and model. J Physiol 562:3-8.

Tsodyks M, Kenet T, Grinvald A, Arieli A (1999) Linking spontaneous activity of single cortical neurons and the underlying functional architecture. Science 286:1943-1946.

Turetsky BI, Bilker WB, Siegel SJ, Kohler CG, Gur RE (2009) Profile of auditory information-processing deficits in schizophrenia. Psychiatry Res 165:27-37.

Uhlhaas PJ, Singer W (2010) Abnormal neural oscillations and synchrony in schizophrenia. Nat Rev Neurosci 11:100-113.

Uhlhaas PJ, Linden DE, Singer W, Haenschel C, Lindner M, Maurer K, Rodriguez E (2006) Dysfunctional long-range coordination of neural activity during Gestalt perception in schizophrenia. J Neurosci 26:8168-8175.

van Aerde KI, Mann EO, Canto CB, Heistek TS, Linkenkaer-Hansen K, Mulder AB, van der Roest M, Paulsen O, Brussaard AB, Mansvelder HD (2009) Flexible spike timing of layer 5 neurons during dynamic beta oscillation shifts in rat prefrontal cortex. J Physiol 587:5177-5196.

van Brederode JF, Spain WJ (1995) Differences in inhibitory synaptic input between layer II-III and layer V neurons of the cat neocortex. J Neurophysiol 74:1149-1166.

von der Malsberg C, Schneider W (1986) A neural cocktail-party processor. Biol Cybernetics 54:29-40.

Vullhorst D, Neddens J, Karavanova I, Tricoire L, Petralia RS, McBain CJ, Buonanno A (2009) Selective expression of ErbB4 in interneurons, but not pyramidal cells, of the rodent hippocampus. J Neurosci 29:12255-12264.

Wagor E, Mangini NJ, Pearlman AL (1980) Retinotopic organization of striate and extrastriate visual cortex in the mouse. J Comp Neurol 193:187-202.

Wang XJ, Buzsaki G (1996) Gamma oscillation by synaptic inhibition in a hippocampal interneuronal network model. J Neurosci 16:6402-6413.

Wen L, Lu YS, Zhu XH, Li XM, Woo RS, Chen YJ, Yin DM, Lai C, Terry AV, Jr., Vazdarjanova A, Xiong WC, Mei L (2010) Neuregulin 1 regulates pyramidal neuron activity via ErbB4 in parvalbumin-positive interneurons. Proc Natl Acad Sci U S A 107:1211-1216.

Whittington MA, Traub RD, Jefferys JG (1995) Synchronized oscillations in interneuron networks driven by metabotropic glutamate receptor activation. Nature 373:612-615.

Whittington MA, Traub RD, Kopell N, Ermentrout B, Buhl EH (2000) Inhibition-based rhythms: experimental and mathematical observations on network dynamics. Int J Psychophysiol 38:315-336.

Winterer G, Ziller M, Dorn H, Frick K, Mulert C, Wuebben Y, Herrmann WM, Coppola R (2000) Schizophrenia: reduced signal-to-noise ratio and impaired phase-locking during information processing. Clin Neurophysiol 111:837-849.